A Physicochemical Approach to Determining the Functions of Microbial Phenazine Metabolites

Thesis by
Korbinian O. Thalhammer

In Partial Fulfillment of the Requirements for the
degree of
Geochemistry

CALIFORNIA INSTITUTE OF TECHNOLOGY
Pasadena, California

2026
(Defended May 21, 2026)

Korbinian Owen Thalhammer
ORCID: 0000-0001-6882-8611

ACKNOWLEDGEMENTS

This thesis is the culmination of research that I performed at Caltech, but it is also the result of relationships, both professional and personal, with people scattered around the world. The work described here depended no more on the experiments detailed in the following pages than on the experiences nurtured by all of these people, most of whom played no part whatsoever in determining the properties of phenazines. While I cannot possibly do justice here to everyone in this invaluable web of friends, mentors, and family members, there are a few people who merit special mention.

First, I am grateful to my parents Rick and Karen Thalhammer, who for so many years brought me outside and explained to me what I was seeing. Mom and Dad, you have taught me that relationships between plants, animals, and people are complicated, and that developing true understanding often requires abandoning my own interpretation and approaching a question from the perspective of another. You also each embody a strong sense of justice that I hope I have inherited.

To Kal, you have shown me the meaning of perseverance while navigating the perils and reaping the rewards of being true to yourself.

To Don Martinez for helping me find my voice.

To Alex Daly, Michael Carroll, and Charlie Passarell, who continue to help me see such different versions of the world and of myself.

To Michael White, Sean Anderson, and Noel Csomay-Shanklin for warm, steady friendship in the mountains and beyond.

To Richard Horak, whose support these many years made my PhD possible *and* immensely enjoyable. While lying supine in the back of Richard's car on the way to the hospital in 2021, I remember thinking I'd found a true friend.

To Jack Wilding, for shouldering incredible responsibility with unassailable grace and good humor.

To Sara Steck and Bill Albright, who feel like extended family at this point. Thank you for taking Amanda and me in during the fires and for all the rockhounding trips and the consistent interest in us and our projects over the years. I'll split wood with you any time.

To John Ciemniecki, for introducing me to the alluring logic of microbial metabolism and for modeling a balance between the wholehearted pursuit of an intellectual passion and the maintenance of a meaningful life beyond the lab.

To Avi Flamholz, for giving me confidence in my project and in myself as a scientist at a time when I sorely needed both. And to Inês Trindade and Xiaoyu Shan, for generously granting me an up-close view of complementary approaches to a scientific problem, and for bringing an unrestrained joy to the lab.

To Nate Glasser, who, through patient training and endless troubleshooting, gave me the skills and confidence to conduct the measurements central to my thesis. And to Nathan Dalleska for fielding my many analytical chemistry questions when I was lost in the wilderness.

I want to express what a pleasure it was to post up with Richard Horak, Ruth Moorman, and Abby Keebler in libraries, cafes, and beer gardens across Pasadena to gripe and write and finally realize, together, the satisfaction of completing our dissertations.

I would also like to extend my warmest gratitude to my academic mentors. Ben Gilbert generously opened the world of geochemistry to me by mentoring me through my first wet chemistry research project. Ed O'Loughlin continues to teach me by example what it means to be a good mentor. Ted Flynn remains a constant source of support and advice as well as a solid, caring friend.

And to my PhD advisor Dianne Newman, thank you for giving me the freedom to pursue a project of my choosing and for having patience when things didn't go according to plan. Beyond the science, you have taught me lessons about how to relate to people and to institutions that I'm confident will serve me well into the future.

My experience at Caltech was shaped by a class field trip accident in 2021 that left me with a chronic illness. The institute responded by shielding itself as best it could from the situation and any attendant liability. In the process, it abandoned me and the other students hurt on this trip by censoring our communications with fellow students, declining to meet with us to discuss a collaborative response, and even trying to deny the workers' compensation claims we filed to cover medical costs that may be lifelong. I consider this a grave violation not only of Caltech's stated mission, but also of its honor code: "No member of the Caltech community shall take unfair advantage of another member of the Caltech community." As a result of this treatment, I decided to share my story publicly and join my peers in an effort to form a graduate student and postdoctoral scholar union.

The process of organizing was the most rewarding thing I did on Caltech's campus. It brought me in touch with others who share the goal of creating a people-centered environment where research and learning of the highest quality can intersect. I'm grateful to my fellow members of the bargaining team and to all of the organizers across campus who put their personal work on hold to secure the first contract of its kind for Caltech researchers. The contract evolved out of thousands of conversations between the people who conduct Caltech's research in the office, in the lab, and in the field. It contains legally binding protections for international workers, establishes a grievance process independent of the Title IX system, and guarantees speedy workers' compensation to researchers injured on the job. This solution is by no means perfect. Like any democracy, it will require constant vigilance, broad participation, and diligent upkeep. But, to me, our union represents a rational response to an institution that has lost touch with its own values.

Finally, for her contagious exuberance for the Earth, and for her unfailing love and support, I dedicate this thesis to Amanda Bednarick.

ABSTRACT

Phenazines are redox-active microbial metabolites produced in diverse ecologic niches from agricultural soils to chronic infections. Hundreds of phenazine analogs are known to exist in nature, but their precise roles in context and the reasons for their chemical diversity remain elusive. While much energy has been devoted to investigating phenazine biology, laboratory experiments designed around phenotypes often neglect important aspects of the environmental conditions in which phenazines function, namely pH and E_H. In this thesis, I propose that an alternative route to determining the true evolved functions of phenazines and other secondary metabolites is to first interrogate their physicochemical properties in relevant context and to then allow the results to guide biological questions. As a case study, I made detailed abiotic lipophilicity measurements of the phenazines produced by the opportunistic pathogen *Pseudomonas aeruginosa*. The measurements revealed an elegant redox-mediated mechanism by which lipophilicity is tuned *in vivo*, sometimes by several orders of magnitude. The increase in biologic retention implied by this finding was born out experimentally by the discovery that the *P. aeruginosa* membrane harbors millimolar concentrations of reduced pyocyanin in low oxygen conditions, a finding that upends the prevailing concept of that metabolite as an extracellular toxin actively secreted by producer cells. This finding in turn raised questions about the integrity of the pyocyanin-saturated membrane and the function of respiratory enzymes therein. The first question inspired a preliminary lipidomics study that points to significant lipid remodeling in the presence of phenazines. The second may be addressed in the future by respirometry methods developed here for interrogating phenazine interactions with the *P. aeruginosa* electron transport chain. In the final chapter, I describe attempts to address whether phenazine-mediated

reduction of Fe(III)-bearing clays in the environment is a viable mechanism of anaerobic survival for environmental phenazine producers. The experiments described throughout this work represent a fundamentally chemical approach to biological questions, and the results speak to the value of that perspective.

GUIDE TO THE THESIS

Chapter one is a published review article that describes the underlying logic of this thesis: that to understand or predict the function of microbial metabolites, it is important to understand the physical and chemical properties of the environments in which the metabolites are produced and to measure the physicochemical properties of the metabolites in a context as close to the native environment as possible. When diligent attention to environmental conditions is coupled with fundamental chemical measurements of a metabolite, abiotic results can provide biological insights.

In chapter two, I take up this challenge, viewing phenazines through the lens of lipophilicity, which is a thermodynamic property related to energies of solvation in fatty versus aqueous solvents. Exploring the lipophilicity of reduced and oxidized *P. aeruginosa* phenazines revealed an unexpectedly strong redox dependence that appears to be related to a deep evolutionary feature of bacterial phenazines. The end of this chapter describes a surprising biological implication of the finding that the reduced form of pyocyanin is significantly more lipophilic than its oxidized form: reduced pyocyanin concentrates heavily in the membrane of producer cells despite the presence of efflux pumps known to transport phenazines out of the cell. This chapter is currently under review for publication.

Chapter three builds on the finding that pyocyanin (and likely other phenazines) can infiltrate the cell membrane and concentrate there. Phenazine disruption of lipid-lipid and lipid-protein interactions could compromise essential physiological functions like membrane rigidity and respiratory enzyme activity, but the producer cell must have evolved strategies to deal with these challenges or it would long ago have poisoned itself. A preliminary measurement of the lipidome reveals increased lipid abundance and significant lipid remodeling in the cell envelopes of wild type *P. aeruginosa* cells compared to phenazine-deficient mutants of the same strain.

Chapter four addresses the effect of phenazines on *P. aeruginosa* respiration by developing techniques related to those used by Friedheim in 1931 when he first discussed the role of pyocyanin as an "accessory respiratory enzyme." The chapter details conditions explored in our laboratory for inhibiting P. aeruginosa respiration and then stimulating it in the presence of the same inhibitor by disrupting the electron transport chain with phenazines. The effects of the phenazines tested correspond to the physicochemical properties of those phenazines, particularly their reaction rates with oxygen and their lipophilicities.

In a return to the environment, Chapter 5 examines the potential for a common environmental phenazine to reduce Fe(III) found in the lattice of clay minerals. That question hinges on the ability of a phenazine to interact electrochemically with cellular and mineral components separated in space. The findings indicate that phenazine-mediated reduction of clay minerals can be accomplished electrochemically or by the metabolism of an environmental phenazine-producing bacterium. The chapter lays the groundwork for

determining whether such an interaction could promote anaerobic survival in natural soils and waters.

In the final chapter, I discuss the implications of my findings and suggest possibilities for future investigations.

PUBLISHED CONTENT AND CONTRIBUTIONS

Chapter one is adapted from a published review article:

Thalhammer, K. O., & Newman, D. K. (2023). A phenazine-inspired framework for identifying biological functions of microbial redox-active metabolites. Current Opinion in Chemical Biology, 75, 102320. https://doi.org/10.1016/j.cbpa.2023.102320

Both authors contributed to outlining the article. K.O.T. conducted the literature review and drafted the article. Both authors edited the manuscript.

Chapter two is adapted from an article currently under review. The current draft is available on bioRxiv:

Thalhammer, K. O., Scurria, M., Li, J., Trindade, I. B., Gutierrez, O., Conway, S. J., & Newman, D. K. (2026). Redox-dependent lipophilicity of phenazine metabolites is modulated by intramolecular hydrogen bonds and controls their biological distribution. *bioRxiv*, 2026-04. https://doi.org/10.64898/2026.04.18.719255

K.O.T. designed the project, carried out the physical experiments, and drafted the manuscript. M.S., O.G., and S.J.C. conducted the physical chemical modeling and provided interpretation. J.L. assisted with electrochemical techniques and calculations. I.B.T. led the membrane fraction separation. D.K.N. secured funding, provided guidance, and assisted with the biochemical measurements. All authors contributed to the editing of the manuscript.

TABLE OF CONTENTS

NOMENCLATURE

PYO – an almost unforgivably bad abbreviation of the word pyocyanin, a pH-sensitive (pKa = 4.9) N-methylated phenazine metabolite produced by *Pseudomonas aeruginosa* and responsible for the blue-green color observed in its planktonic cultures, biofilms, and infections. IUPAC name: 5-Methylphenazin-1(5*H*)-one.

PCN – phenazine-1-carboxamide, a pH-insensitive phenazine metabolite (pK_a < 14.0 and pK_b < 1.5) produced by *Pseudomonas aeruginosa* and other pseudomonads found in the environment

PCA – phenazine-1-carboxylic acid, a pH-sensitive phenazine metabolite produced by *Pseudomonas aeruginosa* and other pseudomonads found in the environment (pKa = 4.24). PCA (or its symmetric counterpart phenazine-1,6-dicarboxylic acid) is an intermediate in all known bacterial phenazine biosynthetic pathways.

Survival assay – this assay, first described by Wang et al., 2010, places stationary phase *Pseudomonas aeruginosa* PA14 cells that were pre-grown aerobically into a strictly anaerobic electrochemical cell where they are dependent on extracellular phenazines and an applied electrochemical potential to survive (via electron shuttling from the cell to the phenazine and finally to the electrode). This assay is described and referenced in Chapter 5.

PBS: abbreviation of phosphate-buffered saline, a common circumneutral carbon-free buffer

PMF: abbreviation of proton motive force, the combination of chemical and electrical potential created by pumping protons out of the cytoplasm during respiration against both a concentration and a charge gradient. Allowing protons to flow back into the cytosol through the ATP-synthase enzyme generates ATP.

Δphz: a strain of *P. aeruginosa* PA14 lacking the biosynthetic machinery necessary to produce phenazines. Specifically: Δphz1/2 DKN330, phenazine-null via deletions of the

phenazine biosynthesis operons phzA1-G1 (PA14_09480 - PA14_09410) and phzA2-G2 (PA14_39970 – PA14_39880)

SHE – standard hydrogen electrode

Chapter 1

A PHENAZINE-INSPIRED FRAMEWORK FOR IDENTIFYING BIOLOGICAL FUNCTIONS OF MICROBIAL REDOX-ACTIVE METABOLITES

Abstract

While the list of small molecules known to be secreted by environmental microbes continues to grow, our understanding of their *in situ* biological functions remains minimal. The time has come to develop a framework to parse the meaning of these "secondary metabolites," which are ecologically ubiquitous and have direct applications in medicine and biotechnology. Here, we focus on a particular subset of molecules, redox active metabolites (RAMs), and review the well-studied phenazines as archetypes of this class. We argue that efforts to characterize the chemical, physical and biological makeup of the microenvironments, wherein these molecules are produced, coupled with measurements of the molecules' basic chemical properties, will enable significant progress in understanding the precise roles of novel RAMs.

Introduction

Natural product chemists and microbial ecologists are well aware of the existence of thousands upon thousands of small organic molecules produced by environmental microbes. Many of these molecules have been isolated in search of novel antibiotic and antitumor agents, and in recent years researchers have developed bioinformatic tools not only to identify biosynthetic gene clusters, but also to propose the structures of the natural products

they produce (1-3). But despite these efforts, the natural *in situ* biological functions of microbial natural products remain underexplored (4). Why are there so many of these molecules and what are they doing? Is it possible to bring conceptual unity to their chemical diversity?

A subset of these microbial natural products, often characterized by vibrant colors that change upon oxidation or reduction, are classified as redox active metabolites (RAMs). We restrict our definition of RAMs to small electron carrier molecules that are secreted extracellularly, oxidized or reduced at a distance, and then returned to the cell where their original oxidation state is restored via cellular electron transfer. Many different types of molecules fit this bill, including quinones, coumarins, and flavins—the key is that they can engage in reversible electron transfer. One important class of RAMs, phenazines, which we will focus on in this review for illustrative purposes, are produced primarily by pseudomonads and streptomycetes (5-7). All phenazines share a common three-ringed structure arranged around a pyrazine core, and this structure is often decorated with various functional groups. While hundreds of phenazine derivatives exist, only a handful have been thoroughly investigated (8). Yet subtle structural differences even within this select RAM class appear to be linked both to different chemical properties and to different biological functions (9). Interestingly, while core phenazine production is under quorum sensing control (i.e. regulated at high cell density), enzymes that modify the core structure are differentially regulated, pointing to the potential for different functions (10).

The best studied phenazines, including pyocyanin (PYO), phenazine-1-carboxylic acid (PCA), and phenazine-1-carboxamide (PCN), are produced by the

opportunistic pathogen Pseudomonas aeruginosa. Like many RAMs, the brilliant blue pyocyanin molecule has long been recognized as an antibiotic able to generate reactive oxygen species, limiting competition from non-producer strains (11, 12). But PYO is also a signaling molecule required for proper biofilm formation (13-15), and in the human host, PYO is an important virulence factor affecting host cell gene regulation, protein activity, and glutathione redox balance (16-25). Like PYO, PCA also appears to act as a diffusible antibiotic, and in wheat cropland soil, PCA-producing strains are effective at limiting the fungal wheat pathogen responsible for take-all disease (26, 27). The same reactive oxygen species-generating ability that can limit *P. aeruginosa's* competitors also makes PYO toxic to the producer strain under certain conditions (28). When reduced carbon is replete, *P. aeruginosa* populations engage energy-dependent PYO defense mechanisms, including efflux pumps and iron-sulfur cluster repair enzymes, but when carbon is limited, PYO-stimulated cell death occurs. In Lysobacter *antibioticus*, a monooxygenase encoded in the myxin biosynthetic gene cluster is involved in self-resistance to that toxic phenazine (29). Indeed, self-resistance by various strategies is necessary among RAM producers, especially those that inhabit aerobic habitats (30-34).

In addition to their antibiotic functions, phenazines can contribute to microbial nutrient acquisition and energy conservation. By way of reductive dissolution of extracellular ferric iron minerals, reduced phenazines have been shown to make both iron and phosphorus more bioavailable (35-38). Within *P. aeruginosa* cells, oxidized phenazines can promote anaerobic survival by facilitating redox-balancing that enables ATP generation via substrate-level phosphorylation (39-41). In a biofilm context, the spatial distribution of specific phenazines have been linked to their functions as electron carriers (42, 51). For example,

PCN has a low midpoint potential and is enriched in the biofilm interior, while PYO, with a higher midpoint potential, specifically binds extracellular DNA farther toward the biofilm's periphery. The rate of PYO-mediated electron transfer through the biofilm is significantly faster than PYO loss from the biofilm, indicating that electron transfer mediated by extracellular DNA-bound phenazines can be an efficient strategy for relieving reductive stress experienced by cells in the biofilm's anoxic core (43).

These diverse, context-dependent functions of the various *P. aeruginosa* phenazines raise questions about the roles of the less familiar phenazines, but also about RAMs more broadly. Which RAMs function primarily as antibiotics? Which are signaling molecules? Which can promote survival under redox stress, and how? We so far lack a systematic approach for analyzing the roles of putative RAMs *en masse*. This review attempts to develop a conceptual framework through which to understand the *in situ* roles of redox-active natural products across environments and species. Challenged with determining the functions of new RAMs, we require some knowledge of the relevant micro-environmental contexts in which the RAMs are produced. Measurements of key physico-chemical properties in those contexts or in experimentally accessible analogs, along with a pointed search for genetic and physiological characteristics in the producer strain, will allow comparisons to known RAMs and RAM producers, situating new RAMs within the context of other, known RAMs, if not explicitly indicating their specific biological functions. Future experimental studies must then validate predictions resulting from this approach.

Context

When we talk about context, what do we mean? Unlike the well-aerated rich media found in most laboratory cultures, conditions experienced by most microbes are heterogeneous, dynamic, and often challenging. Nutrients, including metals and electron donors and acceptors, can be limiting (44). Wetting and drying cycles can drastically change the osmotic potential and ionic strength of aqueous environments, as well as the availability of oxygen. Additionally, many microbes (up to 80% by some estimates) live in biofilms, surrounded by secreted polymers like polysaccharides and extracellular DNA (45). These biofilms thus define the immediate extracellular microenvironment for these microbes, and their composition and properties stand to affect the mobility and reactivity of secreted RAMs. A RAM that is produced by a biofilm-bound microbe and then diffuses into the environment encounters distinct physicochemical contexts: 1) the intracellular environment, where cytosolic conditions, membrane partitioning, and enzyme interactions govern RAM behavior, and 2) the extracellular environment, where aqueous diffusivity will compete with surface interactions—for example, with biofilm components, minerals, natural organic matter, or host tissue - to determine the ultimate fate of the RAM (**Figure 1**). The characteristics of each of these environments, including their redox state, pH, ionic strength, and even temperature will affect the RAM's behavior and influence its utility to the producer cell.

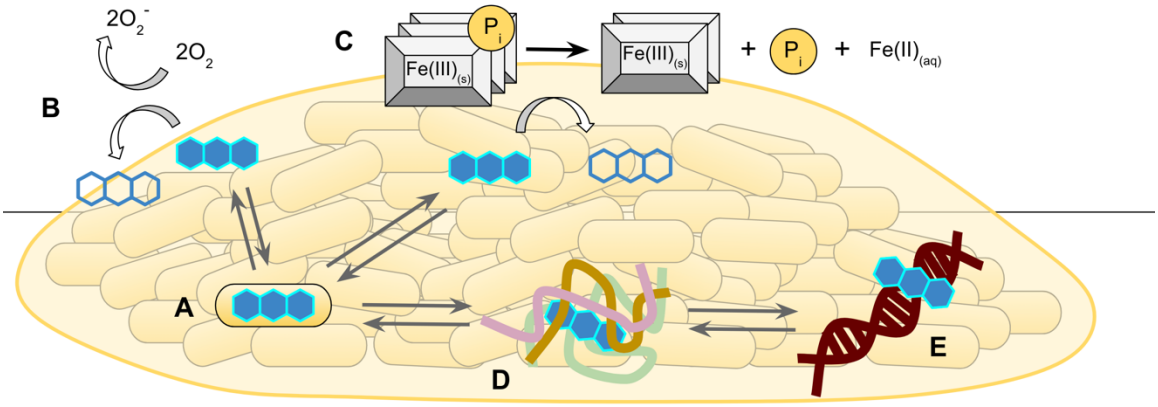

Within the Cell (A)		Beyond the Cell (B-E)	
Controlling Parameters	**Physiological Effects**	**Controlling Parameters**	**Physiological Effects**
lipophilicity, active and passive transport, cytosolic pH and ionic strength, reactions with intracellular components [32, 34]	toxicity, gene regulation, redox reactions with enzymes and cofactors, direct addition to proteins [19, 20, 33-40]	interactions with cell surface proteins, biofilm components, minerals, pH, ionic strength, diffusivity [29, 41-44]	extracellular electron transport to oxic zones, to extracellular enzymes, or to minerals, enhancing nutrient bioavailability [9, 22, 23, 25]

Figure 1: A secreted RAM encounters distinct physicochemical microenvironments including the intracellular space (**a**), where it can affect gene regulation including activating different metabolisms, exerting toxic effects, and/or relieving redox stress; and the biofilm, where it can facilitate extracellular electron transport to oxic interfaces (**b**) or to minerals, thereby enhancing nutrient (e.g. Fe, P) bioavailability (**c**). RAM diffusion and electron transport capabilities within the biofilm depend on interactions with matrix components including polysaccharides (**d**), and extracellular DNA (**e**).

Measurements

The constellation of factors affecting RAM properties in situ is vast, but a reduced set of chemical and physical variables offer a starting point for narrowing and comparing the range

of RAM behavior in context. These include: midpoint potential and redox kinetics, lipophilicity, reductive dissolution and chelation capability, as well as covalent and noncovalent interactions with locally relevant compounds, surfaces, and tissues (**Table 1**). All of these properties are sensitive to a RAM's microenvironment, but despite the diversity of these microenvironments, properties of putative RAMs are often studied under limited conditions, for example in circumneutral aqueous solutions at room temperature. These laboratory conditions do not reflect reality for a RAM producer found in the core of a 37 °C biofilm in an infected wound, where interactions with biofilm components and host tissues dictate RAM mobility and reactivity. Similarly, a microbe adhered to a mineral grain in a soil pore experiencing a wetting/drying cycle endures significant changes in ionic strength and matric potential that will affect the solubility (and hence the utility) of its secreted RAM. Physiological adaptations to this stress, like increasing cell surface hydrophobicity, will affect the partitioning of the RAM into the membrane, enhancing or restricting access to any cellular machinery involved in the redox transformation of the RAM (60).

Table 1: How measurable chemical parameters of RAMs may map onto their expected biological effects, subject to experimental validation.

Measurement	Controlling parameters	Biological effects
Midpoint Potential	pH, enzymatic binding, concentration, temperature (9, 58)	Redox accessibility to enzymes, cofactors, abiotic participants, other RAMs
Redox Kinetics	Reversibility, accessible reductants and oxidants, concentration, temperature (49, 61)	Redox stress relief, reactive oxygen species generation
Lipophilicity	Ionic strength, pH, redox state, temperature (62, 63)	Membrane/cytosol and membrane/extracellular environment partitioning, mobility in biofilm/host tissue/soil
Sorption	Ionic strength, mineral/organic/tissue phases present, temperature (64)	Local concentration enhancement/depletion
Reductive Dissolution	Redox accessibility, ionic strength (9, 38)	Liberation of nutrients for producer and neighbors
Chelation	Competing chelators from other strains or host cells, mineral/metal phases and their oxidations states (35, 37, 65, 66)	Increased nutrient availability for producer, increased or decreased availability for neighbors

Midpoint potential and redox kinetics

The first questions that come to mind when considering a poorly understood RAM include "Can this RAM be reduced or oxidized by the biological system in question?" and if so, "Where is it oxidized and reduced?" The midpoint potential of a RAM will dictate its

accessibility to enzymes, including components of the electron transport chain, to cofactors (like quinones and NADH) within a cell, and to abiotic redox participants like oxygen, nitrate, iron or manganese minerals, and experimental electrodes (9, 22, 36, 43, 48, 61). In some cases, a RAM's potential and structural similarity could even allow it to substitute for a limiting enzymatic cofactor, such as a flavin (48). As demonstrated by the 100 mV potential change between unbound flavin molecules and those bound to Shewanella oneidensis multi-heme cytochrome proteins, binding to a specific enzyme can significantly affect the potential and the kinetics of RAM redox reactivity (58).Midpoint potential is also sensitive to pH and the ratio of oxidized to reduced RAM (36). PYO's reduction potential ranges from 69 mV (normal hydrogen electrode) at pH 5 to −103 mV at pH 8 (9). In *P. aeruginosa* biofilms, pH can vary significantly over micrometer scales, and pH gradients from the core to the edge of the biofilm could theoretically lead not only to altered RAM properties, but also to electrostatic changes in matrix components that affect small molecule penetration (55, 57).

In addition to midpoint potential, the kinetics of reaction between a RAM and likely redox participants in the local environment offer important clues about its fate and function. For example, within the cell, activation of the transcription factor SoxR from Streptomyces coelicolor, *P. aeruginosa*, and *Escherichia coli* by redox active compounds depends not only on midpoint potential, but also on the kinetics of 2Fe–2S cluster oxidation *in vivo* (61). And although nitrate is a thermodynamically acceptable oxidant for PCA, abiotic PCA oxidation by nitrate is not observed, while several bacterial species catalyze nitrate-coupled PCA oxidation rates up to 25 μM/h, suggesting biologically mediated oxidation may contribute significantly to PCA cycling in anoxic environments (49).

Finally, RAM redox reversibility is essential to specific functions, including relief of intracellular redox stress. A RAM incapable of reversible redox chemistry cannot be expected to be recycled numerous times by the producer strain and therefore represents a more significant energetic cost than a reversibly reducible RAM (41). We would therefore infer such a RAM does not contribute appreciably to redox homeostasis but instead possesses a different biological function.

Midpoint potential and redox kinetics

The octanol-water partition coefficient (logP) has long been used as a reproducible and comparable quantitative proxy for lipophilicity of anthropogenic environmental contaminants and attractive drug candidates (62, 67). In the context of environmental RAMs, logP measurements represent a swift, comparable first pass at understanding where a RAM partitions, both intra- and extracellularly. Highly lipophilic RAMs like the archaeal methanophenazine can be expected to partition primarily to the cell membrane (68). When lipophilic RAMs are secreted, they will interact strongly with hydrophobic regions in the biofilm or with lipophilic host tissues or natural organic carbon beyond. Particularly in regimes of high ionic strength, neutral, high logP compounds are prone to "salting out" of aqueous environments, presumably making them inaccessible to the producer strains (62, 63). By contrast, RAMs with low logP values represent candidates for cytosolic redox transformation and will be mobile in aqueous extracellular environments. Changes in logP upon protonation or reduction can affect intracellular RAM concentration, localization and function, for example allowing a RAM to pass back and forth between sites of oxidation and

reduction (46). Adventitious redox interactions with several enzymes are possible for RAMs that migrate throughout the cell (48).

Sorption and covalent interactions

RAM spatial distributions intracellularly, within the biofilm, and in the surrounding environment provide important information about their potential functions (42, 69). Yet experiments and models based on simple aqueous diffusion neglect potentially important interactions between RAMs and cellular or biofilm components. Along with lipophilicity, sorptive interactions-due to electrostatics, Van der Waals forces, and hydrogen bonding-with polysaccharides, extracellular DNA, host tissue, and minerals will alter a RAM's diffusion within its local environment and may even alter physical parameters of that environment. For example, PYO interacts with extracellular DNA, thereby increasing aqueous solution viscosity (59). Determining binding affinity between a RAM and known microenvironmental components through electrochemistry, calorimetry, or even qualitative imaging experiments can begin to illuminate a RAM's *in situ* function (56, 58). A RAM like PCA that diffuses easily out of most biofilm regions likely serves primarily as a diffusible antibiotic or agent of nutrient acquisition, whereas RAMs that bind extracellular DNA may enable electron transfer through biofilms (43, 59). Quantifying the effective diffusion coefficient of a RAM represents an important challenge that can inform interpretation of function.

In some cases, covalent interactions will dictate the fates and effects of RAMs. PCA, for example, bonds covalently to intracellular thiols, potentially leading to protein aggregation and impacting the amount of reduced glutathione in eukaryotic host cells (47). This

reactivity, initiated by a radical mechanism, could also have implications for the activation or inactivation of thiol-bearing proteins in the producer cell or in the extracellular matrix, and will impact extracellular diffusion when PCA encounters thiols in the environment, where they may be present to 10s of μM in dissolved organic matter and to 10s of μmol/g wet weight on the surface of cells (70).

In a soil environment, biofilms exist in direct contact with mineral phases and organic carbon, both dissolved and particulate. Abiotic soil characteristics, including sodium and organic matter content, as well as grain size and pH, have been shown to impact the antibiotic efficacy of PCA-producing Pseudomonas fluorescens biocontrol strains against the fungal wheat pathogen Gaeumannomyces graminis var. *tritici* (27). In particular, higher clay (sub-2 μm diameter particles with high surface area and charge) and organic matter content were correlated with more severe fungal disease, while higher sand content (particles between 62 and 500 μm with lower surface area and charge), pH, and sodium levels were correlated with better-controlled fungal disease. Understanding the strength and reversibility of PCA sorption to mineral surfaces and organic matter under relevant ionic strength and pH regimes could help determine mechanisms responsible for these correlations and inform expectations for PCA behavior in other soils.

Apart from abiotic interactions, if the biofilm is part of the rhizosphere, live plant roots may exert control over local RAM concentrations, either by exuding carbon compounds to recruit and support RAM producers, or by adsorbing or absorbing the RAM directly (71-73). Strong adsorption or active uptake by a living root can hint at particular utility or detriment to the producer strain or to associated plants. Additionally, strong sorption to specific mineral phases can direct hypotheses about RAM utility. For example, sorption experiments showing

strong interactions with a particular metal oxide may suggest microbial attempts at chelation or reductive dissolution or could hint at RAM-mediated mineral respiration. Analogously, in a host infection, extracellular DNA resulting from cell lysis or neutrophil extracellular traps (74, 75) can sequester RAM molecules, providing an opportunity for opportunistic pathogens to survive via extracellular electron transfer.

In addition to informing hypotheses about function, RAM adsorption to extracellular surfaces is essential for determining environmentally relevant experimental conditions, especially RAM concentrations. While some RAMs can be toxic at high concentrations, even to the producer strain, effects of low concentrations of most secondary metabolites, including RAMs, are underexplored (4, 76-79). In some cases, these "antibiotics" may play essential signaling roles at significantly lower concentrations (80). In cross feeding experiments, subinhibitory concentrations of antibiotic secondary metabolites induced antibiotic production and sporulation among various Streptomycete strains (81). Promoter-lux reporter libraries have been used to elucidate previously unappreciated transcriptional changes and ribosomal interactions caused by subinhibitory concentrations (~1 μg/mL, 10-fold lower than the minimum inhibitory concentration) of macrolide-lincosamide-streptogramin antibiotics in Salmonella enterica serovar typhimurium (82). Even if sorption isn't particularly strong or specific, the high surface area of biofilm components and surrounding surfaces may sequester the RAM in certain locations, alternately raising and lowering RAM concentrations in various microenvironments compared with bulk environmental measurements. Concentrating mechanisms of this sort can be key to RAM utilization *in vivo*. In electrochemical experiments, *S. oneidensis* was able to immobilize even minute amounts

(≤ 1 μM) of exogenous PCA at the biofilm–electrode interface to enhance extracellular electron transfer (56). Using a microenvironmentally relevant concentration of a RAM, or the proper ratio of related RAMs, is necessary to elicit experimental responses that are ecologically relevant (83).

Conclusions: from chemical characterization to biological causality

The collection of well-studied RAMs is relatively small, and even the phenazine subset described here is incompletely understood. Motivating *in situ* exploration of RAM function is the promise of new antibiotics that target slow growth metabolisms in biofilms, new knobs for tuning metabolism in the lab or in redox batteries, and a firmer understanding of the evolutionary strategies microbes use to colonize every conceivable ecological niche on Earth (50, 52-54). But our ability to recognize patterns in RAMs' *in situ* functions will depend on comparisons across environmental contexts. The chemical and biological properties described here offer a general framework for gaining intuition about a novel RAM's *in situ* function and comparing it to other known RAMs, feats which may begin to help us glimpse a unity underlying their apparent diversity.

How might we leverage knowledge of the core RAM chemical properties outlined in this review to make accurate predictions about their biological functions? Because RAM chemistry is so versatile, the approach taken to test any given hypothesis will obviously vary with the specific claim, yet certain tools may be generally helpful in identifying correlations and testing causality. To start, correlating *when* specific RAMs are made with specific microenvironmental conditions can provide clues into their biological utility; similarly,

short-term cellular responses to RAM exposure under different conditions (e.g. transcriptional activity in the presence and absence of oxygen) can provide a window into how cells are experiencing RAMs. For example, the observation that phenazine production is correlated with the depletion of oxygen from cultures (84) and/or phosphorus limitation (85) suggested that phenazines might provide a fitness advantage to cells under these conditions. Coupling this observation to the fact that phenazine midpoint potentials are conveniently poised between well-known cellular reductants and oxidants, it became reasonable to postulate that phenazines can serve as alternative electron acceptors when other oxidants are limited, but also as electron donors to distal oxidants (such as ferric oxyhydroxide minerals to which phosphate is adsorbed). This is but one example, and the challenge for the future is to identify new patterns of RAM "behavior" (e.g. regulation of production, physical localization, etc.), that, when coupled to an understanding of their chemistry, can inspire new hypotheses and grant insights into their biological functions.

A next step in testing any such hypothesis is controlling RAM production, ideally by generating mutant strains that lack genes required for RAM biosynthesis—something that is becoming ever easier to do as techniques for genetically manipulating diverse microbes improve—then determining whether the absence of RAMs results in biological effects that are consistent with the hypothesis. Crucial to proving causality is the rescue of the original phenotype by provision of the RAM either via genetic or chemical complementation. Our ability to think beyond a single RAM's effect on a single cell will depend on new methods able to map extracellular RAMs at high resolution, a feat now achievable both electrochemically and optically in the case of phenazines (42, 69, 86). As microscopy at the single cell level improves, and better tools emerge to accurately map and control intra- and

extracellular metabolite distribution in complex environments, a golden age for RAM research is dawning. Indeed, an in-depth understanding of RAM biological functions and broader impacts requires a partnership between chemists and biologists, and we hope this review will inspire researchers in both fields to turn their talents to the many fascinating problems posed by RAMs in diverse contexts, from the soil to the clinic to bioelectronics.

References

1. Newman, D. J., and G. M. Cragg. “Natural Products as Sources of New Drugs over the Last 25 Years.” J Nat Prod 70 (2007): 461–477.
2. Cimermancic, P., M. H. Medema, J. Claesen, K. Kurita, L. C. Wieland Brown, K. Mavrommatis, A. Pati, P. A. Godfrey, M. Koehrsen, J. Clardy, et al. “Insights into Secondary Metabolism from a Global Analysis of Prokaryotic Biosynthetic Gene Clusters.” Cell 158 (2014): 412–421.
3. Blin, K., S. Shaw, A. M. Kloosterman, Z. Charlop-Powers, G. P. van Wezel, M. H. Medema, and T. Weber. “antiSMASH 6.0: Improving Cluster Detection and Comparison Capabilities.” Nucleic Acids Res 49 (2021): W29–W35.
4. Davies, J., and K. S. Ryan. “Introducing the Parvome: Bioactive Compounds in the Microbial World.” ACS Chem Biol 7 (2012): 252–259.
5. Turner, J. M., and Ann J. Messenger. “Occurrence, Biochemistry and Physiology of Phenazine Pigment Production.” Advances in Microbial Physiology (Elsevier, 1986): 211–275.

6. Mavrodi, D. V., W. Blankenfeldt, and L. S. Thomashow. “Phenazine Compounds in Fluorescent *Pseudomonas* spp.: Biosynthesis and Regulation.” Annu Rev Phytopathol 44 (2006): 417–445.
7. Dar, D., L. S. Thomashow, D. M. Weller, and D. K. Newman. “Global Landscape of Phenazine Biosynthesis and Biodegradation Reveals Species-Specific Colonization Patterns in Agricultural Soils and Crop Microbiomes.” eLife 9 (2020): e59726.
8. Glasser, N. R., S. H. Saunders, and D. K. Newman. “The Colorful World of Extracellular Electron Shuttles.” Annu Rev Microbiol 71 (2017): 731–751.
9. Wang, Y., and D. K. Newman. “Redox Reactions of Phenazine Antibiotics with Ferric (Hydr)oxides and Molecular Oxygen.” Environ Sci Technol 42 (2008): 2380–2386.
10. Higgins, S., S. Heeb, G. Rampioni, M. P. Fletcher, P. Williams, and M. Cámara. “Differential Regulation of the Phenazine Biosynthetic Operons by Quorum Sensing in *Pseudomonas aeruginosa* PAO1-N.” Front Cell Infect Microbiol 8 (2018): 252.
11. Baron, S. S., and J. J. Rowe. “Antibiotic Action of Pyocyanin.” Antimicrob Agents Chemother 20 (1981): 814–820.
12. Baron, S. S., G. Terranova, and J. J. Rowe. “Molecular Mechanism of the Antimicrobial Action of Pyocyanin.” Curr Microbiol 18 (1989): 223–230.
13. Dietrich, L. E. P., A. Price-Whelan, A. Petersen, M. Whiteley, and D. K. Newman. “The Phenazine Pyocyanin Is a Terminal Signalling Factor in the

Quorum Sensing Network of *Pseudomonas aeruginosa*." Mol Microbiol 61 (2006): 1308–1321.

14. Dietrich, L. E. P., C. Okegbe, A. Price-Whelan, H. Sakhtah, R. C. Hunter, and D. K. Newman. "Bacterial Community Morphogenesis Is Intimately Linked to the Intracellular Redox State." J Bacteriol 195 (2013): 1371–1380.
15. Costa, K. C., N. R. Glasser, S. J. Conway, and D. K. Newman. "Pyocyanin Degradation by a Tautomerizing Demethylase Inhibits *Pseudomonas aeruginosa* Biofilms." Science 355 (2017): 170–173.
16. Denning, G. M., M. A. Railsback, G. T. Rasmussen, C. D. Cox, and B. E. Britigan. "*Pseudomonas* Pyocyanine Alters Calcium Signaling in Human Airway Epithelial Cells." Am J Physiol Lung Cell Mol Physiol 274 (1998): L893–L900.
17. Denning, G. M., L. A. Wollenweber, M. A. Railsback, C. D. Cox, L. L. Stoll, and B. E. Britigan. "*Pseudomonas* Pyocyanin Increases Interleukin-8 Expression by Human Airway Epithelial Cells." Infect Immun 66 (1998): 5777–5784.
18. Kamath, J. M., B. E. Britigan, C. D. Cox, and D. M. Shasby. "Pyocyanin from *Pseudomonas aeruginosa* Inhibits Prostacyclin Release from Endothelial Cells." Infect Immun 63 (1995): 4921–4923.
19. Denning, G. M., S. S. Iyer, K. J. Reszka, Y. O'Malley, G. T. Rasmussen, and B. E. Britigan. "Phenazine-1-Carboxylic Acid, a Secondary Metabolite of *Pseudomonas aeruginosa*, Alters Expression of Immunomodulatory Proteins by Human Airway Epithelial Cells." Am J Physiol Lung Cell Mol Physiol 285 (2003): L584–L592.

20. Britigan, B. E., M. A. Railsback, and C. D. Cox. “The *Pseudomonas aeruginosa* Secretory Product Pyocyanin Inactivates α1 Protease Inhibitor: Implications for the Pathogenesis of Cystic Fibrosis Lung Disease.” Infect Immun 67 (1999): 1207–1212.

21. O’Malley, Y. Q., K. J. Reszka, G. T. Rasmussen, M. Y. Abdalla, G. M. Denning, and B. E. Britigan. “The *Pseudomonas* Secretory Product Pyocyanin Inhibits Catalase Activity in Human Lung Epithelial Cells.” Am J Physiol Lung Cell Mol Physiol 285 (2003): L1077–L1086.

22. O’Malley, Y. Q., K. J. Reszka, D. R. Spitz, G. M. Denning, and B. E. Britigan. “*Pseudomonas aeruginosa* Pyocyanin Directly Oxidizes Glutathione and Decreases Its Levels in Airway Epithelial Cells.” Am J Physiol Lung Cell Mol Physiol 287 (2004): L94–L103.

23. Usher, L. R., R. A. Lawson, I. Geary, C. J. Taylor, C. D. Bingle, G. W. Taylor, and M. K. B. Whyte. “Induction of Neutrophil Apoptosis by the *Pseudomonas aeruginosa* Exotoxin Pyocyanin: A Potential Mechanism of Persistent Infection.” J Immunol 168 (2002): 1861–1868.

24. Muller, M. “Pyocyanin Induces Oxidative Stress in Human Endothelial Cells and Modulates the Glutathione Redox Cycle.” Free Radic Biol Med 33 (2002): 1527–1533.

25. Kanthakumar, K., G. W. Taylor, D. R. Cundell, R. B. Dowling, M. Johnson, P. J. Cole, and R. Wilson. “The Effect of Bacterial Toxins on Levels of Intracellular Adenosine Nucleotides and Human Ciliary Beat Frequency.” Pulm Pharmacol 9 (1996): 223–230.

26. Mavrodi, D. V., O. V. Mavrodi, J. A. Parejko, R. F. Bonsall, Y.-S. Kwak, T. C. Paulitz, L. S. Thomashow, and D. M. Weller. “Accumulation of the Antibiotic Phenazine-1-Carboxylic Acid in the Rhizosphere of Dryland Cereals.” Appl Environ Microbiol 78 (2012): 804–812.

27. Ownley, B. H., B. K. Duffy, and D. M. Weller. “Identification and Manipulation of Soil Properties to Improve the Biological Control Performance of Phenazine-Producing *Pseudomonas fluorescens*.” Appl Environ Microbiol 69 (2003): 3333–3343.

28. Meirelles, L. A., and D. K. Newman. “Both Toxic and Beneficial Effects of Pyocyanin Contribute to the Lifecycle of *Pseudomonas aeruginosa*.” Mol Microbiol 110 (2018): 995–1010.

29. Liu, J., Y. Zhao, Z. Q. Fu, and F. Liu. “Monooxygenase LaPhzX Is Involved in Self-Resistance Mechanisms during the Biosynthesis of N-Oxide Phenazine Myxin.” J Agric Food Chem 69 (2021): 13524–13532.

30. Xu, Y., A. Willems, C. Au-Yeung, K. Tahlan, and J. R. Nodwell. “A Two-Step Mechanism for the Activation of Actinorhodin Export and Resistance in Streptomyces coelicolor.” mBio 3 (2012): e00191-12.

31. Sakhtah, H., L. Koyama, Y. Zhang, D. K. Morales, B. L. Fields, A. Price-Whelan, D. A. Hogan, K. Shepard, and L. E. P. Dietrich. “The *Pseudomonas aeruginosa* Efflux Pump MexGHI-OpmD Transports a Natural Phenazine That Controls Gene Expression and Biofilm Development.” Proc Natl Acad Sci USA 113 (2016).

32. Tahlan, K., S. K. Ahn, A. Sing, T. D. Bodnaruk, A. R. Willems, A. R. Davidson, and J. R. Nodwell. “Initiation of Actinorhodin Export in *Streptomyces coelicolor*.” Mol Microbiol 63 (2007): 951–961.

33. Sporer, A. J., C. Beierschmitt, A. Bendebury, K. E. Zink, A. Price-Whelan, M. C. Buzzeo, L. M. Sanchez, and L. E. P. Dietrich. “*Pseudomonas aeruginosa* PumA Acts on an Endogenous Phenazine to Promote Self-Resistance.” Microbiology 164 (2018): 790–800.

34. Zhao, Y., J. Liu, T. Jiang, R. Hou, G. Xu, H. Xu, and F. Liu. “Resistance-Nodulation-Division Efflux Pump, LexABC, Contributes to Self-Resistance of the Phenazine Di-N-Oxide Natural Product Myxin in *Lysobacter antibioticus*.” Front Microbiol 12 (2021): 618513.

35. Cox, C. D. “Role of Pyocyanin in the Acquisition of Iron from Transferrin.” Infect Immun 52 (1986): 263–270.

36. Hernandez, M. E., A. Kappler, and D. K. Newman. “Phenazines and Other Redox-Active Antibiotics Promote Microbial Mineral Reduction.” Appl Environ Microbiol 70 (2004): 921–928.

37. Wang, Y., J. C. Wilks, T. Danhorn, I. Ramos, L. Croal, and D. K. Newman. “Phenazine-1-Carboxylic Acid Promotes Bacterial Biofilm Development via Ferrous Iron Acquisition.” J Bacteriol 193 (2011): 3606–3617.

38. McRose, D. L., and D. K. Newman. “Redox-Active Antibiotics Enhance Phosphorus Bioavailability.” Science 371 (2021): 1033–1037.

39. Price-Whelan, A., L. E. P. Dietrich, and D. K. Newman. “Pyocyanin Alters Redox Homeostasis and Carbon Flux through Central Metabolic Pathways in *Pseudomonas aeruginosa* PA14.” J Bacteriol 189 (2007): 6372–6381.

40. Wang, Y., S. E. Kern, and D. K. Newman. “Endogenous Phenazine Antibiotics Promote Anaerobic Survival of *Pseudomonas aeruginosa* via Extracellular Electron Transfer.” J Bacteriol 192 (2010): 365–369.

41. Glasser, N. R., S. E. Kern, and D. K. Newman. “Phenazine Redox Cycling Enhances Anaerobic Survival in *Pseudomonas aeruginosa* by Facilitating Generation of ATP and a Proton-Motive Force.” Mol Microbiol 92 (2014): 399–412.

42. Bellin, D. L., H. Sakhtah, Y. Zhang, A. Price-Whelan, L. E. P. Dietrich, and K. L. Shepard. “Electrochemical Camera Chip for Simultaneous Imaging of Multiple Metabolites in Biofilms.” Nat Commun 7 (2016): 10535.

43. Saunders, S. H., E. C. M. Tse, M. D. Yates, F. J. Otero, S. A. Trammell, E. D. A. Stemp, J. K. Barton, L. M. Tender, and D. K. Newman. “Extracellular DNA Promotes Efficient Extracellular Electron Transfer by Pyocyanin in *Pseudomonas aeruginosa* Biofilms.” Cell 182 (2020): 919–932.e19.

44. Merchant, S. S., and J. D. Helmann. “Elemental Economy.” Advances in Microbial Physiology (Elsevier, 2012): 91–210.

45. Flemming, H.-C., and S. Wuertz. “Bacteria and Archaea on Earth and Their Abundance in Biofilms.” Nat Rev Microbiol 17 (2019): 247–260.

46. Bar-Even, A., E. Noor, A. Flamholz, J. M. Buescher, and R. Milo. "Hydrophobicity and Charge Shape Cellular Metabolite Concentrations." PLoS Comput Biol 7 (2011): e1002166.

47. Heine, D., S. Sundaram, M. Beudert, K. Martin, and C. Hertweck. "A Widespread Bacterial Phenazine Forms S-Conjugates with Biogenic Thiols and Crosslinks Proteins." Chem Sci 7 (2016): 4848–4855.

48. Glasser, N. R., B. X. Wang, J. A. Hoy, and D. K. Newman. "The Pyruvate and α-Ketoglutarate Dehydrogenase Complexes of *Pseudomonas aeruginosa* Catalyze Pyocyanin and Phenazine-1-Carboxylic Acid Reduction." J Biol Chem 292 (2017): 5593–5607.

49. Tsypin, L. M., and D. K. Newman. "Nitrate Reduction Stimulates and Is Stimulated by Phenazine-1-Carboxylic Acid Oxidation by *Citrobacter portucalensis* MBL." mBio 12 (2021): e02265-21.

50. Chukwubuikem, A., C. Berger, A. Mady, and M. A. Rosenbaum. "Role of Phenazine-Enzyme Physiology for Current Generation in a Bioelectrochemical System." Microb Biotechnol 14 (2021): 1613–1626.

51. Jo, J., K. L. Cortez, W. C. Cornell, A. Price-Whelan, and L. E. Dietrich. "An Orphan cbb3-Type Cytochrome Oxidase Subunit Supports *Pseudomonas aeruginosa* Biofilm Growth and Virulence." eLife 6 (2017): e30205.

52. Jo, J., A. Price-Whelan, W. C. Cornell, and L. E. P. Dietrich. "Interdependency of Respiratory Metabolism and Phenazine-Associated Physiology in *Pseudomonas aeruginosa* PA14." J Bacteriol (2020): 202.

53. Schiessl, K. T., F. Hu, J. Jo, S. Z. Nazia, B. Wang, A. Price-Whelan, W. Min, and L. E. P. Dietrich. “Phenazine Production Promotes Antibiotic Tolerance and Metabolic Heterogeneity in *Pseudomonas aeruginosa* Biofilms.” Nat Commun 10 (2019): 762.

54. Lin, Y.-C., M. D. Sekedat, W. C. Cornell, G. M. Silva, C. Okegbe, A. Price-Whelan, C. Vogel, and L. E. P. Dietrich. “Phenazines Regulate nap-Dependent Denitrification in *Pseudomonas aeruginosa* Biofilms.” J Bacteriol 200 (2018).

55. Lawrence, J. R., G. M. Wolfaardt, and D. R. Korber. “Determination of Diffusion Coefficients in Biofilms by Confocal Laser Microscopy.” Appl Environ Microbiol 60 (1994): 1166–1173.

56. Yu, Y.-Y., Y. Zhang, and L. Peng. “Investigating the Interaction between *Shewanella oneidensis* and Phenazine 1-Carboxylic Acid in the Microbial Electrochemical Processes.” Sci Total Environ 838 (2022): 156501.

57. Hunter, R. C., and T. J. Beveridge. “Application of a pH-Sensitive Fluoroprobe (C-SNARF-4) for pH Microenvironment Analysis in *Pseudomonas aeruginosa* Biofilms.” Appl Environ Microbiol 71 (2005): 2501–2510.

58. Okamoto, A., K. Hashimoto, K. H. Nealson, and R. Nakamura. “Rate Enhancement of Bacterial Extracellular Electron Transport Involves Bound Flavin Semiquinones.” Proc Natl Acad Sci USA 110 (2013): 7856–7861.

59. Das, T., S. K. Kutty, R. Tavallaie, A. I. Ibugo, J. Panchompoo, S. Sehar, L. Aldous, A. W. S. Yeung, S. R. Thomas, N. Kumar, et al. “Phenazine Virulence Factor Binding to Extracellular DNA Is Important for *Pseudomonas aeruginosa* Biofilm Formation.” Sci Rep 5 (2015): 8398.

60. Karagulyan, M., M.-O. Goebel, D. Diehl, A. A. Abu Quba, M. Kästner, J. Bachmann, L. Y. Wick, G. E. Schaumann, and A. Miltner. “Water Stress-Driven Changes in Bacterial Cell Surface Properties.” Appl Environ Microbiol 88 (2022): e00732-22.
61. Singh, A. K., J.-H. Shin, K.-L. Lee, J. A. Imlay, and J.-H. Roe. “Comparative Study of SoxR Activation by Redox-Active Compounds.” Mol Microbiol 90 (2013): 983–996.
62. Schwarzenbach, R. P., P. M. Gschwend, and D. M. Imboden. Environmental Organic Chemistry. Wiley, 2003.
63. Turner, A. “Salting Out of Chemicals in Estuaries: Implications for Contaminant Partitioning and Modelling.” Sci Total Environ 314–316 (2003): 599–612.
64. Hirakawa, H., A. Takita, M. Uchida, Y. Kaneko, Y. Kakishima, K. Tanimoto, W. Kamitani, and H. Tomita. “Adsorption of Phenazines Produced by *Pseudomonas aeruginosa* Using AST-120 Decreases Pyocyanin-Associated Cytotoxicity.” Antibiotics 10 (2021): 434.
65. Stone, J. A., and D. Vukomanovic. “Electrospray and Collisionally Activated Dissociation Study of the Association of Pyocyanin with Alkali Metal Cations and Doubly Charged Alkaline Earth and Zinc Cations.” Int J Mass Spectrom 210–211 (2001): 341–359.
66. Morrison, M. M., and D. T. Sawyer. “Flavin Model Systems. 2. Pyocyanine Complexes of Divalent Manganese, Iron, Nickel, Copper, and Zinc in Dimethyl Sulfoxide.” J Am Chem Soc 100 (1978): 211–213.

67. Arnott, J. A., and S. L. Planey. “The Influence of Lipophilicity in Drug Discovery and Design.” Expert Opin Drug Discov 7 (2012): 863–875.

68. Beifuss, U., M. Tietze, S. Bäumer, and U. Deppenmeier. “Methanophenazine: Structure, Total Synthesis, and Function of a New Cofactor from Methanogenic Archaea.” Angew Chem Int Ed 39 (2000): 2470–2472.

69. Bellin, D. L., H. Sakhtah, J. K. Rosenstein, P. M. Levine, J. Thimot, K. Emmett, L. E. P. Dietrich, and K. L. Shepard. “Integrated Circuit-Based Electrochemical Sensor for Spatially Resolved Detection of Redox-Active Metabolites in Biofilms.” Nat Commun 5 (2014): 3256.

70. Joe-Wong, C., E. Shoenfelt, E. J. Hauser, N. Crompton, and S. C. B. Myneni. “Estimation of Reactive Thiol Concentrations in Dissolved Organic Matter and Bacterial Cell Membranes in Aquatic Systems.” Environ Sci Technol 46 (2012): 9854–9861.

71. Zhalnina, K., K. B. Louie, Z. Hao, N. Mansoori, U. N. da Rocha, S. Shi, H. Cho, U. Karaoz, D. Loqué, B. P. Bowen, et al. “Dynamic Root Exudate Chemistry and Microbial Substrate Preferences Drive Patterns in Rhizosphere Microbial Community Assembly.” Nat Microbiol 3 (2018): 470–480.

72. Schwab, A. P., A. A. Al-Assi, and M. K. Banks. “Adsorption of Naphthalene onto Plant Roots.” J Environ Qual 27 (1998): 220–224.

73. Terzaghi, E., G. Raspa, E. Zanardini, C. Morosini, S. Anelli, S. Armiraglio, and A. Di Guardo. “Life Cycle Exposure of Plants Considerably Affects Root Uptake of PCBs.” J Hazard Mater 421 (2022): 126826.

74. DePas, W. H., R. Starwalt-Lee, L. Van Sambeek, S. Ravindra Kumar, V. Gradinaru, and D. K. Newman. “Exposing the Three-Dimensional Biogeography and Metabolic States of Pathogens in Cystic Fibrosis Sputum.” mBio 7 (2016): e00796-16.

75. Schultz, B. M., O. A. Acevedo, A. M. Kalergis, and S. M. Bueno. “Role of Extracellular Trap Release during Bacterial and Viral Infection.” Front Microbiol 13 (2022): 798853.

76. Yim, G., H. H. Wang, and F. R. S. J. Davies. “Antibiotics as Signalling Molecules.” Philos Trans R Soc B Biol Sci 362 (2007): 1195–1200.

77. Yim, G., F. de la Cruz, G. B. Spiegelman, and J. Davies. “Transcription Modulation of *Salmonella enterica Serovar Typhimurium* Promoters by Sub-MIC Levels of Rifampin.” J Bacteriol 188 (2006): 7988–7991.

78. Goh, E.-B., G. Yim, W. Tsui, J. McClure, M. G. Surette, and J. Davies. “Transcriptional Modulation of Bacterial Gene Expression by Subinhibitory Concentrations of Antibiotics.” Proc Natl Acad Sci USA 99 (2002): 17025–17030.

79. McPhee, J. B., S. Lewenza, and R. E. W. Hancock. “Cationic Antimicrobial Peptides Activate a Two-Component Regulatory System in *Pseudomonas aeruginosa*.” Mol Microbiol 50 (2003): 205–217.

80. Mak, S., and J. R. Nodwell. “Actinorhodin Is a Redox-Active Antibiotic with a Complex Mode of Action against Gram-Positive Cells.” Mol Microbiol 106 (2017): 597–613.

81. Ueda, K., S. Kawai, H.-O. Ogawa, A. Kiyama, T. Kubota, H. Kawanobe, and T. Beppu. “Wide Distribution of Interspecific Stimulatory Events on Antibiotic Production among *Streptomyces* Species.” J Antibiot 53 (2000): 979–982.

82. Tsui, W. H. W., G. Yim, H. H. Wang, J. E. McClure, M. G. Surette, and J. Davies. “Dual Effects of MLS Antibiotics.” Chem Biol 11 (2004): 1307–1316.

83. Maddula, V. S. R. K., E. A. Pierson, and L. S. Pierson. “Altering the Ratio of Phenazines in *Pseudomonas chlororaphis* Strain 30-84.” J Bacteriol 190 (2008): 2759–2766.

84. Friedheim, E. A. H. “Pyocyanine, an Accessory Respiratory Enzyme.” J Exp Med 54 (1931): 207–221.

85. Martín, J. F. “Control of Antibiotic Synthesis by Phosphate.” In Advances in Biochemical Engineering, vol. 6, Springer, 1977: 105–127.

86. Nguyen, C. Q., Thrift, W. J., Bhattacharjee, A., Ranjbar, S., Gallagher, T., Darvishzadeh-Varcheie, M., Sanderson, R. N., Capolino, F., Whiteson, K., Baldi, P., Hochbaum, A. I., & Ragan, R. (2018). Longitudinal Monitoring of Biofilm Formation via Robust Surface-Enhanced Raman Scattering Quantification of *Pseudomonas aeruginosa*-Produced Metabolites. ACS Applied Materials & Interfaces, 10(15), 12364–12373. https://doi.org/10.1021/acsami.7b18592

Chapter 2

REDOX-DEPENDENT LIPOPHILICITY OF PHENAZINE METABOLITES IS MODULATED BY INTRAMOLECULAR HYDROGEN BONDS AND CONTROLS THEIR BIOLOGICAL DISTRIBUTION

This chapter has been submitted to bioRxiv and is under review for publication.
Korbinian Thalhammer designed the project, carried out the physical experiments, and drafted the manuscript. Matthew Scurria, Prof. Osvaldo Gutierrez, and Prof. Stuart Conway conducted the physical chemical modeling and provided interpretation. Jinyang Li assisted with electrochemical techniques and calculations. Inês Trindade led the membrane separation. Prof. Dianne Newman secured funding, provided guidance, and assisted with the biochemical measurements. All authors contributed to the editing of the manuscript.

Abstract

Phenazines are redox-active microbial metabolites produced and secreted in diverse ecological contexts from soils to chronic infections. In these disparate environments phenazines can function variously as antibiotics, extracellular electron shuttles, and nutrient scavengers. Key to understanding the impact of these functions is a robust expectation of phenazine retention or diffusion in a given context. But predicting phenazine fate and transport is difficult because of the chemical complexity of their local microenvironments. To address this challenge, we measured the octanol water distribution coefficient (LogD) as a proxy for lipophilicity of three naturally occurring phenazines produced by the opportunistic pathogen *Pseudomonas aeruginosa*: phenazine-1-carboxylic acid, phenazine-1-carboxamide, and pyocyanin. We investigated the behavior of both oxidized and reduced

forms of these phenazines across broad ionic strength and pH conditions. While the ionic context exerts only small effects, the pH and redox state contribute strongly and independently to changes in phenazine lipophilicity. The pH trends are expected, but the observed redox dependence is generally missed by existing lipophilicity calculation methods. Additional LogD measurements with 1-hydroxyphenazine and unsubstituted phenazine, together with density functional theory modeling of phenazines in their reduced and oxidized forms, reveal that intramolecular hydrogen bonding contributes significantly to the increased lipophilicity of reduced phenazines that possess H-bond accepting substituents in the 1-position. These results explain phenazine behavior in a biological context: redox state alone significantly alters retention of pyocyanin in planktonic *P. aeruginosa* cells, with the reduced species being predominantly retained by membranes. We propose that the modulation of phenazine lipophilicity in response to the local redox environment has evolved to give a competitive advantage to bacteria by retaining or dispersing these bioactive molecules. Beyond improving our understanding of natural phenazine fate in diverse microbial contexts, our results emphasize an oft-overlooked theme relevant to rational drug and electrochemical shuttle design: redox state matters.

Introduction

Pseudomonas aeruginosa is a common opportunistic human pathogen that colonizes a wide range of habitats and is known to establish both acute and chronic infections in hospitalized and immunodeficient patients. This bacterium exhibits a high level of metabolic flexibility that enables it to exist in the broad range of environments in which it is found (1). For *P.*

aeruginosa and other microbes, secretion of primary and secondary metabolites can confer a competitive advantage through multiple mechanisms including redox balancing (2) and competitor inhibition (3). Metabolite secretion is controlled by a variety of systems, including ATP-driven transport systems, antiporters, symporters, uniporters, and passive diffusion (4). While the selectivity of enzymatic transport systems depends on structural recognition of the metabolite, passive diffusion across the membrane is governed primarily by the metabolite's physicochemical properties, especially its lipophilicity.

Here we examine the lipophilicity of phenazine metabolites, an important class of secreted, redox-active secondary metabolites produced by *P. aeruginosa* as well as many other bacterial species found in natural soils and waters around the world (5). Phenazines are known to play critical roles in nutrient scavenging, virulence, competitor inhibition, and signaling (6). These functions rely on reversible redox transformations that can be triggered by producer cells, host tissue, competing microbes, and abiotic phases like oxygen and iron oxide minerals (7, 8). Despite this, almost nothing is known about the mechanisms by which phenazine concentrations are spatially controlled, and whether the local redox environment affects compound distribution (9).

In chemically complex environments, lipophilicity is a useful simplifying parameter for understanding and predicting compound distribution. In practice, scientists in disciplines including environmental science and medicinal chemistry lean heavily on the octanol-water partition coefficient (LogP) or the pH-specific distribution coefficient ($LogD_{pH}$) as useful proxies for compound lipophilicity (**Equation 1**). LogP and LogD correlate strongly with

affinity for biological phases, including cell membranes and soil organic matter, which are typically more lipophilic than water (10, 11). As a result, LogP is a useful predictor for the bioaccumulation of anthropogenic toxins such as DDT (12). By the same token, LogP and LogD feature prominently in drug design because of the correlation between the lipophilicity of a drug, its target promiscuity, and our *in vivo* absorption and retention of the molecule (13, 14). While these values can be measured using the shake flask method or chromatography, they are frequently predicted using a range of different algorithms that report calculated LogP or LogD (cLogP or cLogD) (14). Both measurement and prediction of LogP/LogD tend to neglect changes in molecular redox state that are common in biological settings and are relevant to understanding the behavior of redox active metabolites.

$$LogD_x = log_{10}\left(\sum_{i}^{n} f^i {P^i}_{\frac{oct}{water}}\right)$$

Equation 1. The distribution coefficient, $LogD_x$, accounts for the partitioning of all ionization forms of a solute between the octanol and the water phase at pH x. The total number of ionization states is given by n. f^i is the mole fraction of each form of the molecule (controlled by the pKa of the solute and the solution pH) and P^i is the partition coefficient for that form. For solutes that do not ionize, $LogD_x$ collapses to the familiar partition coefficient LogP, which is simply the ratio of the concentrations of solute in octanol and in water.

To explore the redox sensitivity of phenazine lipophilicity, as a case study through which to elucidate general principles, we examined the three main phenazines produced by *P.*

aeruginosa. Like most phenazines, these compounds -- phenazine-1-carboxylic acid (PCA), phenazine-1-carboxamide (PCN), and pyocyanin (PYO) -- undergo reversible, coupled $2e^-$, $2H^+$ redox transformations under physiological conditions (**Scheme 1**). We systematically subjected oxidized and reduced samples of these three phenazines to environmentally relevant pH and ionic strength conditions and measured their octanol/water distribution coefficients. Our results depended heavily on redox state and deviated substantially from predictions made by four leading cLogP prediction algorithms.

To expand our understanding beyond the subset of *P. aeruginosa* phenazines, we conducted additional experiments with phenazine and 1-hydroxyphenazine and performed density functional theory analysis on the compounds studied. We show that lipophilicity, and therefore the expected biological distribution of some phenazines, is modulated in a redox-dependent manner. We suggest this might be a hitherto unappreciated and more broadly applicable mechanism by which the spatial distribution of bioactive molecules is controlled by certain bacteria. These findings have important ramifications for the prediction of redox-active compound lipophilicity, demonstrating that it is essential that the cLogP or cLogD of the compound is calculated not only at the appropriate pH, but also in the relevant redox state. Even then, care must be taken to ensure the chosen algorithm captures the effects of redox-mediated intramolecular hydrogen bonds. Taken together, our results suggest that redox state exerts a fundamental control on lipophilicity for natural and artificial phenazines, and likely for other similar redox-active molecules, a fact that is both underappreciated experimentally and not accounted for *in silico.*

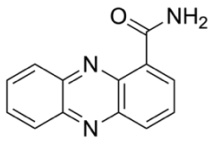

Phenazine-1-carboxamide (PCN)
oxidized

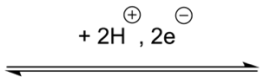

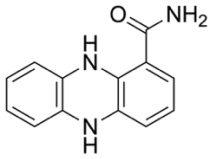

Phenazine-1-carboxamide (PCN)
reduced

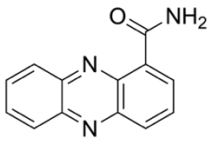

strongest acidic
pKa: 14.2

strongest basic
pKa: 1.3

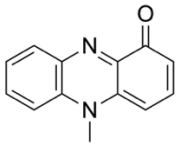

Pyocyanin (PYO)
oxidized

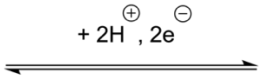

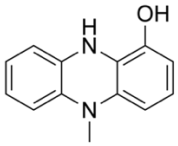

Pyocyanin (PYO)
reduced

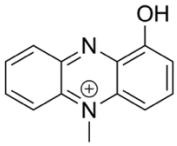

pKa: 4.9

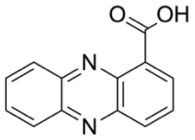

Phenazine-1-carboxylic acid (PCA)
oxidized

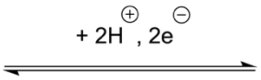

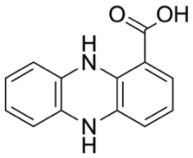

Phenazine-1-carboxylic acid (PCA)
reduced

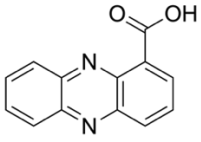

pKa: 4.2

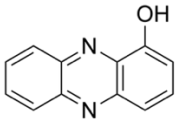

1-Hydroxyphenazine
oxidized

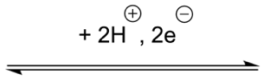

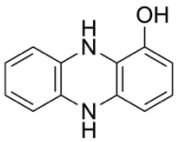

1-Hydroxyphenazine
reduced

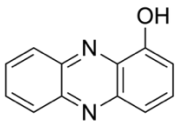

pKa: 8.3

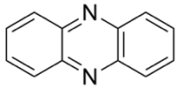

Phenazine
oxidized

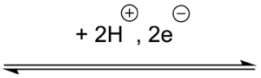

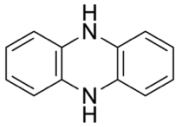

Phenazine
reduced

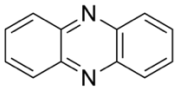

pKa: 2.7

Scheme 1. The redox equilibria and pKa values of phenazine-1 carboxamide (PCN), pyocyanin (PYO), phenazine-1 carboxylic acid (PCA), 1-hydroxyphenazine, and phenazine (15-19). All potentials are relative to the Standard Hydrogen Electrode (8). PCN is not predicted to change ionization state within the physiological pH range (3-10) explored in this study (15). Experiments with 1-hydroxyphenazine and phenazine were only conducted at pH 7.2

Results and Discussion

Existing algorithms fail to predict redox dependence of phenazine lipophilicity

Experimental determination of LogP values is more time and resource intensive than calculation of cLogP values, so we began our study by comparing our initial experimental measurements with cLogP values from four leading prediction algorithms: miLogP, iLOGP, KOWWIN, and XLOGP3 (20-28) (see **Appendix A** for additional algorithm details). Because the algorithms are primarily trained on neutral compounds, we limited our comparison to neutral forms of oxidized and reduced PCA, PCN, PYO, and 1-OH phenazine. But despite the relative simplicity of these phenazine structures, no individual algorithm accurately predicted the redox sensitivity of their lipophilicities (**Figure 1**). The fragment-based miLogP algorithm, developed using a test set of more than 12,000 mostly drug-like molecules, predicts essentially no offset between oxidized and reduced phenazines. The iLOGP algorithm, which considers a whole molecule's solvation energy in water and in octanol, does predict offsets between oxidized and reduced phenazines. But it generally predicts the oxidized form of a phenazine to be more lipophilic, which is the opposite of the experimental trend. The most accurate algorithm, KOWWIN from the US Environmental

Protection Agency, is based on atomic and molecular fragment contributions adjusted with empirical correction factors to account for more complex behavior like hydrogen bonding. The KOWWIN algorithm accurately predicts the enhanced lipophilicity of the reduced forms of PCN, PCA, and PYO, but it exaggerates the effect for PCN and predicts the wrong directionality for 1-OH phenazine, predicting that 1-OH phenazine is more lipophilic when reduced (the opposite is observed experimentally). The atom-based XLogP3 algorithm makes a similar error with 1-OH phenazine and predicts an unobserved redox-sensitive offset for phenazine, suggesting that while these two algorithms accurately capture some aspects of phenazine behavior, they are still missing some subtleties of phenazine redox chemistry. The algorithms all dramatically overestimate the lipophilicity of PYO in both redox forms. Given that these algorithms fail to predict experimental lipophilicities for neutral phenazines, and the fact that several *P. aeruginosa* phenazines are charged under physiological conditions, we continued our investigation by systematically measuring reduced and oxidized phenazine LogD values for PCN, PCA, and PYO across biologically relevant pH and ionic strength conditions.

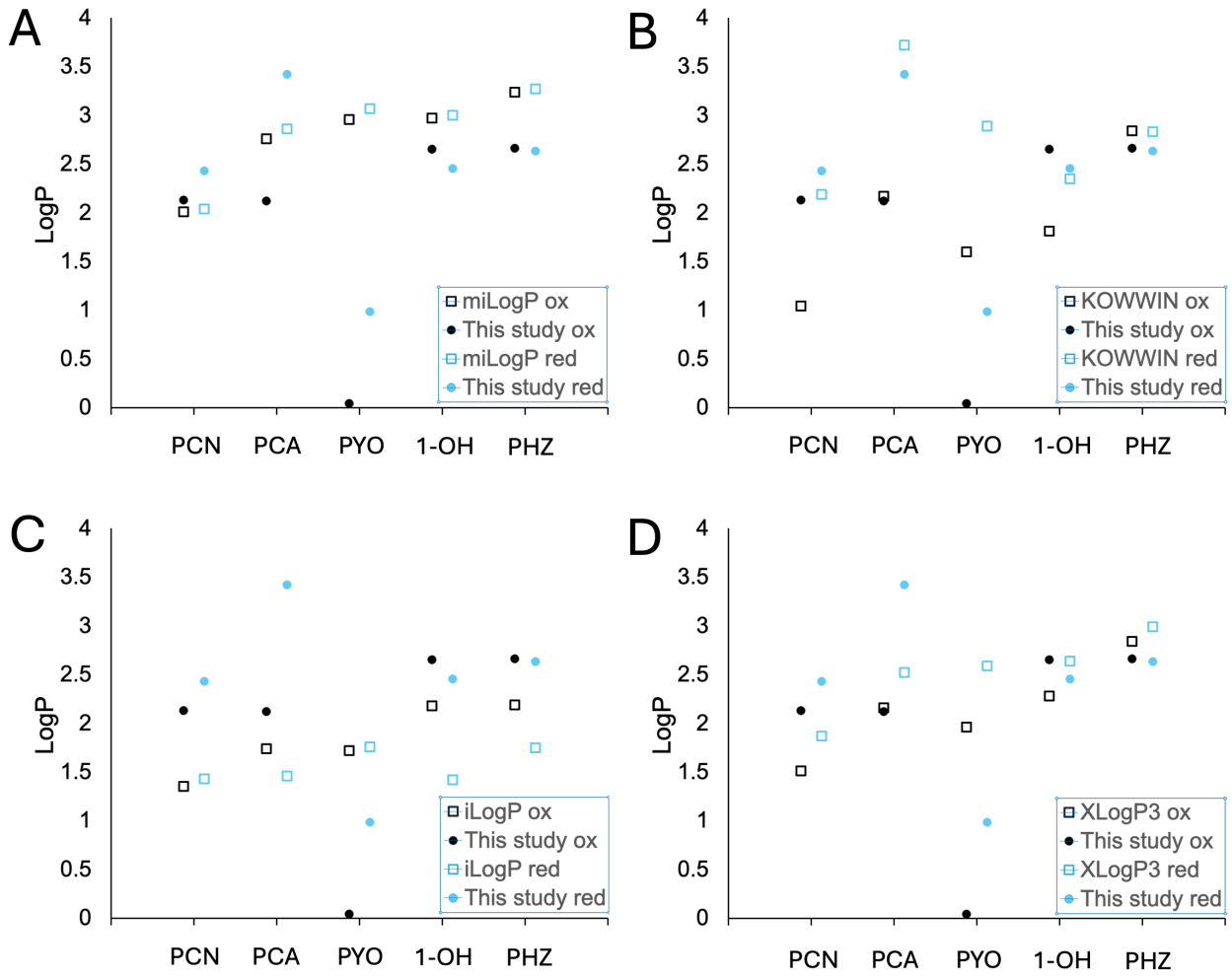

Figure 1: **Existing cLogP prediction algorithms fail to capture redox-dependent lipophilicity changes.** In all panels, closed circles denote experimental values from this study, while open squares indicate cLogP predictions (see **Appendix A** for additional algorithm and measurement details). In all cases, black symbols are for the oxidized phenazine while blue symbols are for the reduced phenazine. A) miLogP predictions. B) KOWWIN predictions C) iLogP predictions. D) XLogP3 predictions. All measurements and predictions are for neutral

forms of the molecules, meaning experiments were conducted at pH 7.2 except in the case of PCA (pH 3).

Phenazine lipophilicity is sensitive to both functionalization and redox state

Across the pH range 3 to 10, reduced PCN maintains a slightly elevated lipophilicity relative to the oxidized form (**Figure 2A**). The difference is most pronounced at high pH. But in a given redox form, PCN exhibits only small variations in LogD between low and high pH, consistent with its predicted pKa values of 14.2 (strongest acidic) and 1.3 (strongest basic), which suggest it exists solely in its neutral form across the measured pH range (15). In contrast, PCA contains a carboxylic acid with a pKa of 4.24 (17). Above this pKa, the majority of the molecules present will be ionized, while below the pKa, we expect the protonated, neutral carboxylic acid form to dominate, permitting greater solubility in the octanol phase and increasing measured lipophilicity. As expected, at low pH, PCA is significantly more lipophilic than at neutral or high pH, regardless of redox state. But in all cases, reduced PCA is more lipophilic than oxidized PCA by about an order of magnitude (**Figure 2B**). Remarkably, according to our measurements, the reduced, neutral form is over 5 orders of magnitude more lipophilic than the oxidized, ionized form. This large range in measured values is supported by the qualitative observation that the neutral, reduced form is highly insoluble in water, while the ionized, oxidized form is highly soluble in water (29). At all pH values, reduced PYO is more lipophilic than oxidized PYO (**Figure 2C**). The difference in lipophilicities is most significant at low pH, where both forms of the molecule are expected to be charged. But a separation of an order of magnitude persists even at high pH, where both forms are neutral (16). The influence of ionic strength was also investigated

systematically, but as results conformed to expectations, the data is shown in the supplement (**Figure A18** and **Table A8** in **Appendix A**).

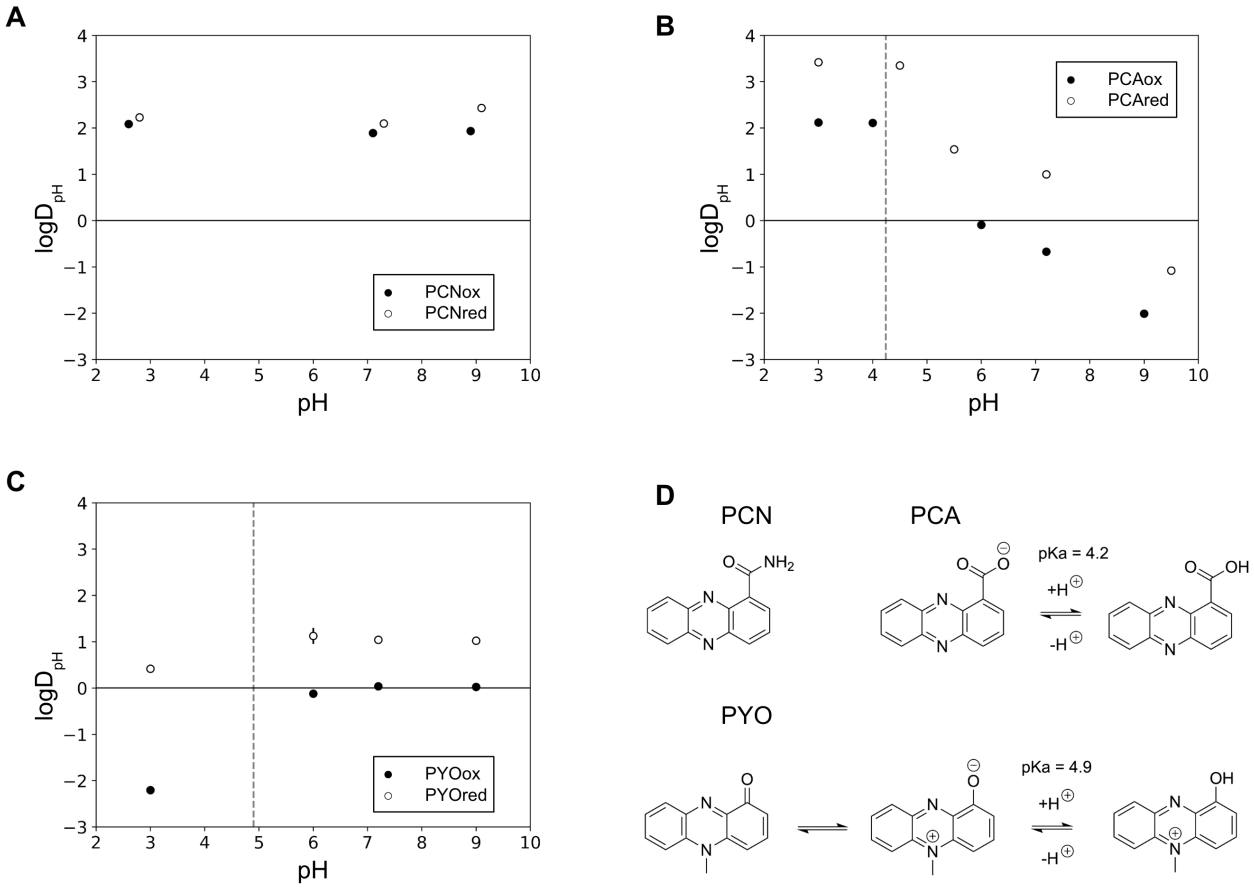

Figure 2. Phenazine lipophilicity is differentially sensitive to pH. Panels A, B, and C: measured $LogD_{pH}$ values for PCN, PCA, and PYO, respectively. Within each panel, open circles represent the reduced form of the phenazine, while closed circles represent the oxidized form. Dashed lines denote pKa values of the oxidized phenazines from the literature. When greater than the size of the marker, standard deviations are depicted as

vertical lines. Phenazines were equilibrated in 20 mM MOPS that was overwhelmed with small amounts of 100 mM HCl or NaOH to achieve the desired pH. Concentrations of phenazines in both the octanol and water phases were measured by HPLC (See **Appendix A** for additional details). Panel D: protonation states with previously measured pKa values (16, 17). PCN is not predicted to change ionization state within the physiological pH range (3-10) explored in this study (15). Measured values are available in the Supporting Information (**Tables A8** and **A9**).

Intramolecular hydrogen bonding contributes significantly to lipophilicity changes

Given the limited structural change between oxidized and reduced phenazines, we were interested in understanding the sometimes substantial redox state-dependent changes in compound lipophilicity. That redox state does not substantially affect the lipophilicity of unsubstituted phenazine (LogD = 2.66 oxidized, 2.63 reduced) led us to hypothesize that the 1-position substituents are likely responsible for the observed changes. The key difference between the oxidized and reduced form of phenazines is the addition of a hydrogen atom to the pyrazine nitrogen, converting it from a hydrogen bond acceptor to a hydrogen bond donor. This changes the ability of this moiety to interact with the substituent at the 1-position on the phenazine ring (30) To test this hypothesis, we probed phenazine-solvent interactions using density functional theory (see **Appendix A** for computational details). The strength of the *intra*molecular hydrogen bond was calculated for all structures, comparing the hydrogen bonded 'closed' form, *versus* the non-hydrogen bonded 'open' form conformation (**Figure A1** and **Table A1**). These were established based on the presence of a new intramolecular

hydrogen bond between the 1-position substituent and pyrazine nitrogen upon rotation of the substituent at the 1-position (31). Energies of solvation in octanol and in water were then calculated and used to predict the effects of intramolecular hydrogen bonding on the cLogD value of a given molecular form (**Figure A2**) (32-34). To compare lipophilicities across redox states, we performed natural bonding orbital (NBO) analysis of phenazines in their reduced and oxidized forms, analyzing for constructive orbital overlap, indicating favorable hydrogen bonding between the pyrazine nitrogen and 1-position substituent (Table A3) (35, 36). We reasoned that a larger energy contribution generated from the second order perturbation theory analysis would result in a stronger NBO interaction which would deter *inter*molecular hydrogen bonding with water, thus increasing overall lipophilicity.

We began by looking at PCA, which, at physiological pH, is negatively charged and can form a strong (14.9 kcal/mol, **Figure 3A**) six-membered hydrogen bonded ring with the carboxylate group in its reduced form, an interaction that is not possible in the oxidized form. We speculated that the formation of this hydrogen bond disperses some of the carboxylate negative charge, resulting in less effective solvation of the molecule by water and consequently an increased lipophilicity compared to the oxidized form. The same situation is observed in PYO: no hydrogen bond is present in the oxidized form, but in the reduced form a hydrogen bond (0.71 kcal/mol, **Figure 3B**) can form between the pyrazine NH and the 1-position hydroxyl group. Again, this results in the reduced pyocyanin being more lipophilic than the oxidized form, as the oxidized form can be more readily solvated by water in the absence of the intramolecular hydrogen bond.

Interestingly, 1-hydroxyphenazine exhibits the opposite change in lipophilicity between the redox states; here the oxidized form is more lipophilic than the reduced form. The hydrogen bonding situation here is more complex, as a 5-membered hydrogen bond can form in both redox states. In the oxidized form of 1-hydroxyphenazine the pyrazine nitrogen lone pair forms a stronger hydrogen bond (3.1 kcal/mol, **Figure 3C**) with the 1-position hydroxyl group. In the reduced form, the 1-position phenolic oxygen donates its lone pair to form a hydrogen bond with the hydrogen atom attached to the pyrazine nitrogen. This hydrogen bond is weaker (0.65 kcal/mol **Figure 3C**), presumably because the oxygen atom is a less effective lone pair donor compared to the nitrogen atom, due to its increased electronegativity, resulting in less electron donation into the antibonding orbital of the N-H bond (37). The weaker hydrogen bond in the reduced form enables more effective solvation by water, meaning that it is less lipophilic than the oxidized form.

When examining PCN, we noticed a more subtle difference in lipophilicity between redox states, which can be explained by analyzing the difference in strength of the intramolecular hydrogen bonds. Due to the structure of PCN, a hydrogen bond can again form in both the reduced and oxidized forms. In the reduced form, a hydrogen bond is predicted to form between the pyrazine NH and the amide carbonyl oxygen atom. In the oxidized form the nitrogen atom of the pyrazine ring donates its lone pair to form a hydrogen bond with one of the amide NH_2 hydrogen atoms. The strengths of these hydrogen bonds are predicted to be similar (**Figure 3D**), likely explaining the more similar lipophilicity between the two redox forms. The lower lipophilicity of the oxidized form is proposed to result from easier solvation

of the more electronegative carbonyl oxygen atom, which is more readily presented to the solvent in this form.

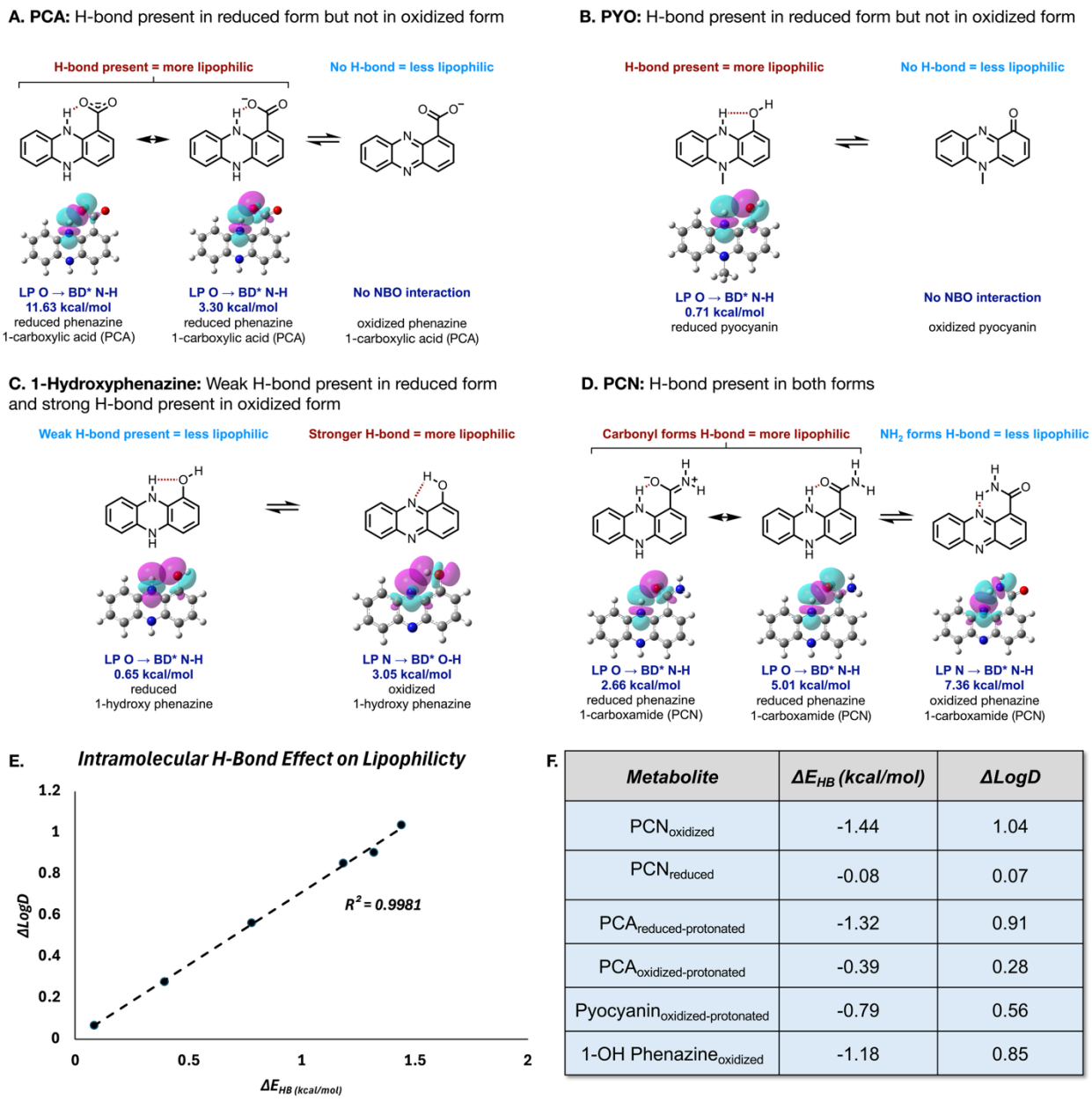

F.

Metabolite	*ΔE_{HB} (kcal/mol)*	*ΔLogD*
$PCN_{oxidized}$	-1.44	1.04
$PCN_{reduced}$	-0.08	0.07
$PCA_{reduced\text{-}protonated}$	-1.32	0.91
$PCA_{oxidized\text{-}protonated}$	-0.39	0.28
$Pyocyanin_{oxidized\text{-}protonated}$	-0.79	0.56
1-OH $Phenazine_{oxidized}$	-1.18	0.85

Figure 3: Intramolecular hydrogen bonding contributes significantly to lipophilicity changes. Natural Bonding Orbitals with their respective interaction energies generated by the

intramolecular hydrogen bond calculated at the uwb97xD/cc-pvDZ-cpcm(H_2O) level of theory for PCA (A), PYO (B), 1-hydroxyphenazine (C), and PCN (D). Predicted hydrogen bonds are indicated using dotted maroon lines. (E&F) Change in LogD values (ΔLogD) due to the formation of an intramolecular hydrogen bond plotted *vs* the change in intramolecular hydrogen bond strength (ΔE_{HB}) due to changes in solvent, calculated at the uwb97xD/6-311+g(d,p)-SMD(solvent)//uwb97xD/cc-pvDZ-cpcm(solvent) level of theory. A larger difference in E_{HB}, when going from water to octanol, directly correlates to a larger increase in lipophilicity when going from the open to closed form. Detailed structures and calculations can be found in the Supporting Information (**Figure A6-A13**).

To isolate and analyze the effect of the intramolecular hydrogen-bond on lipophilicity, we compared the change in LogD values (ΔLogD) due to the formation of an intramolecular hydrogen bond to the change in intramolecular hydrogen bond strength (ΔE_{HB}) due to solvent changes (**Figure 3F**; **Appendix A Figures A3** and **A4**, **Tables A1** and **A2**). As expected, a larger difference in the strength of the hydrogen bond in water as compared to octanol directly correlates to a larger increase in lipophilicity when going from the open to closed form. This demonstrates that the strength of the intramolecular hydrogen bond in octanol will directly impact lipophilicity. Our calculations also suggest that for a given redox state, closed forms of PCA, PCN, and PYO all exhibit increased lipophilicity compared to their 'open' forms.

Taken together, the data described above suggest that intramolecular hydrogen bonding contributes to enhanced lipophilicity of reduced forms of PCA>PYO>PCN, which aligns

well with our experimental observations. Intramolecular hydrogen bonding in 1-OH contributes to slightly increased lipophilicity in the oxidized form. As there is no possibility for intramolecular H-bonding in either the oxidized or reduced forms of unsubstituted phenazine, these compounds exhibit essentially the same lipophilicity.

Redox state controls biological PYO retention

As a case study to assess the biological consequences of redox-mediated changes to PYO's lipophilicity, we experimented with late stationary phase *P. aeruginosa* PA14 cells in liquid culture (see **Appendix A** for additional details). In the first experiment, cells were grown for 20 hours, then subdivided into two aliquots – one centrifuged and washed under anoxic conditions with sparged buffer, where we expect the phenazines to be and remain reduced, the other under normoxic conditions (atmospheric O_2, 21%) with unsparged buffer, where we expect the phenazines to remain oxidized. Extracellular PYO concentrations were measured in the culture supernatant and wash supernatant by HPLC (see **Appendix A** for method details). After three washes with N_2-sparged anoxic buffer, the cells continued to release a quantifiable amount of PYO (3.5 ± 0.4 μM). And after a fourth wash with normoxic buffer, the cells released 11.3 ± 0.1 μM PYO. On the other hand, the cells washed with normoxic buffer released PYO concentrations that were below the limit of quantification (sub 150 nM) by the third wash and that could not be detected (sub 25 nM) by the fourth wash. Together, these results demonstrate that the more lipophilic reduced form of PYO is strongly retained by the bacteria, while the less lipophilic oxidized form of PYO is easily washed away by aqueous buffer. The redox-mediated change to PYO's lipophilicity explains this observed change in cellular retention, which has previously been observed to interfere

with measurement of intracellular NADH/NAD^+ ratios: measurements of NADH/NAD^+ ratios in pyocyanin producers must be made under anoxic conditions because, in normoxic conditions, oxidized PYO skews measurements by diffusing out of the cell pellet and directly oxidizing NADH, leading to artificially low NADH/NAD^+ ratios (38). Moreover, hitherto puzzling observations of quenching of certain oxygen probes by bacterial cultures containing reduced PYO but not oxidized PYO can now be understood in light of our results (39).

Unexpectedly, we observed a large difference between the supernatant PYO concentrations in the normoxic aliquots of cells (60 ± 7 μM) compared to the anoxic aliquots of the same culture (34 ± 3 μM). Calculations made by approximating the volume of the cells suggest that intracellular PYO concentrations in the anoxic condition reached millimolar levels (estimated at >3 mM), roughly 2 orders of magnitude greater than extracellular concentrations observed in the supernatant (see **Appendix A** for retention calculation details).

To validate this estimate and determine whether partitioning into the membrane is responsible for biological PYO retention, we conducted an additional experiment in which 1L of dense *P. aeruginosa* cells grown aerobically in LB (OD_{500} = 4.7), were removed from the shaking incubator and allowed to reduce their extracellular phenazines while standing on the benchtop (the culture changed from blue/green, indicating oxidized PYO, to colorless, indicating reduced PYO). Cells were then pelleted and lysed using a high pressure homogenizer, and the membrane fraction was isolated by ultracentrifugation. Throughout this process, the pellet, the lysed cells, and the membrane fraction remained colorless,

presumably due to abiotic reactions between PYO and NADH and other residual cellular reducing agents. The membrane fraction was weighed and then extracted with MeOH. Upon addition of MeOH during the first extraction, the membrane fraction and added solvent turned bright blue, indicating oxidized PYO. After the third extraction, the ultracentrifuged membrane pellet and the overlying MeOH were colorless. Both the pooled membrane extract and the original culture supernatant were measured by HPLC to determine PYO concentrations. While the extracellular medium contained 0.03 μmol PYO per gram medium (essentially the same concentration as measured in the anoxic aliquot from the first biological retention experiment), the wet membrane fraction contained nearly two orders of magnitude more: 2.2 μmol PYO per gram (See supporting information for membrane concentration calculation details). This suggests that membrane retention, which is expected to correlate directly with lipophilicity, is responsible for significant retention of reduced PYO *in vivo*.

Conclusion

Our results indicate that even minor changes to the substituent at the 1-position (or the symmetric 6-position) can significantly alter phenazine lipophilicity by facilitating intramolecular hydrogen bonding. If a 1-position substituent can accept a hydrogen bond from a reduced pyrazine nitrogen, the lipophilicity of the reduced form compared to the oxidized form can be enhanced by over an order of magnitude. The sensitivity of a fundamental property like lipophilicity to substitutions at the 1-position is particularly intriguing given PCA or its symmetric counterpart 1,6-phenazine dicarboxylic acid are intermediates in all the known biosynthetic pathways for microbial phenazine. Changes in

lipophilicity due to the local pH and redox environment, especially dramatic changes of the magnitude observed for PCA, likely dictate natural phenazines' abilities to traverse membranes, biofilms, soils, and tissues. In general, higher lipophilicities are expected to correlate with increased retention in organic phases and decreased water solubility and aqueous transport. As is the case for quinones and quinols, changes in lipophilicity likely also influence phenazine affinities for protein binding pockets (40), enhancing or limiting their interaction with components of the electron transport chain or with detoxifying or degrading enzymes.

The ability to effect such significant changes to a fundamental thermodynamic property through the modification of a single molecular substituent gives phenazine producers a remarkable evolutionary handle for tuning the functions of these secreted metabolites to the needs most pressing in their respective niches. Unlike many secondary metabolites, including most antibiotics, which are large or complex enough that their basic properties are difficult to change without significant structural modification, phenazine lipophilicity is highly sensitive to minor structural alterations, which can often be accomplished by a single enzyme. Perhaps this flexibility helps explain their prevalence and structural diversity across diverse niches (6, 41), including host-microbe systems.

In the case of reduced pyocyanin, the measured enhancement in lipophilicity predicts increased biological retention, which is observed in anoxic cell pellets, despite the expected expression of an entire suite of efflux pumps capable of actively pumping phenazines out of the cell (42, 43). There is thus good reason to believe that lipophilicity changes can play an

important role even in contexts where active biological processes compete with abiotic processes like diffusion and partitioning. The extremely elevated levels of pyocyanin measured in the membrane suggest a different biological role than is typically appreciated for this metabolite, which is often treated as both toxic and primarily extracellular. One possible explanation is that in oxygen limited environments, PYO, and possibly other phenazines, play a direct role like that of quinones in the *P. aeruginosa* electron transport chain. In the archaeal methanogen *Methanosarcina mazei*, the hydrophobic methanophenazine plays a role similar to ubiquinone, accepting electrons from dehydrogenase enzymes and donating electrons to a heterodisulfide reductase enzyme (43). In *P. aeruginosa*, phenazines are produced in aerobic cultures during early stationary phase, as oxygen becomes limited due to increased consumption by the high density of cells. Furthermore, PCN and PYO are known to accept electrons from dehydrogenase enzymes in the electron transport chain (45, 46) and donate their electrons to quinones (46, 47). Direct participation in redox reactions coupled to cellular survival could help explain the elevated intracellular concentrations found in this study. But even compared to known quinone concentrations in growing *Escherichia* coli (47), our measurements are elevated by a factor of 5-10, suggesting further study is needed to illuminate the function of PYO in the membrane.

Octanol and water are imperfect substitutes for the complexities of the cell membrane and the cytosol, which are unlike any media used regularly in the lab (49). But the indication from simple, reductionist shake flask measurements that redox state is a fundamental control on phenazine lipophilicities led us to determine that simple modifications to the phenazine

core structure provide microbial phenazine producers the opportunity to tune phenazine mobility strongly both within and beyond the cell. The understanding that this modulation stems from facilitation of intramolecular hydrogen bonding may help explain the profusion of phenazine analogs in different environmental niches. In addition, the suggestion from LogD measurements that reduced PYO might be retained by the membrane inspired our determination of the intracellular and intramembrane concentrations of the reduced metabolite. That it is retained primarily within the cell, despite being conventionally described as a "secreted" metabolite, both challenges our conceptualization of these compounds and points to an underappreciated physiological role for phenazines in the membrane. These results reinforce the ability of the octanol-water partition coefficient to transcend the complexity of bulk biological environments and lead to new understanding. While LogD measurements and cLogP predictions are generally used to predict environmental fate and inform pharmaceutical research, here they offer fresh insight into subcellular and extracellular metabolite localization, pointing us toward a new biological role for a molecule that has been studied for nearly 100 years (50).

Acknowledgments

We thank Dr. Nate Glasser, Dr. Nathan Dalleska, and the members of the Newman Lab for insightful suggestions that improved this study. Grants from the NIH (1R01AI189726-01A1) and ARO (Cooperative Agreement Number W911NF-22-2-0210) supported our research. The views and conclusions contained in this document are those of the authors and should not be interpreted as representing the official policies, either expressed or implied, of

the Army Research Office or the U.S. Government. The U.S. Government is authorized to reproduce and distribute reprints for Government purposes notwithstanding any copyright notation herein. S.J.C. is grateful to Michael and Alice Jung for endowing the Jung Chair in Medicinal Chemistry and Drug Discovery at UCLA, which partially supported this work. O.G. acknowledges NIH NIGMS (R35GM137797) for funding and the Hoffman2 Cluster at UCLA Office of Advanced Research Computing's Research Technology Group for providing computational resources (https://hprc.tamu.edu, https://www.hoffman2.idre.ucla.edu/). I.B.T. was supported by an EMBO Postdoctoral Fellowship (ALTF 191-2023).

References

1. Frimmersdorf, E., Horatzek, S., Pelnikevich, A., Wiehlmann, L., & Schomburg, D. (2010). How *Pseudomonas aeruginosa* adapts to various environments: a metabolomic approach. *Environmental Microbiology*, 12(6), 1734–1747. https://doi.org/10.1111/j.1462-2920.2010.02253.x

2. van Hoek, M. J., & Merks, R. M. (2012). Redox balance is key to explaining full vs. partial switching to low-yield metabolism. *BMC Systems Biology*, 6(1), 22. https://doi.org/10.1186/1752-0509-6-22

3. Santamaria, G., Liao, C., Lindberg, C., Chen, Y., Wang, Z., Rhee, K., Pinto, F. R., Yan, J., & Xavier, J. B. (2022). Evolution and regulation of microbial secondary metabolism. *eLife*, 11. https://doi.org/10.7554/elife.76119

4. Konings, W. N., Poolman, B., & Driessen, A. M. (1992). Can the excretion of metabolites by bacteria be manipulated? *FEMS Microbiology Letters,* 88(2), 93–108. https://doi.org/10.1111/j.1574-6968.1992.tb04959.x

5. Dar, D., Thomashow, L. S., Weller, D. M., & Newman, D. K. (2020). Global landscape of phenazine biosynthesis and biodegradation reveals species-specific colonization patterns in agricultural soils and crop microbiomes. *eLife*, 9. https://doi.org/10.7554/elife.59726

6. Mavrodi DV, Blankenfeldt W, Mavrodi OV, Weller DM, Thomashow LS. 2025. Microbial phenazines: biosynthesis, structural diversity, evolution, regulation, and biological significance. *Microbiol Mol Biol Rev* 89:e00147-23. https://doi.org/10.1128/mmbr.00147-23

7. Grahl, N., Kern, S. E., Newman, D. K., & Hogan, D. A. (2013). The Yin and Yang of Phenazine Physiology. In Microbial Phenazines (pp. 43–69). *Springer Berlin Heidelberg*. https://doi.org/10.1007/978-3-642-40573-0_3

8. Wang, Y., & Newman, D. K. (2008). Redox reactions of phenazine antibiotics with ferric (hydr)oxides and molecular oxygen. *Environmental Science & Technology*, 42(7), 2380–2386. https://doi.org/10.1021/es702290a

9. Thalhammer, K. O., & Newman, D. K. (2023). A phenazine-inspired framework for identifying biological functions of microbial redox-active metabolites. *Current Opinion in Chemical Biology*, 75, 102320. https://doi.org/10.1016/j.cbpa.2023.102320

10. Hansch, Corwin., & Fujita, Toshio. (1964). p-σ-π Analysis. A method for the correlation of biological activity and chemical structure. *Journal of the American Chemical Society*, 86(8), 1616–1626. https://doi.org/10.1021/ja01062a035

11. Uchida, M. & Kasai, T. (1980). Adsorption and mobility of fungicidal dialkyl dithiolanylidenemalonates and their analogs in soil. Journal *of Pesticide Science*, 5(4), 553–558. https://doi.org/10.1584/jpestics.5.553

12. Connell, D. W., Miller, G. J., Mortimer, M. R., Shaw, G. R., & Anderson, S. M. (1999). Persistent lipophilic contaminants and other chemical residues in the southern hemisphere. *Critical Reviews in Environmental Science and Technology*, 29(1), 47–82. https://doi.org/10.1080/10643389991259173

13. Hill, A. P., & Young, R. J. (2010). Getting physical in drug discovery: a contemporary perspective on solubility and hydrophobicity. *Drug Discovery Today*, 15(15–16), 648–655. https://doi.org/10.1016/j.drudis.2010.05.016

14. Young, R. J., Green, D. V. S., Luscombe, C. N., & Hill, A. P. (2011). Getting physical in drug discovery II: the impact of chromatographic hydrophobicity measurements and aromaticity. *Drug Discovery Today*, 16(17–18), 822–830. https://doi.org/10.1016/j.drudis.2011.06.001

15. Ou, J., Li, H., Ou, X., Yang, Z., Chen, M., Liu, K., Teng, Y., & Xing, B. (2020). Degradation, adsorption and leaching of phenazine-1-carboxamide in agricultural soils. *Ecotoxicology and Environmental Safety*, 205, 111374. https://doi.org/10.1016/j.ecoenv.2020.111374

16. Michaelis, L., Hills, E. S., and Schubert, M. P. *Biochem. Z*. 255, 66 (1932).

17. Brisbane, P. G., Janik, L. J., Tate, M. E., & Warren, R. F. (1987). Revised structure for the phenazine antibiotic from *Pseudomonas fluorescens* 2-79 (NRRL B-15132). *Antimicrobial Agents and Chemotherapy,* 31(12), 1967–1971. https://doi.org/10.1128/aac.31.12.1967

18. Perkampus, H. -H., & Rössel, Th. (1958). Untersuchungen über die pH-Abhängigkeit der Absorptionsspektren und über die Basizität einiger N-heterocyclischer Oxyverbindungen Oxyacridine und Oxyphenazine. *Zeitschrift Für Elektrochemie, Berichte Der Bunsengesellschaft Für Physikalische Chemie*, 62(1), 94–105. https://doi.org/10.1002/bbpc.19580620114chemicalize

19. Chemicalize was used for prediction of pKa values for phenazine, *JChem* n.n.n (version number), 201n (NNNN), ChemAxon (http://www.chemaxon.com)

20. Molinspiration Cheminformatics free web services. https://www.molinspiration.com, Slovensky Grob, Slovakia.

21. Daina, A., Michielin, O., & Zoete, V. (2014). iLOGP: A simple, robust, and efficient description of n-octanol/water partition coefficient for drug design using the GB/SA approach. *Journal of Chemical Information and Modeling*, 54(12), 3284–3301. https://doi.org/10.1021/ci500467k

22. US EPA. [2026]. Estimation Programs Interface Suite™ for Microsoft® Windows, v 4.11]. United States Environmental Protection Agency, Washington, DC, USA. (Used for KOWWIN logP estimate)

23. Mannhold, R., & Rekker, R. F. (2000). The hydrophobic fragmental constant approach for calculating log P in octanol/water and aliphatic hydrocarbon/water systems. *Perspectives in Drug Discovery and Design*, 18(1), 1–18. https://doi.org/10.1023/a:1008782809845

24. Meylan, W. M., & Howard, P. H. (1995). Atom/fragment contribution method for estimating octanol–water partition coefficients. *Journal of Pharmaceutical Sciences*, 84(1), 83–92. https://doi.org/10.1002/jps.2600840120

25. Meylan, W. M., Howard, P. H., & Boethling, R. S. (1996). Improved method for estimating water solubility from octanol/water partition coefficient. *Environmental Toxicology and Chemistry*, 15(2), 100–106. https://doi.org/10.1002/etc.5620150205

26. Meylan, W. M., & Howard, P. H. (2000). Estimating log P with atom/fragments and water solubility with log P. *Perspectives in Drug Discovery and Design*, 19(1), 67–84. https://doi.org/10.1023/a:1008715521862

27. Wang, R., Fu, Y., & Lai, L. (1997). A new atom-additive method for calculating partition coefficients. *Journal of Chemical Information and Computer Sciences*, 37(3), 615–621. https://doi.org/10.1021/ci960169p

28. Cheng, T., Zhao, Y., Li, X., Lin, F., Xu, Y., Zhang, X., Li, Y., Wang, R., & Lai, L. (2007). Computation of octanol−water partition coefficients by guiding an additive model with knowledge. *Journal of Chemical Information and Modeling*, 47(6), 2140–2148. https://doi.org/10.1021/ci700257y

29. Chiou, C. T., Schmedding, D. W., & Manes, Milton. (1982). Partitioning of organic compounds in octanol-water systems. *Environmental Science & Technology*, 16(1), 4–10. https://doi.org/10.1021/es00095a005

30. Chen, D., Zhao, M., Tan, W., Li, Y., Li, X., Li, Y., & Fan, X. (2019). Effects of intramolecular hydrogen bonds on lipophilicity. *European Journal of Pharmaceutical Sciences*, 130, 100–106. https://doi.org/10.1016/j.ejps.2019.01.020

31. José Manuel Guevara-Vela; Gallegos, M.; Valentín-Rodríguez, M. A.; Costales, A.; Tomás Rocha-Rinza; Ángel Martín Pendás. On the relationship between hydrogen bond strength and the formation energy in resonance-assisted hydrogen bonds. *Molecules* **2021**, *26* (14), 4196–4196.

32. Michalík, M.; Vladimír Lukeš. The validation of quantum chemical lipophilicity prediction of alcohols. *Acta Chimica Slovaca* 2016, 9 (2), 89–94.

33. Ho, J.; Ertem, M. Z. Calculating free energy changes in continuum solvation models. *The Journal of Physical Chemistry B* 2016, 120 (7), 1319–1329.

34. Marenich, A. V.; Cramer, C. J.; Truhlar, D. G. Universal solvation model based on solute electron density and on a continuum model of the solvent defined by the bulk dielectric constant and atomic surface tensions. *The Journal of Physical Chemistry* B 2009, 113 (18), 6378–6396.

35. Glendening, E. D.; Landis, C. R.; Weinhold, F. NBO 6.0: Natural bond orbital analysis program. *Journal of Computational Chemistry* **2013**, *34* (16), 1429–1437.

36. Reed, A. E.; Curtiss, L. A.; Weinhold, F. Intermolecular interactions from a natural bond orbital, donor-acceptor viewpoint. *Chemical Reviews* **1988**, *88* (6), 899–926.

37. Anslyn, E. V.; Dougherty, D. A. Modern Physical Organic Chemistry (pp 171-180); Univ. Science Books: Sausalito, Calif., 2008.

38. Filloux, A., & Ramos, J.-L. (eds.), *Pseudomonas* Methods and Protocols, Methods in Molecular Biology, vol. 1149, Ch. 26: Extraction and Measurement of NAD(P)+ and NAD(P)H. Suzanne E. Kern, Alexa Price-Whelan, and Dianne K. Newman. DOI 10.1007/978-1-4939-0473-0_26.

39. Branning J. M., Jr., Ruff, B. M., Saccomano, S. C., Flamholz, A. I., Newman, D. K., Cash, K. J. A fluorous phase oxygen optical nanosensor for mitigating redox-active microbial metabolite interference. *Submitted to RCS*.

40. Rich, P. R., & Harper, R. (1990). Partition coefficients of quinones and hydroquinones and their relation to biochemical reactivity. *FEBS Letters*, 269(1), 139–144. https://doi.org/10.1016/0014-5793(90)81139-f

41. Turner, J. M., & Messenger, Ann. J. (1986). Occurrence, biochemistry and physiology of phenazine pigment production. *Advances in Microbial Physiology* (pp. 211–275). Elsevier. https://doi.org/10.1016/s0065-2911(08)60306-9

42. Sakhtah, H., Koyama, L., Zhang, Y., Morales, D. K., Fields, B. L., Price-Whelan, A., Hogan, D. A., Shepard, K., & Dietrich, L. E. P. (2016). The *Pseudomonas aeruginosa* efflux pump MexGHI-OpmD transports a natural phenazine that controls gene expression and biofilm development. *Proceedings of the National Academy of Sciences*, 113(25). https://doi.org/10.1073/pnas.1600424113

43. Meirelles, L. A., Perry, E. K., Bergkessel, M., & Newman, D. K. (2021). Bacterial defenses against a natural antibiotic promote collateral resilience to clinical antibiotics. *PLOS Biology*, 19(3), e3001093. https://doi.org/10.1371/journal.pbio.3001093

44. Beifuss, U., Tietze, M., Bäumer, S., & Deppenmeier, U. (2000). Methanophenazine: structure, total synthesis, and function of a new cofactor from methanogenic archaea. *Angewandte Chemie International Edition*, 39(14), 2470–2472. https://doi.org/10.1002/1521-3773(20000717)39:14<2470::aid-anie2470>3.0.co;2-r

45. Glasser, N. R., Wang, B. X., Hoy, J. A., & Newman, D. K. (2017). The pyruvate and α-ketoglutarate dehydrogenase complexes of *Pseudomonas aeruginosa* catalyze pyocyanin and phenazine-1-carboxylic acid reduction via the subunit dihydrolipoamide dehydrogenase. *Journal of Biological Chemistry*, 292(13), 5593–5607. https://doi.org/10.1074/jbc.m116.772848

46. Ciemniecki, J. A., & Newman, D. K. (2023). Dehydrogenases are the predominant phenazine reductases in the electron transport chain of *Pseudomonas aeruginosa. Molecular Microbiology*, 119(5), 560–573. https://doi.org/10.1111/mmi.15049

47. Tsypin, L. M., & Newman, D. K. (2021). Nitrate reduction stimulates and Is stimulated by phenazine-1-carboxylic acid oxidation by *Citrobacter portucalensis* MBL. *mBio*, 12(4). https://doi.org/10.1128/mbio.02265-21

48. Unden, G., & Bongaerts, J. (1997). Alternative respiratory pathways of *Escherichia coli*: energetics and transcriptional regulation in response to electron acceptors. *Biochimica et Biophysica Acta (BBA) - Bioenergetics*, 1320(3), 217–234. https://doi.org/10.1016/s0005-2728(97)00034-0

49. Parry, B. R., Surovtsev, I. V., Cabeen, M. T., O'Hern, C. S., Dufresne, E. R., & Jacobs-Wagner, C. (2014). The bacterial cytoplasm has glass-like properties and Is fluidized by metabolic activity. *Cell*, 156(1–2), 183–194. https://doi.org/10.1016/j.cell.2013.11.028

50. Friedheim, E., & Michaelis, L. (1931). Potentiometric study of pyocyanine. *Journal of Biological Chemistry*, 91(1), 355–368. https://doi.org/10.1016/s0021-9258(18)76619-2

Chapter 3

PHENAZINE PRODUCTION INDUCES LIPID REMODELING IN THE *PSEUDOMONAS AERUGINOSA* CELL ENVELOPE

KOT conceptualized the project, performed the experiments prior to lipid extraction, and interpreted the results. Dr. Binyou Wang performed the lipid extraction, detection, and data analysis.

Abstract

The cell envelope of the opportunistic pathogen *Pseudomonas aeruginosa* plays several crucial roles, protecting against environmental change, facilitating active and passive transport of nutrients, excluding toxins, and enabling the production and maintenance of a proton motive force (PMF). Because of these vital functions, the properties of the membranes that constitute this envelope are closely controlled by the cell, which changes the specific lipid composition of the inner and outer membrane in response to environmental factors like temperature, nutrient availability, and antibiotic stress. The recently documented redox-sensitive lipophilicity of the phenazine metabolites produced by *Pseudomonas aeruginosa* and the elevated levels of pyocyanin measured in the membrane fraction of lysed cells suggest that phenazines might impact membrane properties by partitioning into these lipid-rich phases and disrupting important lipid-lipid and lipid-protein interactions. Here we demonstrate that WT *P. aeruginosa* PA14 cells grown to late stationary phase in a condition promoting phenazine production possess starkly different lipid compositions compared to identically grown Δphz mutants lacking phenazine biosynthesis genes. Whether these changes are the result of genetic regulation, perhaps caused by direct interaction of phenazines with regulatory enzymes like the transcription factor SoxR, or the result of more

generic responses to changes in membrane properties like fluidity will require a series of more detailed follow up studies which I outline at the end of this chapter.

Introduction

The Pseudomonas aeruginosa cell envelope, like those of other gram-negative bacteria, consists of an asymmetric outer membrane, containing a high proportion of the lipopolysaccharide LipidA in the outer leaflet, and an inner membrane separating the periplasm from the cytoplasm (1). Between these two membranes lies the cell wall, which in P. aeruginosa is composed primarily of a rigid layer of peptidoglycan (**Figure 1**). The composition of the outer and inner membranes consists of a diverse blend of lipids with tunable combinations of various headgroups -- primarily phosphatidylethanolamine and phosphatidylglycerol -- attached to fatty acid tails of various lengths and degrees of unsaturation (2, 3). Changes in membrane lipid composition affect membrane properties like fluidity, as well as the presence and character of specific lipid domains that in turn affect the assembly and function of respiratory enzymes (4, 5).

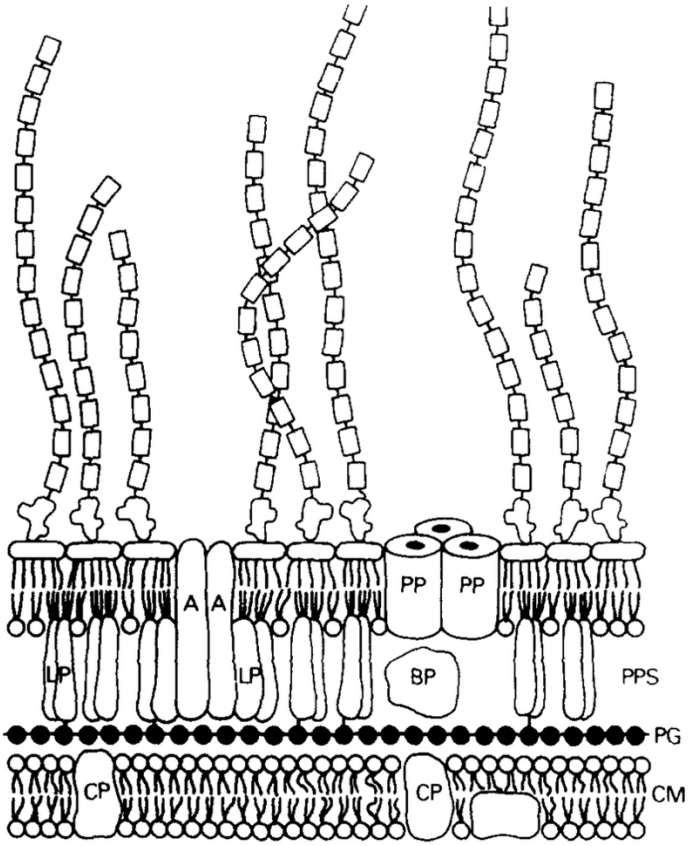

Figure 1: Architecture of the gram negative bacterial cell envelope. The outer membrane consists of a lipopolysaccharide-rich outer leaflet (long appendages depicted here are primarily Lipid A in P. aeruginosa) and an inner lipid leaflet containing both lipoproteins (LP) and transmembrane peptidoglycan-associated proteins (A) that share the periplasmic space (PPS) with nutrient binding proteins (BP). Pore forming trimeric proteins (PP) permit solute passage through the outer membrane. The inner cytoplasmic membrane (CM) is located just inside the rigid peptidoglycan cell wall (PG) and is composed of a lipid bilayer interspersed with carrier proteins (CP) and respiratory chain components including the quinone pool and dehydrogenase and terminal oxidase enzymes capable of generating a proton motive force (not pictured). Reproduced with permission from Biochimica et Biophysica Acta 737 (1983), 51-115 (1).

Because membrane properties are so closely linked to critical cellular functions, *Pseudomonas aeruginosa* is known to alter its membrane properties in response to environmental stress. When confronted with decreasing extracellular pH, P. aeruginosa responds by increasing the viscosity and lowering the permeability of its inner membrane (6.) When limited by phosphorous availability, *P. aeruginosa* diminishes the ratio of typical phosphorous-containing lipid headgroups in favor of phosphorous-free glycolipids. In addition to addressing nutrient stress common in infection contexts, this adaptation increases cells' resistance to the antibiotic polymyxin B and may decrease susceptibility to phage attacks (7, 8).

The stress of entering stationary phase, typically characterized by nutrient or oxidant limitation due to crowding, also provokes significant lipid remodeling. As it enters stationary phase, *P. aeruginosa* cyclopropanates many of its fatty acids (2). This response has also been observed when *P. aeruginosa* forms biofilms or is confronted by oxidative stress (3, 9). Because of their unique structures, cyclopropanated fatty acids are believed to both stabilize membranes by limiting along-chain motion within their fatty acyl groups, and enhance internal membrane fluidity by promoting disorder toward the center of the lipid bilayer (10-12).

Coincident with the start of stationary phase, wild type (WT) *P. aeruginosa* cells generally begin producing phenazines, often resulting in extracellular concentrations over 100μM by late stationary phase (13). Beyond planktonic conditions, phenazines are also believed to be essential in biofilm contexts, where they promote extracellular electron transfer from the biofilm's oxygen-starved core to the aerobic periphery (14, 15). Phenazines are redox-active

and can cause oxidative stress by generating superoxide and by stealing reducing equivalents directly from cellular components in the membrane and the cytosol (16, 17). The transcription factor SoxR, when oxidized by pyocyanin, causes a phenazine-specific regulatory response that includes expression of multidrug efflux pumps (18). As detailed in Chapter 1, reduction of the three main phenazines produced by P. aeruginosa PA14 (PCA, PCN, and PYO) results in intramolecular hydrogen bonding that causes the phenazines to become more lipophilic. In the case of pyocyanin, which is generally considered a specific target of the efflux pumps under the control of SoxR, the abiotic change in lipophilicity appears to be significant enough to cause dramatic accumulation in the membrane (19, 20). Membranes extracted from stationary phase planktonic cells contained pyocyanin at a concentration approximately 100 times that found in the extracellular medium.

This incredible concentration of this highly reactive metabolite in the cell membrane is 5-10 times higher than that of native quinones (21) and could reasonably interfere with both lipid-lipid and lipid-protein interactions that are vital to cellular survival. Disruptions in the hydrophobic forces holding the lipid bilayer together could cause devastating structural changes with attendant effects on permeability (22, 23). A “leaky” inner membrane could both diminish exclusion of extracellular toxins and, by allowing protons to leak back across the membrane, could dramatically increase the metabolic flux required to maintain a sufficient PMF. Both of these energy sinks could prove catastrophic in the nutritionally limited context of a biofilm or in planktonic stationary phase. In addition, lipid-quinone and lipid-protein interactions essential to the function of the respiratory chain could also be disrupted by large quantities of pyocyanin or other hydrophobic phenazines in the membrane.

Given that *P. aeruginosa* cells evolved to produce phenazines, it is reasonable to believe that they also evolved strategies to mitigate any deleterious phenazine-mediated membrane disruptions and preserve critical respiratory functions. Indeed, phenazine-deficient Δphz mutants of P. aeruginosa PA14 exposed to exogenous pyocyanin during exponential growth appear to upregulate SoxR controlled efflux pumps but also several hypothetical proteins (13), two of which have orthologs apparently related to lipid modification: PA3515, is an ortholog of pmtA, a phospholipid methyltransferase known to affect PYO production and biofilm formation (24); and PA3520 is a putative periplasmic substrate binding protein with 97% structural similarity to protein 5T1P in *Campylobacter jejuni* and a predicted ligand identical to P. aeruginosa's most abundant lipid headgroup phosphatidylethanolamine (PE) (25, 26). But, possibly because phenazines have not previously been appreciated to accumulate in cell membranes, to our knowledge no work has been done to understand the specific effects of endogenous phenazines on *P. aeruginosa* lipid composition. To test our hypothesis that cells change their lipid composition in response to endogenous phenazines, we conducted a preliminary lipidomics study to search for changes in membrane composition between WT *P. aeruginosa* PA14 cells and phenazine-deficient Δphz cells.

Lipid Nomenclature

For the purposes of this report, lipids will be referred to using an abbreviation of the style XX(N:M) in which XX is a letter code referring to the headgroup and (N:M) is a description of the combined fatty acyl tails composed of N total carbons with M total double bonds. When available, information about individual acyl groups will be reported using the same N:M nomenclature with the possible addition of information about the location and orientation of double bonds as (YE) for a trans double bond at carbon number Y, or (YZ) for a cis double bond at carbon Y. **Table 1** describes the headgroups measured in this study.

Table 1: Descriptions of the major lipid headgroups measured in this study. R groups refer to generic fatty acyl tails attached to the headgroup by ester bonds.

Abbreviation	Name	Structure
DG	Diacylglycerol	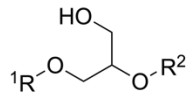
DGDG	Diglycosyldiacylglycerol	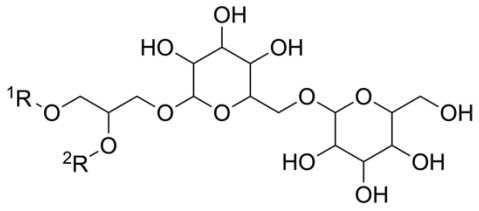
CL	Cardiolipin	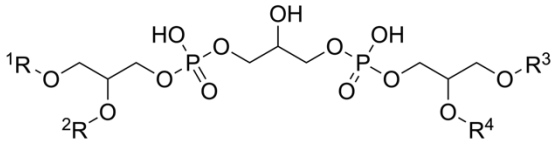

MLCL	Monolysocardiolipin	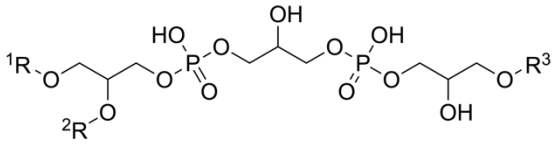
PA	Phosphatidic acid	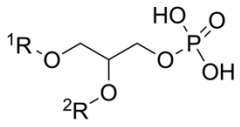
LPA	Lysophosphatidic acid	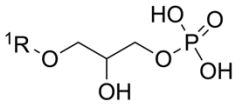
PC	Phosphatidylcholine	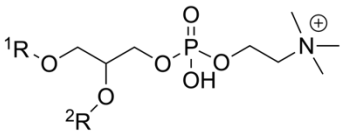
LPC	Lysophosphatidylcholine	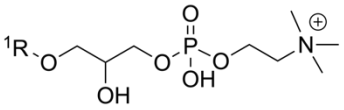
PE	Phosphatidylethanolamine	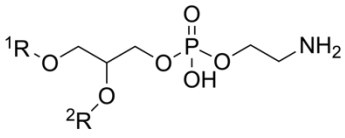

LPE	Lysophosphatidylethanolamine	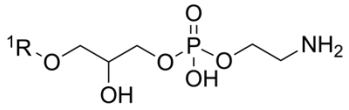
PG	Phosphatidylglycerol	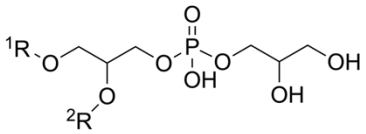
LPG	Lysophosphatidylglycerol	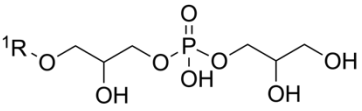

Methods

Culture conditions

Four biological replicates each of wild type (WT) and Δphz *P. aeruginosa* cells were inoculated from LB agar plates into 5 mL tubes of LB medium. Cells were grown aerobically at 37 ºC with shaking (250 RPM) for 20 hours, by which time they had reached late stationary phase. Culture densities were measured by absorbance at 500 nm to avoid interference from pyocyanin produced by WT cells. Cells were then harvested by centrifugation and supernatant was diluted 1:1 with MeOH for phenazine measurement by HPLC. Cell pellets were washed twice with fresh PBS and stored at -20 ºC until lipid extraction, described below.

Liquid chromatography phenazine measurements

Phenazine measurements were performed on a Waters Alliance HPLC connected to a Waters 2998 PDA detector set to detect wavelengths from 200-800nm at 20Hz with 1.2nm resolution. We used a C18 column (XBridge BEH 2.5µm particle size, 3 x 100mm) and the following basic gradient method (final pH $\geq$ 9), using solvent A (H_2O + 2% *v/v* MeOH + 0.1% *v/v* NH_4OH) and Solvent B (acetonitrile + 2% *v/v* MeOH + 0.1% *v/v* NH_4OH) at 0.5 mL/min: 0-6 minutes: linear gradient from 98%A, 2%B to 80%A, 20%B; 6-8 minutes: linear gradient to 5%A, 95%B; 8-9 minutes hold at 5%A, 95%B; 9-9.1 minutes: linear gradient to 98%A, 2%B; 9.1-16 minutes: hold at 98%A, 2%B.

A standard curve was prepared using the same method and was used to assess concentrations of PCA, PCN, and PYO down to 150nM. Prior to introducing them to the column, pellet supernatant samples were diluted 1:1 with MeOH and incubated at 0 °C for at least one hour to encourage protein precipitation. Samples were then centrifuged at 16,000 x g for 1 minute, and the resulting supernatant was stored at 10 °C until measurement.

Phenazines were monitored at the following retention times and wavelengths: PCA: 364 nm, 2.5 minutes; PYO: 313 nm, 6.3 minutes; PCN: 248 nm, 12.0 minutes. Concentrations were determined by comparing peak areas at the stated wavelengths to standard curves of authentic standards produced using the same chromatography and detection methods.

Lipid extraction

Lipid extraction was performed using a tert-butyl methyl ether (MTBE)-based protocol (27). PBS-washed cell pellets were resuspended in 70 µL water, followed by addition of 232 µL methanol and 20 µL (10× diluted) internal standard mixture. Subsequently, 840 µL MTBE was added and samples were incubated for 1 h at room temperature with shaking. Phase separation was induced by adding 150 µL water, followed by incubation for 5 min at room

temperature and centrifugation at 1,000 × g for 10 min. The upper organic phase (750 µL) was collected and transferred to glass autosampler vials (Thermo, 6PSV9-1PG) and dried overnight under vacuum.

Liquid Chromatography for Lipid Separation

Dried lipid extracts were reconstituted in 500 µL of Solvent B (isopropanol/acetonitrile/ water, 88:10:2, vol/vol) containing 10 mM ammonium formate and 0.1% (vol/vol) formic acid. Lipids were separated by reversed-phase LC on a Vanquish Core system (Thermo Fisher Scientific) equipped with an Accucore C30 column (150 × 2.1 mm, 2.6 mm, 150 Å, Thermo Fisher Scientific). Mobile phase A from LC system was acetonitrile/water, 60:40, *v/v* with 10 mM ammonium formate and 0.1% *v/v* formic acid and Mobile phase B from LC system was isopropanol/acetonitrile/water, 88:10:2, vol/vol both containing 10 mM ammonium formate and 0.1% *vol/vol* formic acid. Separation was performed at 45 °C at a flow rate of 0.26 mL/min using the following gradient: 0–2 min, 30–43% B (curve 5); 2.1–12 min, 43–55% B (curve 5); 12–18 min, 65–85% B (curve 5); 18–20 min, 85–100% B (curve 5); 20–25 min, 100% B isocratic; 25.1–28 min, 100%–30% B (curve 5) followed by 7 min re-equilibration at 30% B.

Mass spectrometry for Lipid Detection

LC was coupled to an Orbitrap Exploris™ 240 mass spectrometer (Thermo Fisher Scientific) with a heated electrospray ionization (HESI) source. Mass spectra were acquired in positive and negative modes with the following ESI parameters: sheath gas, 40 (Arb); auxiliary gas, 10 (Arb); sweep gas, 0 (Arb); spray voltage, (+)3.25 kV (positive ion mode); (−)3 kV (negative ion mode); Ion transfer tube temperature, 300 °C; S-lens RF level, 70; Vaporizer temperature, 275 °C. Data acquisition for lipid identification wasperformed in data-dependent acquisition mode (DDA) full scan with MS/MS. The full scan has the

resolution of 120,000, AGC target set to standard mode, maximum injection time set to auto mode in a scan range of m/z 100–1,200. Data-dependent MS/MS scans were acquired with a resolution of 15,000, AGC target set to standard mode, maximum injection time set to auto mode, isolation window of 1 m/z and stepped normalized collision energies of 20, 30 and 40. A data-dependent MS2 was triggered (Cycle time of 1.2 s) when an AGC target of 2.5e3 was reached followed by a dynamic exclusion for 10 s. All isotopes and charge states >1 were excluded. Full scan spectra were acquired in profile type and MS/MS scans were acquired in centroid type. Data for lipid quantification in individual samples were acquired in full scan MS mode with the following parameters: resolution of 120,000, AGC target set to standard mode, maximum injection time set to auto mode in a scan range of m/z 100-1200.

Lipid identification and quantification

Raw data were processed using Compound Discoverer v3.4 (Thermo Scientific) coupled with Lipid search workflow using the following parameters: m/z tolerance for precursor mass selection set to 5 ppm; minimum peak intensity threshold 30,000; S/N threshold set to 1.5; Peak rating threshold set to 0.4; Gap fill enabled with a 1.5 S/N threshold, 3 minimum scans per peak. For lipid identification, triacylgylcerols, diacylglycerols were identified as [M + NH4]+ adducts. Lysophosphatidylcholines, and acyl-, ether- and vinyl ether-PC, acylcarnitines, ceramides, cardiolipins and sphingomyelins were analyzed as [M + H]+ adducts. Lysophosphatidylethanolamines, and acyl-, ether- and vinyl ether-PE, phosphatidylserines, phosphatidylinositols and phosphatidylglycerol were analyzed as [M−H]- adducts. Acyl-, ether- and vinyl ethers were identified as [M−H]- adducts (28). Quantification was performed by peak integration of the extracted ion chromatograms of

most common ion adducts. Peak integration was first performed by CD then manually curated and adjusted. Identified lipids were normalized to peak areas of added internal standards to decrease analytical variation. Raw lipidomics data were analyzed using Compound Discoverer and exported as .csv files and plotted in GraphPad Prism 11.0.0 (GraphPad Software).

Results and Discussion

This study was designed as a coarse search for changes in lipid composition between WT and Δphz cells grown under phenazine-producing conditions. As expected, both WT and Δphz cells had reached late stationary phase when they were harvested at 20 h. At this time point, the WT cultures had produced an average of 35.4 ± 1.4 μM PCA, 55.7 ± 2.0 μM PYO, and 1.7 ± 0.1 μM PCN, and no phenazines were detectable in the supernatant of Δphz cultures (**Table 2**).

Table 2: Cell densities and measured extracellular phenazine concentrations from the cultures used in this study. Cells were grown to late stationary phase (20hr) in aerobic LB medium at 37 °C. Phenazine concentrations were measured by HPLC as described above. No phenazines were detectable in Δphz samples. Averages are reported ± the standard error.

Sample	OD_{500}	[PCA] μM	[PYO] μM	[PCN] μM
WT1	4.2	37.7	54.3	1.7
WT2	4.4	36.4	57.2	1.9
WT3	3.9	36.1	60.3	1.8

WT4	4.2	31.2	51.1	1.6
Average WT	**4.2**	**35.4 ± 1.4**	**55.7 ± 2.0**	**1.7 ± 0.1**
Δphz1	4.2	-	-	-
Δphz2	4.5	-	-	-
Δphz3	4.3	-	-	-
Δphz4	4.4	-	-	-
Average Δphz	**4.4**	**-**	**-**	**-**

LCMS lipidomics data was normalized in two separate ways: first to give a sense of relative lipid contents between strains, and second to reveal within-strain enrichments in individual lipids. To determine the lipid abundance differences between strains, we normalized lipid ion counts based on the assumption that the number of cells present in the different experimental conditions are the same. In this scheme, a larger ion count for a particular lipid class than the mean signal for that class indicates an enhanced abundance of that lipid.

While WT and Δphz cells do not grow significantly differently, Δphz generally does exhibit a slight growth advantage and OD_{500} values are not directly comparable between strains. These caveats notwithstanding, what does appear to be the case based on between-strain normalization is that WT cells produce more of essentially all measured lipid types than Δphz cells (**Figure 2)**. Considering the slight growth advantage of Δphz cells relative to WT, this normalization likely underestimates the difference between the strains, suggesting this result

is robust. In future experiments, normalizing to colony forming units or total protein measured by Bradford assay could prove more accurate than relying on OD measurements. Increased lipid production was found to be a hallmark of *P. aeruginosa* strains resistant to quaternary ammonium antibiotics, but the same effect was not noted for chloramphenicol resistant cells (29). In general, lipid bilayers cannot increase substantially in thickness because of the physicochemical forces holding the membrane together. The increased lipid abundance thus implies the possibility of morphological changes to WT *P. aeruginosa* cells compared to their Δphz counterparts. One possibility is that cells increase their surface area by elongation. Alternatively, cells could create outer membrane vesicles that extend outward and eventually separate from the surface of an otherwise normal cell. If vesicles containing high concentrations of reduced PYO diffused to an oxic zone, they would presumably release their phenazine "payload," either poisoning nearby competitors in an environmental niche or causing damage to host cells in an infection context. Electron microscopy observations may reveal morphological changes to the cell envelope and could also be used to look for outer membrane vesicles.

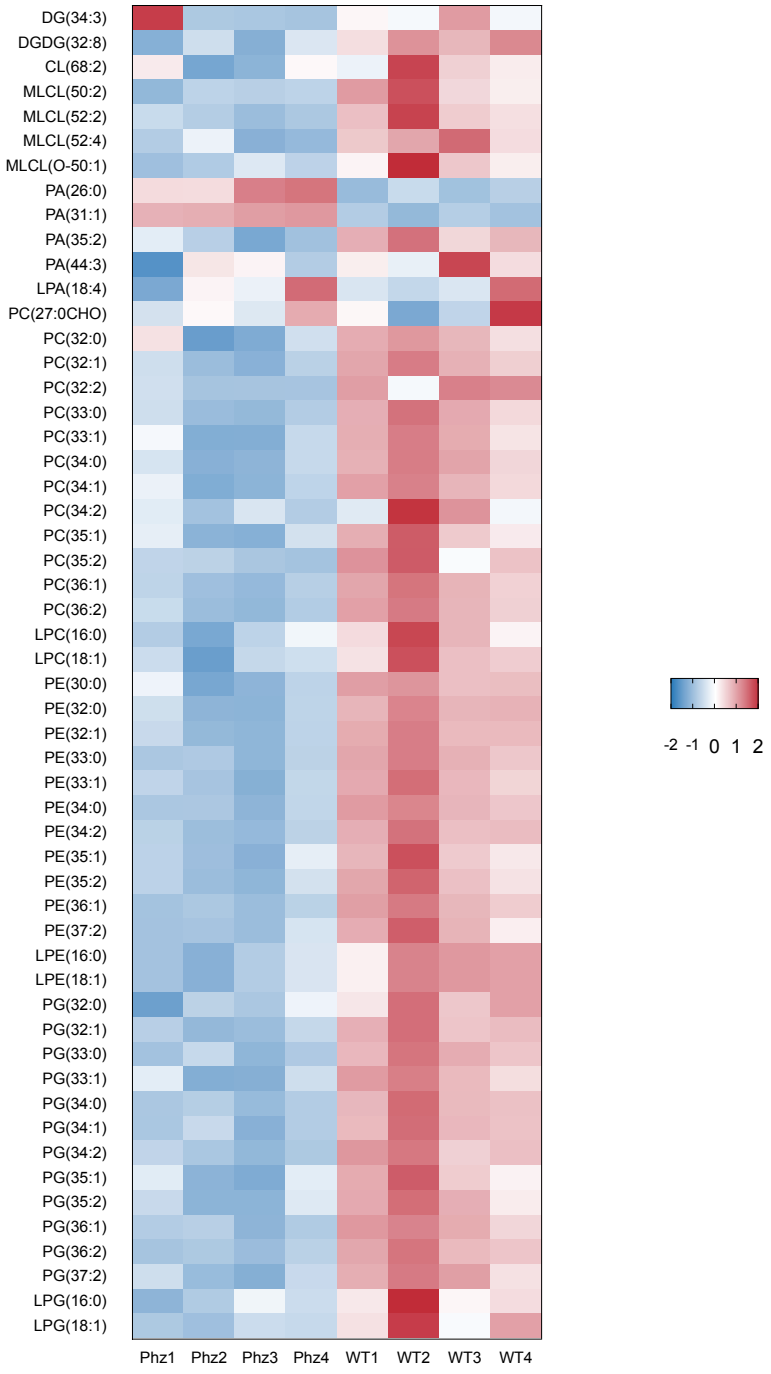

Figure 2: Stationary phase WT cells exposed to endogenous phenazines possess more total lipids than Δphz cells exposed to no phenazines. The z-score shown in the heat map is calculated according to $z = \frac{x-\mu}{\sigma}$ where x is the raw ion count for that lipid class, μ is the population mean across all 8 samples for that lipid class, and σ is the standard deviation of the

population. For this analysis, culture density was presumed to be the same in both conditions so that ion counts could be compared as a proxy for lipid abundance. This likely represents a slight underestimation of Δphz densities and thus likely results in a slight underestimation of the difference between the lipid composition of the strains. All lipids are named according to the nomenclature described in the Lipid Nomenclature section above. Associated headgroup structures appear in Table 1.

To determine whether the general increased lipid abundance seen in the WT cells is a simple scaling of the same lipid composition observed in the Δphz cells, we normalized the ion counts from individual lipid classes to the total lipid ion count within each replicate (**Figure 3**). This normalization gives a sense of relative enrichments of specific lipids within each strain. The resulting heat map demonstrates significant differences between the WT and Δphz lipid ratios, indicating substantially different lipid compositions at the 20 h time point. For example, Δphz cells appear to possess proportionally more diacylglycerol DG(34:3) and cardiolipin CL(68:2) than WT cells. Similarly, Δphz cells appear to generally favor phosphatidic acid (PA) derivatives compared to their WT counterparts. The relative enrichment of PA(26:0) and PA(31:1) in Δphz cells is particularly notable given these are the only two lipids measured at higher abundance in Δphz cells than in WT cells. While more granular data is not available for every lipid measured, we were able to positively identify the acyl chains of PA(26:0) as 14:0 and 16:0 and those of PA(31:1) as 17:0, and 14:1(9Z).

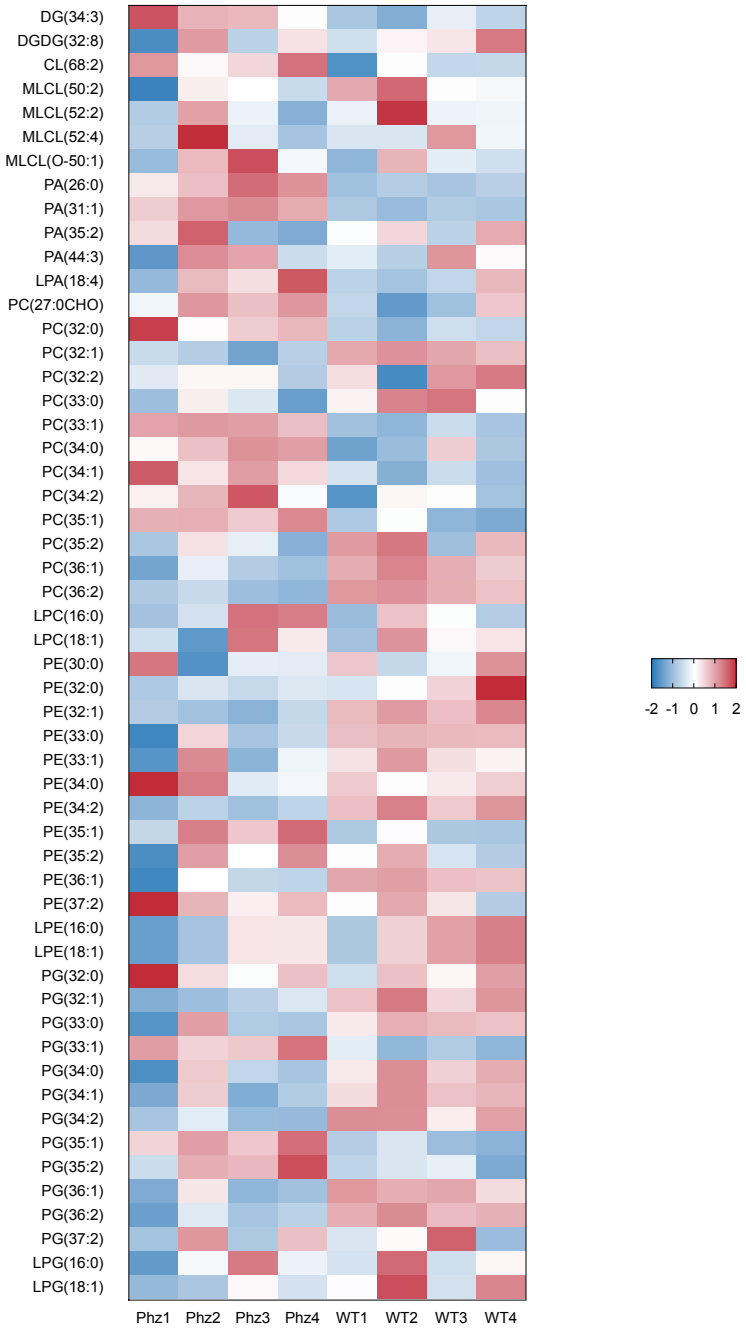

Figure 3: Stationary phase WT cells exposed to endogenous phenazines possess different ratios of lipids than Δphz cells exposed to no phenazines. Lipid abundances are normalized by dividing the ion count for the given lipid class by the total ion count of that sample. Following this calculation, the z-score depicted is then calculated using the mean (μ) and standard deviation (σ) of all 8 samples according to $z = \frac{x-\mu}{\sigma}$.

Internally normalized ratios of phosphatidylcholine (PC) and phosphatidylethanolamine (PE) suggest that Δphz cells and WT cells accumulate different ratios of these lipids based on acyl chain identity. Broadly, WT cells appear to favor PC(32:1), (32:2), and (33:0) as well as (35:2), (36:1), and (36:2). Δphz cells by contrast display enrichments in PC (32:0), (33:1), (34:0), (34:1), (34:2), and (35:1). Existing lipidomics studies report phosphatidylethanolamine as the dominant lipid type in *P. aeruginosa* cells grown under a variety of conditions (Hancock et al. Benamara et al.). In our experiment, WT cells are enriched relative to Δphz cells in all measured PE and lyso-phosphatidylethanolamine (LPE) species except PE (35:1) and PE (35:2). Phosphatidylglycerol enrichments follow a similar pattern: WT cells are enriched in nearly all measured PG species with the notable exceptions of PG (35:1) and PG (35:2). WT cells also possess a smaller proportion of PG (33:1) than their Δphz counterparts.

I will avoid interpreting these preliminary results, including the apparent preferences for specific fatty acyl chain lengths, too closely for a few reasons. First, the extraction protocol observed in this study might have suffered from the unwanted action of lipases and phospholipases that remained active during the PBS washes prior to lipid extraction with methyl tert-butyl ether (30). The resulting unintentional modification of the lipid pool, including potentially significant levels of deacylation, means that significant information might have been lost during the initial preparation of harvested cells. Because the abundance, activity, and selectivity of the lipases between the two strains are unknown, modifications to the WT pool could have been very different from those to the

Δphz pool. Second, the methods for identifying lipids in this study, including the internal standards used, reflect lipids found in eukaryotic cells and give no detailed information about some *P. aeruginosa*-specific lipids like cyclopropanated fatty acids, which are known to be abundant in stationary phase cells (2, 3). Finally, the normalization protocols used here can be improved upon by using total protein or a count of viable cells rather than a simple OD measurement. Nevertheless, there are clear differences in both the sheer abundance of lipid molecules and in the ratios of the types of lipids between the WT and Δphz groups. In broad strokes, this implies that the presence or production of phenazines has measurable consequences for the lipidome.

The observed differences in the lipid profiles between these conditions could conceivably stem from several different causes. First, the lipidome changes in WT cells could be the direct result of phenazine-mediated regulatory changes. Pyocyanin activates SoxR, which upregulates efflux pumps, but it is also a terminal signaling factor, causing regulatory changes in dozens of genes, many of which remain unannotated (13, 19). As noted above, two of these unannotated proteins are similar to orthologs that appear to interact with lipids, suggesting pyocyanin could be playing a direct role in modifying the lipidome. Given several of the up- and down-regulated genes detected after pyocyanin exposure are still completely unannotated, their involvement in lipid synthesis, modification, or degradation remains to be determined. Similar regulatory data for PCA shows that it too changes gene regulation in exponential PA14 cultures. Perhaps these three phenazines regulate a small orchestra of genes that tune the membrane based on the specific phenazine cocktail present under a given condition.

Alternatively, phenazines could indirectly affect membrane composition by changing important properties of the membrane or of membrane-associated proteins such that the cell senses the disturbance and responds in a more generic way. For example, if the presence of phenazines disrupts lipid-lipid interactions and thus makes the membrane more or less fluid, perhaps a nonspecific regulatory response to saturate or cyclopropanate lipids could counteract those effects in a phenazine-agnostic way. Or if, as has been suggested in infected human host cell lipids, phenazines provoke damaging lipid peroxidation in the producer cell, perhaps a non-specific lipid repair response takes over and modifies the lipid pool to limit further damage.

When considering phenazine effects on lipid-lipid interactions and bulk membrane properties, it might be possible to draw lessons from eukaryotic membrane modifications. In eukaryotic cells, rigid, planar, polycyclic sterols like cholesterol promote the formation of distinct membrane microdomains, also known as lipid rafts, by drawing saturated acyl chains more closely together, increasing bilayer density and rigidity (31). These lipid rafts typically contain flotillin proteins, which recruit lipid-raft-associated enzymes that are often implicated in signaling pathways. Bacterial lipid rafts have also been observed, and are often stabilized by polycyclic isoprenoid lipids called hopanoids (32, 33). As in eukaryotic cells, these microdomains are more compact and rigid than the rest of the cell membrane, and they contain flotillin proteins (34).

Like cholesterol and hopanoids, unsubstituted phenazine is polycyclic and lipophilic. In its oxidized state, the pyrazine core of all phenazines is strictly planar, and although its reduced form adopts a slight bend at the reduced bridging nitrogens, the ring structure remains rigid and lipophilic. Given the high concentration of reduced PYO found in the

P. aeruginosa membrane, it may be that phenazines play some rafting role in the membrane, rigidifying portions of the membrane, altering membrane permeability, and potentially solvating proteins.

Examining expression levels of *P. aeruginosa* native FloA and FloT flotilins under phenazine producing conditions may provide information about their relevance when phenazines are prevalent in the membrane (34). Given the observation that *B. subtilis* biofilm formation is dependent on a functional membrane-associated protein that in turn depends on polycyclic isoprenoid lipids that likely form rafts, it is also worth considering whether there are signaling pathways in *P. aeruginosa* that depend on phenazine rafts or phenazine-lipid rafts (32). The clear regulatory difference between wild type colony biofilms and biofilms formed by Δphz cells may be a starting point for such an investigation (35).

In general, lipid rafts are difficult to isolate completely but are significantly enriched in the detergent-resistant fraction of membrane extracts (32). Conducting a membrane fractionation in the presence of a reducing agent and a phenazine may provide direct access to lipid domains rigidified by phenazine interactions, but the presence of detergents might also disrupt the *in vivo* phenazine interactions of primary interest. Measurements of biophysical membrane properties using fluorescent dyes are likely to encounter confounding effects from the absorption and fluorescence emission spectra of reduced phenazines, but direct measurements using atomic force microscopy could circumvent this issue (36).

While this study and the experimental work described in Chapter 2 made no attempt to separate the inner and outer leaflets of *P. aeruginosa* to quantify the relative

concentrations of phenazines in those two domains, a precise understanding of phenazine localization within these different membranes will undoubtedly assist the determination of any biological function. Physical separation of these leaflets is possible, but the required disruption by detergents and the separation via density gradients may complicate any interpretation of the results. Molecular dynamics simulations of phenazines in *P. aeruginosa* membrane lipids may make a complementary localization investigation possible *in silico*, and could also reveal spatial orientation and location within a bilayer, which is not currently possible to observe directly (37). Phenazine partition experiments conducted with micelles composed of individual lipid components found in the *P. aeruginosa* membrane may offer additional information about the specific lipids with which phenazines preferentially associate (38).

A provocative but unexplored hypothesis is that rather than acting as a toxin, phenazines concentrated in the membrane could be playing an essential role in the stationary phase cell's respiratory chain. P. aeruginosa phenazines have been shown to oxidize dehydrogenase enzymes and reduce quinones (17), suggesting they might participate as intracellular electron shuttles, perhaps in a way that is beneficial only when oxygen or nutrients are limited. The large concentration of reduced PYO measured in the membrane would certainly affect the thermodynamics of electron transfer reactions by increasing the reaction quotient for any electron transfer from reduced PYO to another species (perhaps a quinone). Because of the proximity of respiratory chain components, recently oxidized (and hence more polar) PYO molecules would presumably be near enough to dehydrogenase enzymes or other reduced membrane components to pick up more electrons before diffusing out of the membrane. This could be especially important if

phenazines are concentrated in lipid rafts surrounding the NADH dehydrogenases. Whatever the precise dynamics, reduced PYO appears to be the dominant form in the membrane by far. What value, if any, is accrued by including this additional step in the electron transport chain remains to be elucidated, but it could conceivably be related to changing the route of PMF generation under challenging conditions. Because phenazine reductions and oxidations are proton-coupled, there could be some proton pumping action in which reduced phenazines translocate protons within the membrane or from the interior of the membrane to the exterior, although this hypothesis runs counter to the observation that PYO causes a net reduction in *P. aeruginosa* membrane potential. Our current understanding of phenazine interactions in the cell envelope are summarized in **Figure 4**.

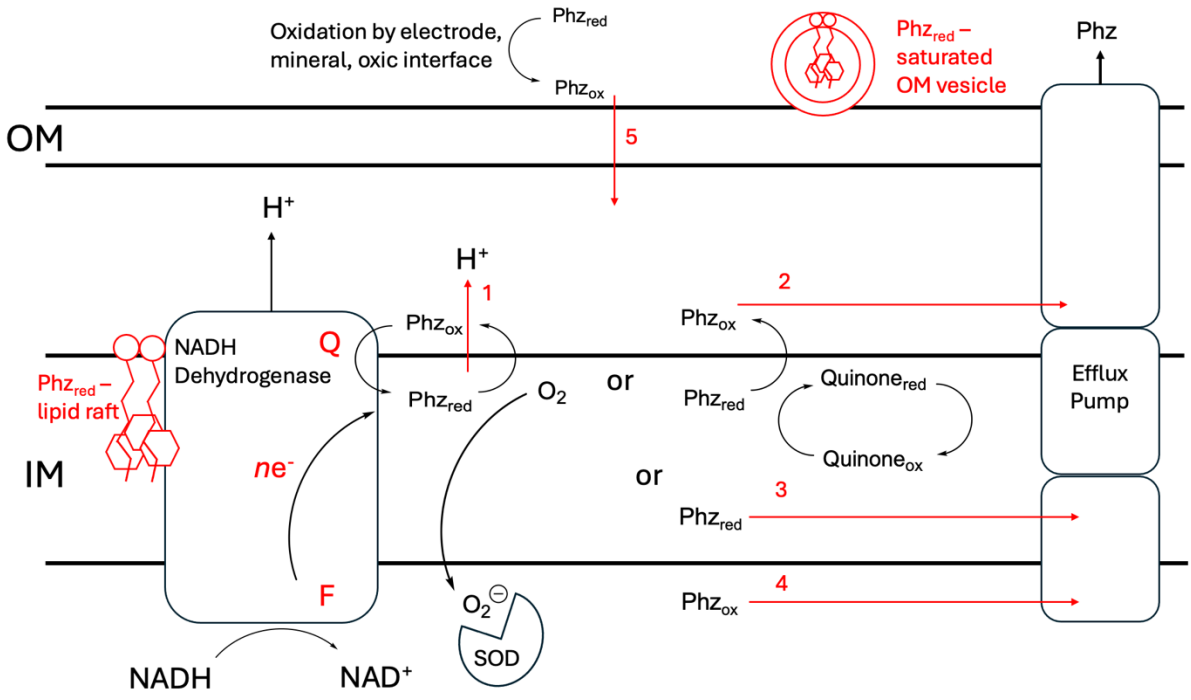

Figure 4: Current knowledge and outstanding questions regarding phenazine interactions in the membrane. Outer and inner membranes are denoted by OM and IM,

respectively. Red denotes structures and steps that are hypothesized but not characterized. In general, our current understanding is that phenazines are reduced by NADH dehydrogenases in the inner membrane and are pumped out of the cell by efflux pumps in the Mex family (16, 17, 19), although the high concentration of PYO observed in the membrane fraction (including both IM and OM) in Chapter 2 suggests this model is incomplete. The components of the figure, beginning at the left side of the inner membrane and working counter-clockwise, highlight the following gaps in knowledge: The existence and possible enzyme-solvating effects of phenazine-lipid rafts in the inner or outer membrane are open questions motivated by the work of this thesis. Within the dehydrogenase complexes known to transfer electrons to phenazines, the precise binding location of the phenazines (Q denotes a quinone binding site, while F denotes a flavin binding site) and the number of electrons transferred per step (ne^-) are not well understood, although phenazines in the membrane are thought to exist in their fully reduced forms (following two electron, two proton reduction) because the semiquinone forms are not known to be kinetically stable, and membrane interactions are unlikely to improve the stability of these radicals. Arrow 1 suggests the possibility that phenazine reduction and re-oxidation in the membrane and periplasmic space, respectively, could contribute to proton pumping, contributing to the formation of a proton motive force. While theoretically possible, this hypothesis runs counter to the observation that PYO causes a net lowering of the membrane potential in *P. aeruginosa* (39) Reduced phenazines in the membrane may reduce oxygen, forming superoxide, or may reduce benzoquinone, as has been observed *in vitro (*17). Phenazines are transported by efflux pumps, but whether the pumps express a particular affinity for reduced or oxidized phenazines is not known (13, 19). Another open question is the precise location from which phenazines are pumped; they may conceivably be

pumped either from the periplasm, from the membrane, or from the cytosol (arrows 2-4). While phenazines do leave the cell via active pumping, the increased lipid abundance observed in phenazine-producing WT cells suggests either a geometric change in cell morphology to increase membrane area, or the formation of outer membrane vesicles, which could be formed of phenazine-lipid rafts. Finally, while phenazines are known to support anaerobic survival through extracellular electron transport, it remains unclear whether oxidized phenazines re-enter the cell through abiotic diffusion, through a passive transport mechanism like a porin, or through some form of active transport (arrow 5).

Disentangling the detailed causes and effects of phenazine influence on the *P. aeruginosa* lipidome will require controlled studies using Δphz mutants provided with known concentrations of phenazine, alone and in combination, and possibly at various stages of growth. The gold standard, capable of removing confounding effects of oxygen concentration, nutrient availability, and growth state, would be a set of chemostat experiments in which cells growing at a constant rate are consistently supplied with fresh medium containing known concentrations of nutrients, oxygen, and phenazine. Alternatively, a phenazine-dependent, oxygen-free, growth-arrested state like the survival assay described in Chapter 5 could prove an excellent context for understanding non-growth metabolic turnover through lipid degradation or synthesis, especially using thoughtful incorporation of either deuterium or carbon labels.

Whatever growth or non-growth experimental state is chosen, strict control over cell metabolic state and concentrations of nutrients, oxygen, and phenazine is essential, as is immediate quenching of unwanted lipase and phospholipase activity in harvested cells.

This can be accomplished with cycloheximide, or another strong protein inhibitor, or by quenching cells in boiling ethanol for 15 minutes or by flash freezing then freeze drying prior to extraction (30). Finally, developing a lipidomics analysis protocol calibrated to detect and quantify specific *P. aeruginosa* lipids, including cyclopropanated fatty acids that are known to play important roles in membrane properties, should grant more solid insight into the effect these "extracellular" phenazine metabolites have when they accumulate intracellularly.

References

1. Lugtenberg, B., & Van Alphen, L. (1983). Molecular architecture and functioning of the outer membrane of *Escherichia coli* and other gram-negative bacteria. *Biochimica et Biophysica Acta (BBA) – Reviews on Biomembranes, 737*(1), 51–115. https://doi.org/10.1016/0304-4157(83)90014-X
2. Hancock, I. C., & Meadow, P. M. (1969). The extractable lipids of *Pseudomonas aeruginosa*. *Biochimica et Biophysica Acta (BBA) – Lipids and Lipid Metabolism, 187*(3), 366–379. https://doi.org/10.1016/0005-2760(69)90010-1
3. Benamara, H., Rihouey, C., Abbes, I., Ben Mlouka, M. A., Hardouin, J., Jouenne, T., & Alexandre, S. (2014). Characterization of membrane lipidome changes in *Pseudomonas aeruginosa* during biofilm growth on glass wool. *PLOS ONE, 9*(9), e108478. https://doi.org/10.1371/journal.pone.0108478
4. Kaur M., Mozaheb N., Paiva T.O., Herent M., Goormaghtigh F., Paquot A., Terrasi R ., Mignolet E., Décout J., Lorent J.H., Larondelle Y., Muccioli G.G., Quetin-Leclercq J., Dufrêne Y.F., Mingeot-Leclercq M. (2024). Insight into the outer

membrane asymmetry of *P. aeruginosa* and the role of MlaA in modulating the lipidic composition, mechanical, biophysical, and functional membrane properties of the cell envelope. *Microbiol Spectrum,* 12:e01484-24. https://doi.org/10.1128/spectrum.01484-24

5. Mitchison-Field, L. M. Y., & Belin, B. J. (2023). Bacterial lipid biophysics and membrane organization. *Current Opinion in Microbiology, 75*, 102315. https://doi.org/10.1016/j.mib.2023.102315

6. Mozaheb N. , Rasouli P. , Kaur M. , Van Der Smissen P., Larrouy-Maumus G., Mingeot-Leclercq M. 2023. A Mildly Acidic Environment Alters *Pseudomonas aeruginosa* Virulence and Causes Remodeling of the Bacterial Surface. Microbiol Spectrum.11:e04832-22. https://doi.org/10.1128/spectrum.04832-22

7. Rebekah A Jones, Holly Shropshire, Caimeng Zhao, Andrew Murphy, Ian Lidbury, Tao Wei, David J Scanlan, Yin Chen, Phosphorus stress induces the synthesis of novel glycolipids in *Pseudomonas aeruginosa* that confer protection against a last-resort antibiotic, *The ISME Journal*, Volume 15, Issue 11, November 2021, Pages 3303–3314, https://doi.org/10.1038/s41396-021-01008-7

8. Lyon, R., Jones, R.A., Shropshire, H., Aberdeen, I., Scanlan, D.J., Millard, A. et al. (2022) Membrane lipid renovation in Pseudomonas aeruginosa - implications for phage therapy? Environmental Microbiology, 24(10), 4533–4546. https://doi.org/10.111/1462-2920.16136.

9. Ezeduru, V., Shao, A. R., Venegas, F. A., McKay, G., Rich, J., Nguyen, D., & Thibodeaux, C. J. (2024). Defining the functional properties of cyclopropane fatty

acid synthase from *Pseudomonas aeruginosa PAO1*. *Journal of Biological Chemistry*, *300*(9). 10.1016/j.jbc.2024.107618

10. David, P. (2015). A Ring to Rule Them All: The Effect of Cyclopropane Fatty Acids on the Fluidity of Lipid Bilayers. 10.1021/acs.jpcb.5b00958
11. Dufourc, E. J., Smith, I. C., & Jarrell, H. C. (1983). A 2H-NMR analysis of dihydrosterculoyl-containing lipids in model membranes: structural effects of a cyclopropane ring. *Chemistry and Physics of Lipids*, *33*(2), 153-177.https://doi.org/10.1016/0009-3084(83)90019-1
12. Dufourc, E. J., Smith, I. C., & Jarrell, H. C. (1984). The role of cyclopropane moieties in the lipid properties of biological membranes: a deuterium NMR structural and dynamical approach. *Biochemistry*, *23*(10), 2300-2309.https://doi.org/10.1021/bi00305a033
13. Dietrich, L. E. P., Price-Whelan, A., Petersen, A., Whiteley, M., & Newman, D. K. (2006). The phenazine pyocyanin is a terminal signalling factor in the quorum sensing network of *Pseudomonas aeruginosa*. *Molecular Microbiology, 61*(5), 1308–1321. https://doi.org/10.1111/j.1365-2958.2006.05306.x
14. Saunders, S. H., Edmund, C. M., Yates, M. D., Otero, F. J., Trammell, S. A., Stemp, E. D., ... & Newman, D. K. (2020). Extracellular DNA promotes efficient extracellular electron transfer by pyocyanin in *Pseudomonas aeruginosa* biofilms. *Cell*, *182*(4), 919-932. https://doi.org/10.1016/j.cell.2020.07.006
15. Li, J., Squyres, G. R., Duong, K., Reichhardt, C., Parsek, M. R., & Newman, D. K. (2026). Extracellular matrix chemistry tunes bacterial biofilm metabolism and

optimizes fitness. *Proceedings of the National Academy of Sciences*, *123*(15), e2528666123. https://doi.org/10.1073/pnas.2528666123

16. Glasser, N. R., Wang, B. X., Hoy, J. A., & Newman, D. K. (2017). The pyruvate and α-ketoglutarate dehydrogenase complexes of *Pseudomonas aeruginosa* catalyze pyocyanin and phenazine-1-carboxylic acid reduction via the subunit dihydrolipoamide dehydrogenase. *Journal of Biological Chemistry*, *292*(13), 5593-5607.https://doi.org/10.1074/jbc.M116.772848

17. Ciemniecki, J. A., & Newman, D. K. (2023). NADH dehydrogenases are the predominant phenazine reductases in the electron transport chain of *Pseudomonas aeruginosa*. *Molecular microbiology*, *119*(5), 560-573. https://doi.org/10.1111/mmi.15049

18. Palma, M., Zurita, J., Ferreras, J. A., Worgall, S., Larone, D. H., Shi, L., ... & Quadri, L. E. (2005). *Pseudomonas aeruginosa* SoxR does not conform to the archetypal paradigm for SoxR-dependent regulation of the bacterial oxidative stress adaptive response. *Infection and immunity*, *73*(5), 2958-2966. 10.1128/IAI.73.5.2958-2966.2005

19. Sakhtah H, Koyama L, Zhang Y, et al. The *Pseudomonas aeruginosa* efflux pump MexGHI-OpmD transports a natural phenazine that controls gene expression and biofilm development. Proceedings of the National Academy of Sciences of the United States of America. 2016 Jun;113(25):E3538-47. DOI: 10.1073/pnas.1600424113.

20. Thalhammer, K. O., Scurria, M. Li, J. Trindade, I. B., Gutierrez, O., Conway, S. J., & Newman, D. K. (2026). Redox-dependent lipophilicity of phenazine metabolites

is modulated by intramolecular hydrogen bonds and controls their biological distribution. *bioRxiv,* 2026-04. https://doi.org/10.64898/2026.04.18.719255

21. Unden, G., & Bongaerts, J. (1997). Alternative respiratory pathways of *Escherichia coli*: energetics and transcriptional regulation in response to electron acceptors. *Biochimica et Biophysica Acta (BBA)-Bioenergetics*, *1320*(3), 217-234. https://doi.org/10.1016/S0005-2728(97)00034-0

22. Chen, E. H. L., Wang, C. H., Liao, Y. T., Chan, F. Y., Kanaoka, Y., Uchihashi, T., ... & Chen, R. P. Y. (2023). Visualizing the membrane disruption action of antimicrobial peptides by cryo-electron tomography. *Nature Communications*, *14*(1), 5464.https://doi.org/10.1038/s41467-023-41156-2

23. Valdez-Lara, A. G., Jaramillo-Granada, Á. M., Ortega-Zambrano, D., García-Marquez, E., García-Fajardo, J. A., Mercado-Uribe, H., & Ruiz-Suárez, J. C. (2025). Disruption of biological membranes by hydrophobic molecules: a way to inhibit bacterial growth. *Frontiers in microbiology*, *15*, 1478519. https://doi.org/10.3389/fmicb.2024.1478519

24. Thees AV, Pietrosimone KM, Melchiorre CK, Marden JN, Graf J, Lynes MA, Maltz-Matyschsyk M. PmtA Regulates Pyocyanin Expression and Biofilm Formation in *Pseudomonas aeruginosa*. Front Microbiol. 2021 Nov 15;12:789765. doi: 10.3389/fmicb.2021.789765.

25. Caprari, S., Brandi, V., Pasquadibisceglie, A., & Polticelli, F. (2020). Uncovering the structure and function of *Pseudomonas aeruginosa* periplasmic proteins by an *in silico* approach. *Journal of Biomolecular Structure and Dynamics*, *38*(15), 4508–4520. https://doi.org/10.1080/07391102.2019.1683468

26. Imperi, F., Ciccosanti, F., Perdomo, A.B., Tiburzi, F., Mancone, C., Alonzi, T., Ascenzi, P., Piacentini, M., Visca, P. and Fimia, G.M. (2009), Analysis of the periplasmic proteome of *Pseudomonas aeruginosa*, a metabolically versatile opportunistic pathogen. Proteomics, 9: 1901-1915. https://doi.org/10.1002/pmic.200800618

27. Matyash, V., Liebisch, G., Kurzchalia, T. V., Shevchenko, A., & Schwudke, D. (2008). Lipid extraction by methyl-tert-butyl ether for high-throughput lipidomics. *Journal of Lipid Research, 49*(5), 1137–1146. https://doi.org/10.1194/jlr.D700041-JLR200

28. Lange, M., Angelidou, G., Ni, Z., Criscuolo, A., Schiller, J., Blüher, M., & Fedorova, M. (2021). AdipoAtlas: A reference lipidome for human white adipose tissue. *Cell Reports Medicine*, *2*(10). https://doi.org/10.1016/j.xcrm.2021.100407

29. E. A. Anderes, W. E. Sandine, and P. R. Elliker. 1971. Lipids of antibiotic-sensitive and -resistant strains of *Pseudomonas aeruginosa*. *Canadian Journal of Microbiology*. **17**(11): 1357-1365. https://doi.org/10.1139/m71-217

30. Ratledge, C., & Wilkinson, S. G. (1988). *Microbial Lipids* (Vol. 1, pp. 16–18). Academic Press.

31. Silvius, J. R. (2003). Role of cholesterol in lipid raft formation: lessons from lipid model systems. Biochimica et Biophysica Acta (BBA) - Biomembranes, 1610(2), 174–183. https://doi.org/10.1016/s0005-2736(03)00016-6

32. Bramkamp, M., & Lopez, D. (2015). Exploring the Existence of Lipid Rafts in Bacteria. Microbiology and Molecular Biology Reviews, 79(1), 81–100. https://doi.org/10.1128/mmbr.00036-14

33. Sáenz, J. P., Sezgin, E., Schwille, P., & Simons, K. (2012). Functional convergence of hopanoids and sterols in membrane ordering. Proceedings of the National Academy of Sciences, 109(35), 14236–14240. https://doi.org/10.1073/pnas.1212141109

34. Álvarez-Mena, A., Morvan, E., Martinez, D., Berbon, M., Savietto Scholz, A., Grélard, A., Turpin, S., Dufourc, E. J., Bramkamp, M., & Habenstein, B. (2025). Bacterial flotillins as destabilizers of phospholipid membranes. Biochimica et Biophysica Acta (BBA) - Biomembranes, 1867(1), 184399. https://doi.org/10.1016/j.bbamem.2024.184399

35. Ramos, I., Dietrich, L. E. P., Price-Whelan, A., & Newman, D. K. (2010). Phenazines affect biofilm formation by *Pseudomonas aeruginosa* in similar ways at various scales. Research in Microbiology, 161(3), 187–191. https://doi.org/10.1016/j.resmic.2010.01.003

36. Robinson, M., Filice, C. T., McRae, D. M., & Leonenko, Z. (2023). Atomic force microscopy and other scanning probe microscopy methods to study nanoscale domains in model lipid membranes. Advances in Physics: X, 8(1). https://doi.org/10.1080/23746149.2023.2197623

37. Li, A., Schertzer, J. W., & Yong, X. (2018). Molecular dynamics modeling of *Pseudomonas aeruginosa* outer membranes. Physical Chemistry Chemical Physics, 20(36), 23635–23648. https://doi.org/10.1039/c8cp04278k

38. Yeagle, P. L., & Young, J. E. (1986). Factors contributing to the distribution of cholesterol among phospholipid vesicles. Journal of Biological Chemistry, 261(18), 8175–8181. https://doi.org/10.1016/s0021-9258(19)83893-0

39. Horak, R. D., Ciemniecki, J. A., & Newman, D. K. (2024). Bioenergetic suppression by redox-active metabolites promotes antibiotic tolerance in *Pseudomonas aeruginosa*. Proceedings of the National Academy of Sciences, 121(46). https://doi.org/10.1073/pnas.2406555121

Chapter 4

METHODS FOR RESPIROMETRY IN *PSEUDOMONAS AERUGINOSA* PA14

Abstract

If, as appears to be the case for PYO, lipophilic phenazines accumulate in the cell, it stands to reason that they have physiological effects there. The cell has clearly evolved to manage phenazine-associated redox damage, but, through interactions with the electron transport chain (ETC), phenazines may actually be playing a beneficial role that has not been fully described. To enable direct interrogations of the respiratory effects of phenazines, we developed methods for detecting oxygen consumption by respiring *P. aeruginosa* cells. Methodological details developed in this chapter will likely prove useful for those wishing to probe the phenazine-ETC connection further, perhaps by combining respiratory chain mutants and chemical inhibitors with phenazine treatments.

Introduction

In addition to raising questions about the *P. aeruginosa* lipidome, the high concentration of reduced PYO observed in the *P. aeruginosa* cell membrane raises the possibility that it has an evolved function in that part of the cell. Friedheim first referred to PYO as an "accessory respiratory enzyme" in 1931, in recognition of the PYO-mediated increase in respiration rates across various species. Friedheim concluded that PYO appeared to interact with cytochromes or some other component of the respiratory chain that is inhibited by cyanide and carbon monoxide (1). In other species, this respiration rate increase, which both upsets cellular redox balance and produces reactive oxygen species, has long been considered deleterious and is cited as a facet of pyocyanin's function as a virulence factor (2, 3). Similar functions have also made the compound attractive as a potential cancer treatment (4).

But within the *P. aeruginosa* cell, only relatively recently has detailed work begun to illuminate exactly where and how PYO and the other endogenous phenazines PCA and PCN react with components of the cell. We now know these phenazines are reduced at different rates and to different extents by various dehydrogenase enzymes found in the membrane (5, 6), and that the reduced species are capable of reducing ubiquinone. But the primary dehydrogenases do not account for all of the reduction observed in vitro, and ubiquinone reduction certainly does not appear to be the only electron sink for reduced phenazines, considering their rapid reactions with oxygen and the observed production of reactive oxygen species *in vivo* (3, 7, 8). Our picture of how endogenous phenazines participate in the electron transport chain and exactly what, if any, benefit they provide to cells thus remains incomplete.

To enable future studies on the role of phenazines in the *P. aeruginosa* electron transport chain, we sought to develop techniques for measuring respiration rates under the influence of individual phenazines. Our preliminary investigations revealed several methodological details that may prove useful to future efforts.

Methods and Preliminary Results

Initial experiments relied on a Clark electrode, which measures current in a liquid culture as a proxy for oxygen tension. Initial experiments relied on a Clark electrode, which measures current in a liquid culture as a proxy for oxygen tension. The Clark electrode consists of a platinum working electrode and a silver counter electrode, both submerged in an electrolyte solution and encapsulated in a small tube. Dissolved oxygen crosses a Teflon membrane to enter the tip of the tube, where it is reduced to water using electrons from the electrode and

protons from the surrounding solution. The resulting current is recorded and can be calibrated to known oxygen tensions.

For all experiments, cells were grown in MOPS minimal medium buffered at pH 7.2 and supplemented with 25 mM glucose. Cells were harvested by centrifugation at 6800 rpm for 10 minutes, and the resulting pellets were resuspended at an OD of 10 in PBS at pH 7.0 supplemented with 10 mM glucose and 500 μM EDTA until the experiment was carried out. Multiple short experiments were conducted from the same stock of cells prepared in this fashion, although allowing the cells to rest for more than an hour appeared to alter their metabolic state. We found EDTA aided the penetration of both inhibitors and phenazines, presumably by chelating divalent cations Ca^{2+} and Mg^{2+}, thereby limiting cross linking in the lipopolysaccharide of the cell wall.

Measurements were conducted on the benchtop by placing 4.5 mL of PBS (containing 10 mM glucose) in a small upright tube equipped with a stir bar and inserting the electrode from above to collect a reference baseline of about 30 s. This step often proved to be quite challenging due to our model of the Clark electrode, which was sensitive to electromagnetic fields as slight as those generated by the charging cord of the laptop to which it was attached. After collection of a sufficient baseline, experiments were initiated by carefully pipetting 0.5 mL of dense EDTA-treated cells from the holding tube into the stirred tube to achieve a final OD of 1. In a typical experiment, the respiration of the newly introduced cells caused the measured voltage to drop at a steady rate from the fully oxygenated value (approximately 120 mV) to 0 within about 120 s. Depending on how long the cells had been held before being introduced to the experiment, the voltage sometimes dropped precipitously at first (presumably due to the introduction, along with the cells, of a volume of completely

deoxygenated media) before relaxing to a less intense and generally reproducible rate we attributed to cellular respiration.

Our initial attempts to identify inhibitors for *P. aeruginosa* respiratory chain components revealed no apparent change in respiration rate after treatment with potassium cyanide, sodium arsenate, oligomycin, CCCP, or DCCD (data not shown). Because inhibitors often have horseshoe shaped dose responses with a "goldilocks" concentration of efficacy, we swept a range of about three orders of magnitude for each of these inhibitors ranging from a few μM to a few mM. *P. aeruginosa* is known to have redundant terminal oxidases, which might have explained the inefficacy of cyanide, but we attributed the general lack of any perceivable effect of any of these inhibitors to inconsistent penetration of the cell envelope. Perhaps longer treatment or a different concentration of EDTA prior to measurement could reveal the expected susceptibilities to these inhibitors. It might also be possible that adding TRIS to the buffer system could increase permeability (Glasser, personal communication).

Despite these difficulties, we did find that sodium azide, introduced at an exceptionally high concentration of 20mM, produced near total inhibition of respiration (**Figure 1**) (9). This inhibition manifested as a break from the consistent negative respiration slope to a line of either zero slope or of slightly positive slope. The positive slope was interpreted as the diffusion of atmospheric oxygen back into the partially deoxygenated solution. It is important to note that on certain occasions concentrations of 200mM azide produced almost no effect. There appears to be an aspect of the inhibitor sensitivity that is highly dependent on the precise details of cell preparation ahead of the experiment. Variables we considered (along with parenthetical recommendations) included: length of pregrowth (20 hr or late stationary phase), concentration and length of pretreatment with EDTA (500 μM for 30 min), the

addition of glucose (10 mM glucose did not appear to be necessary, but we used it for consistency. Friedheim noted different respiration rates in the presence of PYO using carbon-free phosphate buffer compared to pyruvate-supplemented buffer), and the length of time cells were allowed to rest in the EDTA solution before an experiment (between 30 and 90 minutes appeared most consistent).

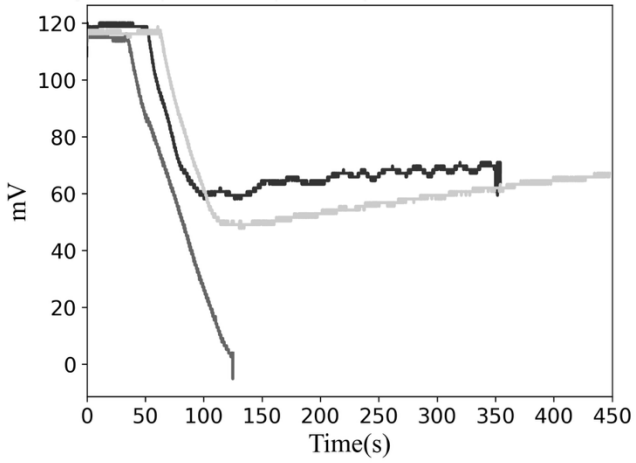

Figure 1: Azide inhibits P. aeruginosa respiration but CCCP has no uncoupling effect. Measurements taken with a Clark electrode in PBS supplemented with 10 mM glucose. After collection of a baseline, cells pretreated with 500 μM EDTA and 10 mM glucose were added to a final OD of 1. The leftmost medium gray line is representative of respiration rates observed in experiments conducted without inhibitors. The lightest gray line reflects respiration by cells treated with 20 mM sodium azide, which was applied at about 110 s. The darkest line shows an experiment in which cells were treated with 20 mM sodium azide at about 90 s and were then provided 100 μM CCCP at about 140 s. Positive slopes were believed to result from diffusion of oxygen back into the slightly deoxygenated buffer.

After determining that sodium azide inhibited *P. aeruginosa* respiration, we began experimenting with the effect of adding phenazines to azide-treated cells. We observed that PCA had no measurable effect, but that PCN was slightly stimulatory (**Figure 2**). Cells treated with PYO had a much more dramatic reaction, switching instantaneously from complete inhibition to consuming oxygen at about one third their pre-azide rate.

We conducted an additional test with the redox active secondary metabolite toxoflavin, produced by *Burkholderia* species *glumae* and *gladioli*. Toxoflavin, like PYO, undergoes redox reactions with cellular components (10). Toxoflavin had an even more significant effect than PYO, essentially returning oxygen consumption to its initial uninhibited rate.

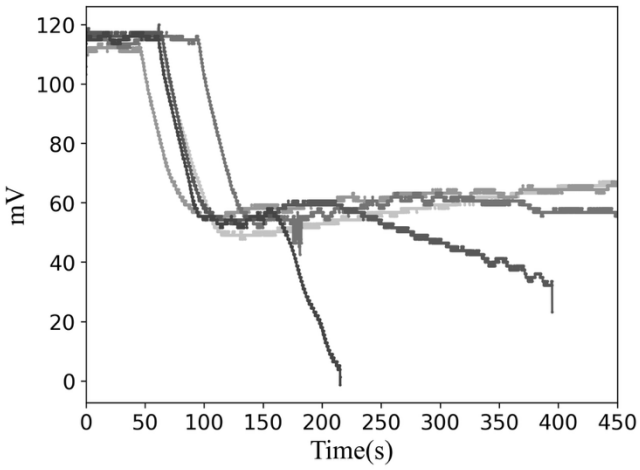

Figure 2: Measurements taken with a Clark electrode in PBS supplemented with 10 mM glucose. After collection of a baseline, cells pretreated with 500 μM EDTA and 10 mM glucose were added to a final OD of 1. In all experiments plotted here, cells were treated with 20 mM azide to inhibit their respiration, which is visible as the break from the initial negative slope to a slightly positive slope. The lightest line represents cells treated with 20mM sodium azide and nothing else. In an attempt to uncouple respiration and overcome the azide inhibition, cells were treated

with various redox active metabolite. Traces in order of increasing darkness represent cells treated with 200μM of either PCA (no visible effect), PCN (slight effect), PYO (major effect), or toxoflavin (largest effect).

Unfortunately, our attempts at generating data of high enough quality to quantify respiration rates reproducibly were thwarted by the sensitivity of the electrode to external interference. We thus ultimately moved to a different and much more stable instrument: the Ocean Optics NeoFox FOSPOR-R oxygen sensor, which relies on a fluorescence system that pulses an excitation LED at an embedded proprietary fluorescent dye encapsulated within a thin metal tube. The tube is open at one end to the experimental solution through a proprietary coating that is ethanol compatible (helpful for sterilization between experiments). We were initially concerned that reduced phenazines might quench the fluorescent probe as has been noted with dissolved dyes, but control experiments conducted in an anaerobic glovebox demonstrated no detectable effect from reduced PCA, PCN or PYO except their reaction with dissolved oxygen in the buffer (**Figure 3**). This probe should enable both higher resolution and significantly better reproducibility than the Clark electrode.

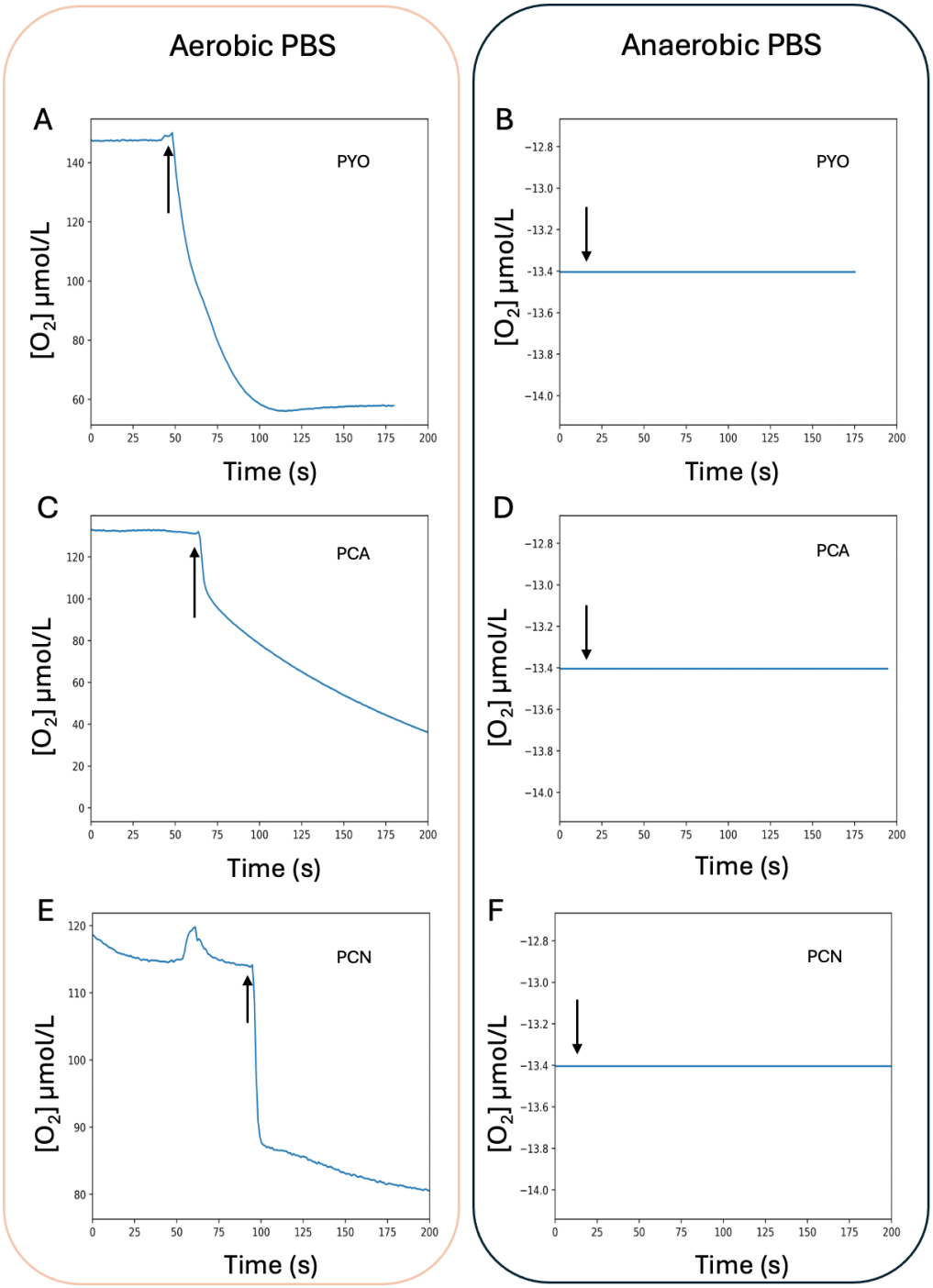

Figure 3: Ocean Optics FOSPOR-R respirometer measures oxygen consumption without interference from reduced phenazines. All panels show oxygen concentration measurements in PBS before and after the addition (black arrows) of a volume of reduced phenazine solution sufficient to achieve a 200µM final concentration (phenazine identity is

reported in the top right of each panel). Panels A, C, and E show measurements made in aerobic buffer. Panels B, D, and F show measurements in anaerobic buffer (N_2 sparged).

Conclusions

We now have a stable platform for measuring oxygen consumption rates in *P. aeruginosa* and other cell suspensions in order to quantify the effects of phenazines on respiration. Azide is a reliable total inhibitor of P. aeruginosa respiration at a concentration of 20 mM, but care must be taken to pretreat cells with EDTA and to use them while they are reasonably fresh. However, azide is known to reduce quinones, which suggests that it might also be able to interact with phenazines or toxoflavin (11). Despite this caveat, our initial work with azide-inhibited P. aeruginosa cells suggests the following order of increasing azide-inhibited respiratory stimulation: PCA < PCN < PYO < toxoflavin. We believe the return to oxygen consumption after treatment with these redox active metabolites represents a decoupling of the respiratory chain in which electrons are transferred onto a phenazine or toxoflavin which then transfers electrons directly onto oxygen, bypassing downstream components of the ETC. The strength of interactions likely relies on a combination of cell penetration to access components of the ETC and oxygen reaction rates. Lipophilicity of the reduced phenazines at pH 7 is PCN > PYO >> PCA, while the speed of reaction with oxygen is PYO >> PCA > PCN (7, 12). PYO possesses both a fast oxygen consumption rate and a favorable lipophilicity, making it an ideal candidate for decoupling the respiratory chain when small amounts of oxygen are present. Identifying and quantifying the relative contributions from components of the respiratory chain remains a challenge that has been partially met through the use of clever biochemical techniques, including the use of specific ETC inhibitors on

genetic mutants with ETC deficiencies (5, 6, 13). Respirometry may be another useful angle on this problem, but given the relative resistance of *P. aeruginosa* to inhibitors, determining the identities and concentrations of effective inhibitors on short respirometry experimental timescales should be explored with an emphasis on promoting cell envelope penetration through the use of buffers and chelating agents.

References

1. Friedheim, E. A. (1931). Pyocyanine, an accessory respiratory enzyme. *The Journal of experimental medicine*, *54*(2), 207.
2. Lau GW, Hassett DJ, Ran H, and Kong F (2004) The role of pyocyanin in *Pseudomonas aeruginosa* infection. Trends Mol Med 10: 599–606.
3. Muller M (2002) Pyocyanin induces oxidative stress in human endothelial cells and modulates the glutathione redox cycle. Free Radic Biol Med 33: 1527–1533.
4. Moayedi, A., Nowroozi, J., & Sepahy, A. A. (2018). Cytotoxic effect of pyocyanin on human pancreatic cancer cell line (Panc-1). *Iranian journal of basic medical sciences*, *21*(8), 794. 10.22038/IJBMS.2018.27865.6799
5. Glasser, N. R., Wang, B. X., Hoy, J. A., & Newman, D. K. (2017). The Pyruvate and α-Ketoglutarate Dehydrogenase Complexes of *Pseudomonas aeruginosa* Catalyze Pyocyanin and Phenazine-1-carboxylic Acid Reduction via the Subunit Dihydrolipoamide Dehydrogenase. Journal of Biological Chemistry, 292(13), 5593–5607. https://doi.org/10.1074/jbc.m116.772848
6. Ciemniecki, J. A., & Newman, D. K. (2023). NADH dehydrogenases are the predominant phenazine reductases in the electron transport chain of *Pseudomonas*

aeruginosa. Molecular Microbiology, 119(5), 560–573. https://doi.org/10.1111/mmi.15049

7. Wang, Y., & Newman, D. K. (2008). Redox Reactions of Phenazine Antibiotics with Ferric (Hydr)oxides and Molecular Oxygen. Environmental Science & Technology, 42(7), 2380–2386. https://doi.org/10.1021/es702290a
8. Rada, B., & Leto, T. L. (2013). Pyocyanin effects on respiratory epithelium: relevance in *Pseudomonas aeruginosa* airway infections. *Trends in microbiology*, *21*(2), 73-81. http://dx.doi.org/10.1016/j.tim.2012.10.004
9. Wilson, D. F., & Chance, B. (1967). Azide inhibition of mitochondrial electron transport I. The aerobic steady state of succinate oxidation. *Biochimica et Biophysica Acta (BBA)-Bioenergetics*, *131*(3), 421-430.
10. Latuasan, H. E., & Berends, W. (1961). On the origin of the toxicity of toxoflavin. *Biochimica et biophysica acta*, *52*(3), 502-508. https://doi.org/10.1016/0006-3002(61)90408-5
11. Hendrix, K., Bleyen, N., Mennecart, T., Bruggeman, C., & Valcke, E. (2019). Sodium azide used as microbial inhibitor caused unwanted by-products in anaerobic geochemical studies. *Applied Geochemistry*, *107*, 120-130. 10.1016/j.apgeochem.2019.05.014
12. Thalhammer, K. O., Scurria, M., Li, J., Trindade, I. B., Gutierrez, O., Conway, S. J., & Newman, D. K. (2026). Redox-dependent lipophilicity of phenazine metabolites is modulated by intramolecular hydrogen bonds and controls their biological distribution. openRxiv. https://doi.org/10.64898/2026.04.18.719255

13. Franco, A., Chukwubuikem, A., Meiners, C., & Rosenbaum, M. A. (2024). Exploring phenazine electron transfer interaction with elements of the respiratory pathways of *Pseudomonas putida* and *Pseudomonas aeruginosa*. *Bioelectrochemistry*, *157*, 108636.

Chapter 5

PRELIMINARY INVESTIGATIONS OF PHENAZINE-MEDIATED REDUCTION OF IRON(III)-BEARING CLAYS

Abstract

Phenazine-mediated reductive dissolution of Fe(III) oxyhydroxide minerals raises intriguing questions about bioremediatory and survival implications of environmental iron reduction by phenazine producers. While reductive dissolution of iron oxyhydroxide minerals releases dissolved Fe(II), which facilitates damaging Fenton reactions that harm producer bacteria, Fe(III)-bearing clay minerals generally retain nearly all of their Fe(II) through the reduction process and can even undergo multiple redox cycles without significant damage to the mineral lattice. Fe(II) transfer from clays to organic and heavy metal contaminants is a well-explored bioremediation technique because of the ubiquity of both clay minerals and microbial processes that reduce them. But in the case of phenazine producers, clay reduction may offer an additional benefit to the microbe: the supply of terminal oxidant in oxygen-limited waters and soils with limited harmful side reactions. Here we investigate the capacity for phenazines to reduce clays in an abiotic electrochemical system and explore the culture conditions in which phenazines appear to aid biotic reduction of a nontronite clay mineral. The methods developed here will enable progress toward a quantitative understanding of phenazine-mediated Fe(III)-bearing clay reduction and assist with the search for a clay-mediated survival phenotype.

Introduction

Phenazines react abiotically with iron oxyhydroxide minerals, liberating soluble Fe(II) as well as nutrients like inorganic phosphate that are often found adsorbed to the mineral surface (1-3). This observation, coupled with the finding that phosphorous limitation enhances phenazine biosynthesis, supports a hypothesis that phenazines may assist environmental microbes with nutrient scavenging in phosphorous limited environments (4). In a low-oxygen soil or water environment where phenazines are thought to be produced, iron reduction may also prove useful as a terminal oxidant. In anaerobic laboratory conditions, P. aeruginosa Δphz cells deficient in phenazine biosynthesis are capable of long-term (> 7 day) survival when supplied with an exogenous phenazine and an electrode poised to re-oxidize that phenazine (5). Iron(III) oxyhydroxide minerals appear an appealing environmental substitute for the laboratory electrode, but because soluble Fe(II) facilitates damaging Fenton reactions in the presence of phenazines which would presumably require energetically expensive damage repair mechanisms in a severely limited metabolic condition, it is likely that Fe(III) oxyhydroxide minerals are poor terminal oxidants for phenazine producers. Ferruginous smectites and other Fe(III)-bearing clays on the other hand are well known to undergo reversible redox cycles mediated by microbes and oxygen (6). These cycles result in the release of small amounts of Fe(II), generally thought to come from mineral edge sites, but the bulk of the redox-accessible iron remains bound in octahedral sites in the mineral lattice. Once reduced, iron-rich clays can transfer electrons to organic contaminants and metals like antimony, uranium, and mercury (7). The reversibility of iron-bearing clay redox cycling and the limited release of dissolved Fe(II) suggest these clays might serve as terminal oxidants for environmental phenazine producers.

Shewanella oneidensis is known to reduce clays as a means of anaerobic survival through its outer membrane multiheme cytochromes, but it is also capable of transferring electrons to clays using diffusible flavins (9). Whereas reduction via cytochrome requires direct microbe-mineral contact, flavins are known to enable mineral reduction at a distance (10). In batch cultures, various Pseudomonad species have been observed to reduce clays, but the effect of that reduction on survival has not been thoroughly explored (11). Moreover, the mechanism responsible for that reduction has not been identified. Phenazines seem a logical hypothesis for such a reduction, but to my knowledge no work has so far been done to determine whether phenazines can donate electrons to clay, much less whether phenazine producers can survive using that process to facilitate carbon catabolism. In this chapter, I discuss my progress toward understanding the interaction between the environmental phenazine producer *Pseudomonas synxantha* and Fe(III)-bearing clay minerals.

Methods

Clay minerals were obtained from the Clay Minerals Society. Analysis of their chemical composition and x-ray determined structures are available from the same. Briefly, NAu-1 is a nontronite containing approximately 33% iron by weight, almost entirely in the Fe(III) octahedral form. SWy-3 is a smectite containing approximately 3% iron by weight, also primarily in the Fe(III) octahedral form.

Clay preparation to ensure consistent size fraction and interstitial cation identity

Bulk NAu-1 arrived as a single chunk of consolidated material and was first pulverized into uniform powder using a shatter box. SWy-3 arrived as a fine powder and was therefore not

pulverized. From this point, each clay was treated identically. To replace interstitial cations, 30 g of clay were placed into a 250 mL centrifuge bottle and were suspended in 200 mL of 100 mM NaCl. The clay was shaken for 3 hours and was then centrifuged for 10 minutes at 10,000 RPM. The supernatant was decanted and the pellet was resuspended by sonication. This NaCl wash was repeated twice. Next, three identical washes were carried out with deionized water (> 18 MΩ).

After the final wash, the resulting pellet was resuspended via sonication in sodium hexametaphosphate to ensure complete dispersion and allow for fractionation of clay particle size by settling. The dispersed clay was transferred to a 1L graduated cylinder and allowed to settle for several hours. The top several centimeters of solution were sampled to obtain the sub 2 μm fraction of clay particles (13). This process was completed three times and the resulting fractions were centrifuged into a combined clay pellet which was finally resuspended in 1 mM sodium chloride for experiments.

Abiotic phenazine-mediated clay reduction

PCA and clay were suspended in a sealed, stirred electrochemical reactor from Stony Lab. The reactor possesses ports (sealable with rubber O-rings) that provide access for electrodes (working, counter, and reference) as well as a sparging needle to introduce inert gas and an exit needle, which allows the sparging gas to leave the reactor chamber and prevent pressure buildup.

To transfer electrons to the phenazine, we used a graphite working electrode and a platinum counter electrode both submerged directly in the reaction fluid, as well as a Ag/AgCl

reference electrode connected to the reaction solution via a 3% agarose salt-bridge doped with 3M KCl. On the other side of the salt bridge, the reference electrode was submerged in an oxidized PCA solution equimolar with that in the reaction chamber.

After sparging the media thoroughly with N_2, we moved the sparging needle from beneath the surface of the reaction liquid and placed it directly above the liquid to allow a continuous stream of N_2 to flow into the reaction chamber and out the exit port. Prior to the start of the experiment, we ensured the media was anoxic by conducting a cyclic voltammogram. Because clays are not capable of receiving electron transfer directly from electrodes, the resulting voltammogram recorded only the behavior of dissolved PCA. To begin the experiment, we set the working electrode to apply a potential of -500 mV (SHE) for a period of several hours and we recorded the current as a measurement of the number of electrons transferred throughout the experiment.

Culture conditions

For experiments examining the reduction of clay by *P. synxantha*, we used a MOPS minimal medium buffered only lightly at pH 7.2 with the following components (unless otherwise noted, all reported concentrations are mM): $CaCl_2$: 0.68; $MgSO_4$. : 0.41; NH_4Cl : 16.00; KH_2PO_4 : 25 mM or 10 μM; glucose : 55.51; MOPS 25.00 or 125.00. After adjusting the pH to 7.2 with NaOH, we also added SL-10 trace metals to 1x final concentration. In cases where phosphorous concentration was adjusted, we used a pH 7 mixture of mono and dibasic potassium phosphate.

To determine the ability of WT and Δphz strains of *P. synxantha* to reduce Fe(III)-bearing clay using phenazines, we grew 5 mL overnight cultures aerobically at 30 ºC in a minimal medium containing various amounts and combinations of MOPS buffer (+buffer = 125 mM, -buffer = 25 mM) and potassium phosphate (+P = 2.5 mM, -P = 10 μM) with or without the addition of 100 μM PCA dissolved in 0.2 M NaOH or the equivalent volume of 0.2 M NaOH. We then transferred 2mL of the late stationary phase cells to Eppendorf tubes and added 4 mg of ≤ 2 μm particles of NAu-1 suspended in sodium hexametaphosphate. The tubes were then left sealed in the anaerobic chamber for two weeks.

At the end of the experiment, the extent of reduction was determined qualitatively by comparing the color of the clay pellets after centrifugation of the culture tubes. Because fully reduced NAu-1 is a deep blue green while fully oxidized and NAu-1 is a pale yellow, color is a reasonable qualitative proxy for reduction extent. In some cases, it has been used spectrophotometrically, but the scattering introduced by the presence of cells as well as potential interference from PCA absorption bands precluded use of this method in this study (13). In the future, attempts should be made to replicate the methods of Gorski et al., using highly efficient low molecular weight electron shuttles like diquat to measure the extent of clay reduction electrochemically (14).

Results and Discussion

For phenazine-producing microbes to survive via phenazine-mediated clay reduction, phenazines must be able to reduce Fe(III)-bearing clays. Our abiotic experiments demonstrate that the phenazine PCA is capable of reducing both NAu-1 and SWy-3. However, integration of the current traces in **Figure 1** reveals a discrepancy between the

measured and expected relative electron accepting capacity of the clays. Because NAu-1 contains 11 times as much octahedral Fe(III) as SWy-3, we expect that it should be capable of accepting 11 times as much total charge. This result is expected when using highly efficient electron shuttles like diquat to transfer electrons between an electrode and a clay. However, we find that in our PCA condition, NAu-1 is only capable of accepting about 1.25 times as much charge as SWy-3, indicating that PCA may not be a very efficient electron shuttle for reducing iron in the clay lattice.

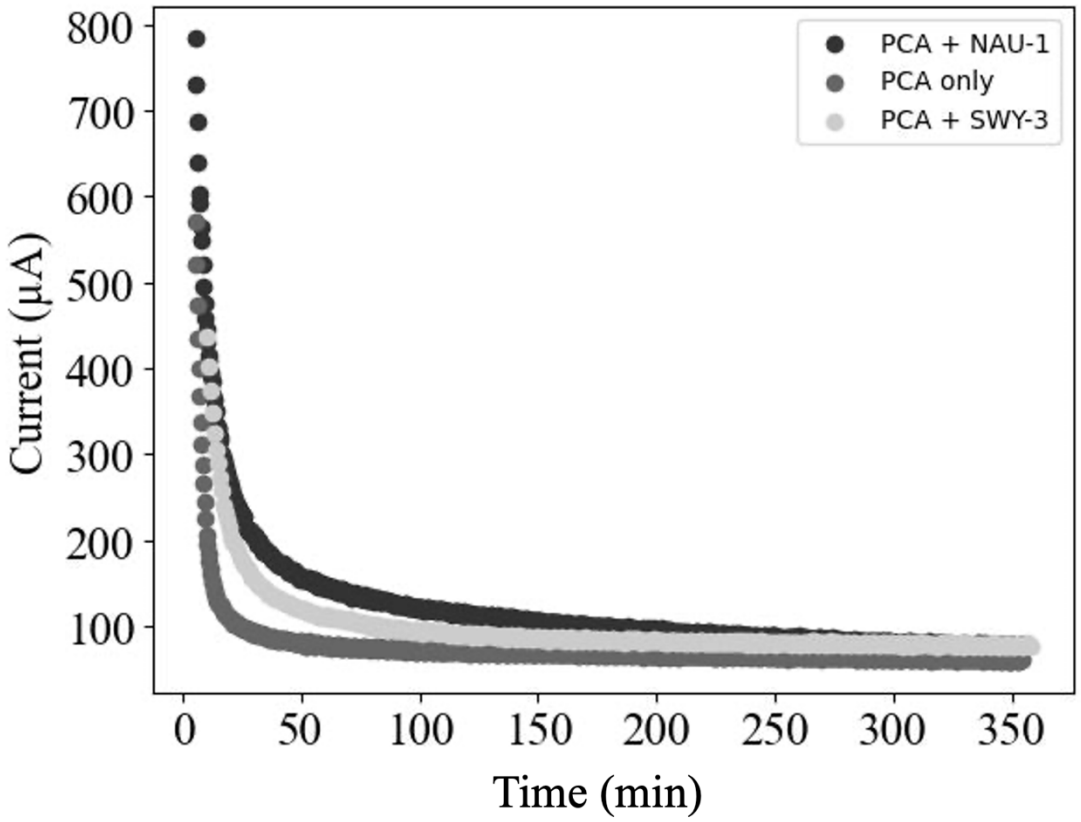

Figure 1: Reduction of PCA and PCA+clay solutions by a graphite working electrode poised at –500mV (SHE). A larger area under a curve indicates a greater total current transferred by the working electrode (and thus more total electrons accepted by the PCA or PCA+clay combination). NAU-1 is a nontronite clay containing ~33 weight % ferric iron. SWY-3 is a smectite containing ~3 weight % ferric iron.

To determine conditions under which P. synxantha cells reduce iron-bearing clay and whether phenazines are essential for that process, we swept a series of phosphorous concentration and buffer strength conditions using stationary phase cultures transferred from aerobic pregrowth to an anaerobic condition. Carbon was supplied in great excess and cells were provided with the nontronite clay NAu-1 after their transition to anoxia. In all cases we tested, WT P. synxantha cells produced and reduced PCA, visible in the solution above

the cell/clay pellets in its fluorescent yellow reduced form. (**Table 1 and Figure 2**). In three out of four cases, reduction of the clay pellet by these WT cultures is clear, although in tube A1 (+P, -Buffer), the pellet is so brown that it is unclear by eye whether the clay is reduced or simply discolored by some microbial compound.

Table 1: Experimental conditions and conclusions from an experiment with Δphz and WT Pseudomonas synxantha cells grown to stationary phase and then transferred to an anaerobic chamber and provided with oxidized NAu-1. +P indicates 2.5 μM phosphorous, while –P indicates only 10 μM phosphorous. +Buffer indicates 125 mM MOPS at a starting pH of 7.2, while –Buffer indicates 25 mM MOPS at a starting pH of 7.2. +PCA indicates 100 μM PCA in 0.2 M NaOH, while -PCA indicates only the addition of an equal volume of the 0.2 M NaOH carrier solvent. Conclusions about clay reduction are drawn based on the color of NAu-1 after two weeks in contact with the cells: more blue-green coloration indicates a greater extent of reduction. Images of the culture tubes at the end of the experiment can be found in **Figure 2**.

Sample	Strain	P	Buffer	Exogenous PCA	Final pH	Degree of Clay Reduction
A1	WT	+	-	-	5.0	unclear
A2	WT	-	-	-	5.0	intermediate
A3	WT	+	+	-	6.5	significant
A4	WT	-	+	-	6.5	significant

B1	Δphz	+	-	-	4.5	none
B2	Δphz	-	-	-	5.0	none
B3	Δphz	+	+	-	6.5	significant
B4	Δphz	-	+	-	5.5	none
C1	Δphz	+	-	+	5.5	significant
C2	Δphz	-	-	+	5.5	significant
C3	Δphz	+	+	+	6.5	significant
C4	Δphz	-	+	+	6.0	significant

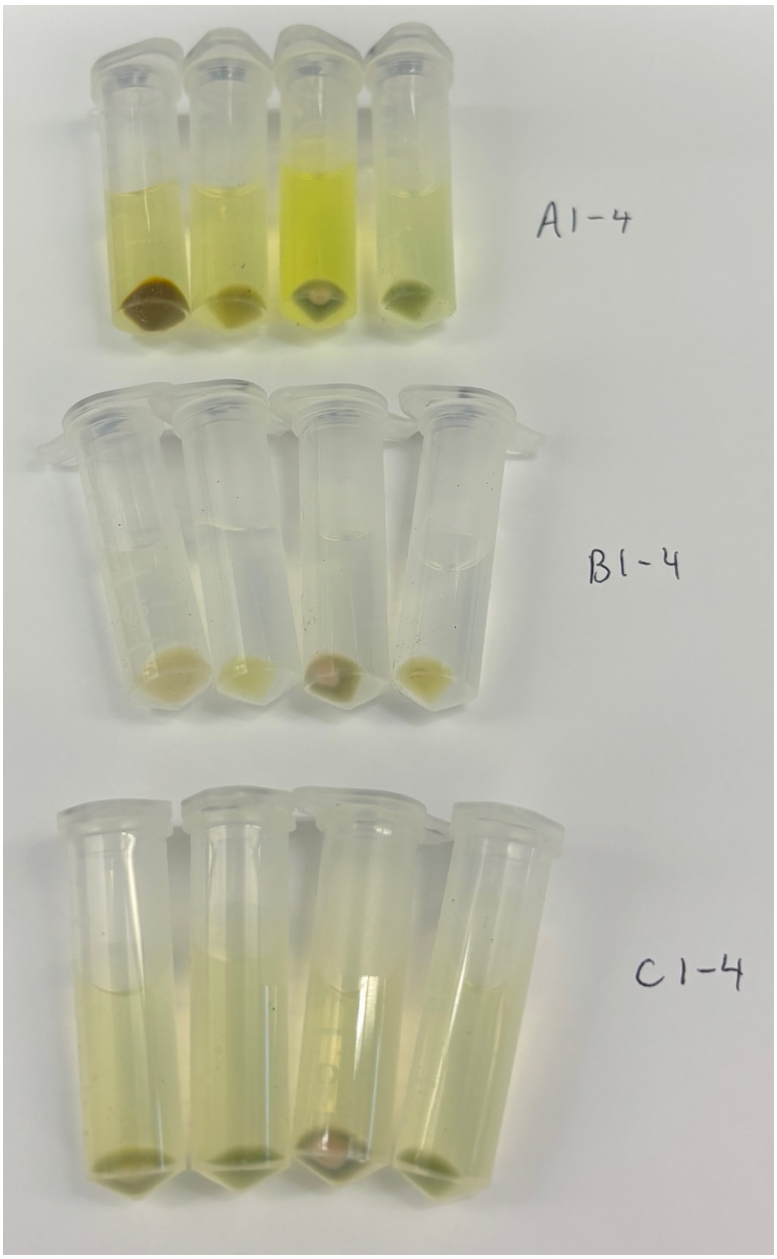

Figure 2: Phenazines enhance NAu-1 reduction by *P. synxantha*. Final time point image from cultures of WT and Δphz P. synxantha incubated anaerobically at 25 °C for 2 weeks. **Table 1** above contains comprehensive descriptions of the culture conditions corresponding to each tube including phosphorous and buffer additions. Tubes A1-4 contain WT cultures. Tubes B1-4 contain Δphz cultures with no exogenous PCA. Tubes C1-4 contain Δphz cultures provided with 100 μM exogenous PCA.

In our experiments with *P. synxantha* Δphz*,* cells provided with no exogenous phenazine were generally not able to reduce phenazines under the given conditions, while those under the same conditions that were provided with 100 μM PCA were able to reduce the clay. In one condition (tube B3: +P, +Buffer), Δphz cells were able to reduce the clay, although not as fully as when provided exogenous PCA. This indicates the presence of some phenazine-orthogonal mechanism for clay reduction, perhaps some other small diffusible molecule that has yet to be identified.

Conclusions

In this study we determined that the environmentally-relevant phenazine PCA is capable of transferring electrons to Fe(III)-bearing clays NAu-1 and SWy-3 when reduced by a graphite working electrode. To our knowledge, this is the first demonstration that reduced phenazines can reduce clays. Our electrochemical results indicate that PCA may not be as efficient at transferring electrons to clays as well-known clay-compatible electron shuttles like diquat, although an alternative explanation is that PCA might require a higher driving force than the -500 mV (SHE) applied in this study. Our experiments with WT *P. synxantha* demonstrate that it produces PCA and reduces clay in anoxia across multiple phosphorous and pH conditions. Our experiments with *P. synxantha* Δphz cells under similar conditions show that they are generally incapable of reducing NAu-1 without exogenously supplied PCA, but that in a condition where they can reduce the clay slightly without PCA, the degree of reduction is enhanced by the presence of PCA. These results indicate that at least some of the requirements for long term anaerobic survival by phenazine-mediated clay reduction can be met, namely that an environmentally relevant strain of phenazine producer can use its native

phenazine PCA to transfer electrons to a clay in anaerobic conditions. Future work should focus on measuring the extent of biotic reduction possible under anaerobic conditions, preferably using the methods developed by Gorski et al., to enable calculations of the clay supply necessary to sustain a survival metabolism (14). Experiments using dialysis tubing or similar membranes to separate clay from phenazine producing bacteria will enable the differentiation of phenazine-mediated clay reduction at a distance from the cell from any processes that require microbe-clay contact. Although *P. synxantha* is not known to possess transmembrane cytochromes like those found in *S. oneidensis*, the concentration of reduced phenazine in the cell membrane might permit faster reduction when the membrane is in contact with the clay. The environmentally-accessible pKa of PCA and the effect of the molecule's charge on its lipophilicity and presumably its concomitant membrane permeability suggests that more acidic buffers might enhance clay reduction rates by giving PCA easier access to membrane associated ETC components. An additional point of consideration is the choice of nutrients in the media. It was noted in early experimental attempts that a component (or components) of LB permitted reduction of clays by several cell types including phenazine deficient mutants. Rich media should be avoided because of the confounding effects of unidentified redox-active components. Finally, whatever conditions are chosen to investigate this phenotype, care must be taken when plating CFUs from anaerobic cultures because of unwanted Fenton and phenazine interactions upon exposure to oxygen. Plates made with LB supplemented with nitrate might allow *P. synxantha* to outgrow in the safety of an anaerobic chamber.

References

1. Hernandez, M. E., Kappler, A., & Newman, D. K. (2004). Phenazines and Other Redox-Active Antibiotics Promote Microbial Mineral Reduction. *Applied and Environmental Microbiology*, 70(2), 921–928. https://doi.org/10.1128/aem.70.2.921-928.2004
2. McRose, D. L., & Newman, D. K. (2021). Redox-active antibiotics enhance phosphorus bioavailability. *Science*, 371(6533), 1033–1037. https://doi.org/10.1126/science.abd1515
3. McRose, D. L., Li, J., & Newman, D. K. (2023). The chemical ecology of coumarins and phenazines affects iron acquisition by pseudomonads. *Proceedings of the National Academy of Sciences*, 120(14). https://doi.org/10.1073/pnas.2217951120
4. Alcalde, R. E., Jeckel, H., Zhang, O., Avila, R. L., Dalleska, N., Mavrodi, D., Yang, C., & Newman, D. K. (2025). Phosphorus stress and spatial confinement lower the threshold for quorum-sensing activation of redox-active metabolite production in *Pseudomonas synxantha*. *openRxiv*. https://doi.org/10.1101/2025.11.11.687776
5. Wang, Y., Kern, S. E., & Newman, D. K. (2010). Endogenous Phenazine Antibiotics Promote Anaerobic Survival of *Pseudomonas aeruginosa* via Extracellular Electron Transfer. *Journal of Bacteriology*, 192(1), 365–369. https://doi.org/10.1128/jb.01188-09

6. Pentráková, L., Su, K., Pentrák, M., & Stucki, J. W. (2013). A review of microbial redox interactions with structural Fe in clay minerals. *Clay Minerals*, 48(3), 543–560. https://doi.org/10.1180/claymin.2013.048.3.10

7. Cai, S., Li, F., Yan, C., Min, Y., Li, W., Xiang, T., Sang, F., & Song, B. (2026). Reduced Fe-bearing clay minerals in environmental remediation: Mineral fundamentals, reduced state activation, applications, and enhancement strategies. *Coordination Chemistry Reviews*, 563, 218042. https://doi.org/10.1016/j.ccr.2026.218042

8. Kostka, J. E., Stucki, J. W., Nealson, K. H., & Wu, J. (1996). Reduction of Structural Fe(III) in Smectite by a Pure Culture of *Shewanella Putrefaciens* Strain MR-1. *Clays and Clay Minerals*, 44(4), 522–529. https://doi.org/10.1346/ccmn.1996.0440411

9. Cooper, R. E., Goff, J. L., Reed, B. C., Sekar, R., & Dichristina, T. J. (2015). Breathing Iron: Molecular Mechanism of Microbial Iron Reduction by *Shewanella oneidensis*. *Manual of Environmental Microbiology* (p. 5.2.1-1-5.2.1-13). ASM Press. https://doi.org/10.1128/9781555818821.ch5.2.1

10. Michelson, K., Alcalde, R. E., Sanford, R. A., Valocchi, A. J., & Werth, C. J. (2019). Diffusion-Based Recycling of Flavins Allows *Shewanella oneidensis* MR-1 To Yield Energy from Metal Reduction Across Physical Separations. *Environmental Science & Technology*, 53(7), 3480–3487. https://doi.org/10.1021/acs.est.8b04718

11. Gates, W. P., Wilkinson, H. T., & Stucki, J. W. (1993). Swelling Properties of Microbially Reduced Ferruginous Smectite. *Clays and Clay Minerals*, 41(3), 360–364. https://doi.org/10.1346/ccmn.1993.0410312

12. Gee, G. W., & Bauder, J. W. (1986). Particle-size Analysis. In SSSA Book Series (pp. 383–411). Wiley. https://doi.org/10.2136/sssabookser5.1.2ed.c15

13. Komadel, P., Lear, P. R., & Stucki, J. W. (1990). Reduction and Reoxidation of Nontronite: Extent of Reduction and Reaction Rates. *Clays and Clay Minerals*, 38(2), 203–208. https://doi.org/10.1346/ccmn.1990.0380212

14. Gorski, C. A., Aeschbacher, M., Soltermann, D., Voegelin, A., Baeyens, B., Marques Fernandes, M., Hofstetter, T. B., & Sander, M. (2012). Redox Properties of Structural Fe in Clay Minerals. 1. Electrochemical Quantification of Electron-Donating and -Accepting Capacities of Smectites. *Environmental Science & Technology*, 46(17), 9360–9368. https://doi.org/10.1021/es3020138

Chapter 6
CONCLUSIONS

The natural functions of phenazines in membranes

The prevailing view in the literature is that phenazines function as extracellular metabolites. Their cited functions all involve the transfer of electrons from the cell to the phenazine molecule, which then leaves the cell to interact elsewhere in the environment. For example, as generators of toxic reactive oxygen species, phenazines must leave the producer cell in the reduced state and diffuse to a source of oxygen, limiting competition in the producer cells' environmental niche. As agents of reductive mineral dissolution, reduced phenazines must diffuse to a mineral surface, where they transfer electrons to dissolve the mineral and facilitate nutrient acquisition by producer cells. Phenazine-mediated extracellular electron transfer, which under laboratory conditions confers a survival benefit to planktonic cells lacking alternative electron acceptors, is also believed to provide a lifeline to cells in the anoxic cores of *P. aeruginosa* biofilms. All of these functions rely on phenazine interactions beyond the confines of the cell. But given their higher lipophilicity in the reduced form, it appears at first glance that the cells got it backward. Why keep a dangerous metabolite around by incorporating an intramolecular hydrogen bond only in the reduced form, especially when that toxin can supposedly do so much good for you when it's out interacting elsewhere in the environment? Perhaps the cells know more than they are letting on.

The direct observation that PYO concentrates in the membrane at a rate almost 100 times greater than in the extracellular media exceeds the expectation from the partition coefficient alone, which suggests only about a 10x excess in a lipophilic phase compared to an aqueous

one. In a planktonic culture grown to stationary phase in LB, this accumulation occurs within about 5 minutes. In addition to offering a compelling refutation of the prevailing model that reduced PYO diffuses away from the cells to relieve them of reducing equivalents, this measurement suggests that *P. aeruginosa* PA14 cells may in fact have evolved to survive or even prefer high concentrations of PYO in their membranes.

In his 2023 thesis, partially supported by respirometry measurements of the sort described in Chapter 4 of this thesis, Dr. John Ciemniecki proposed an intentional short-circuiting of the ETC, in which reduced phenazines react with oxygen, bypassing the downstream portions of the electron transport chain (1). He suggested the bypass might enable a deliberate reduction in the bioenergetic poise of the cell as a mechanism to prepare for long term survival or to avoid the damaging effects of antibiotics, as Horak et al. soon thereafter showed can be the case for cells treated with tobramycin (2). One possible twist to this hypothesis that may be worth considering is that an extremely concentrated pool of PYO in the membrane makes the whole surface of the cell oxygen-reactive. In a sense, membrane-associated PYO may poise the cell to field even a very minute concentration of oxygen and take full advantage of it. In fully oxygenated conditions, terminal oxidases are constantly bombarded by oxygen molecules. P. aeruginosa possesses several different terminal oxidases with different affinities for oxygen, but if it has evolved to function even at oxygen tensions well below the K_m of its highest affinity oxidase, perhaps its "accessory respiratory enzyme" pyocyanin lends a hand when the going gets toughest (3). A membrane saturated with PYO should conceivably be able to push electrons through the electron transport chain with PYO present (from NADH dehydrogenase to PYO to ubiquinone instead of the typical direct dehydrogenase-to-ubiquinone transfer) as long as there is sufficient oxygen for the terminal

oxidases to function. When the oxygen concentration dips too low, the terminal oxidases slow down even as the cell continues to require a metabolic flux for biosynthetic and energetic reasons, and by populating the membrane with reduced PYO, the cell continues to push electrons from NADH to the NADH dehydrogenases to PYO. If any small amount of oxygen diffuses to the cell, it will immediately contact either an oxidase or a PYO molecule, creating the possibility for the NADH pool to push more reducing equivalents out of the cytoplasm and into the membrane via the dehydrogenases. This mechanism could permit survival during periods of very low oxygen. And when oxygen levels return to normal, the reduction in PYO's lipophilicity should cause it to diffuse rapidly out of the cell as observed in the pellet retention assay in Chapter 2. This model will likely require significant work to corroborate or disprove, but it now seems clear that there is some evolved role for PYO in the cell membrane.

Phenazines as molecular probes

Given their redox sensitivity and fluorescence profiles, phenazines have been condemned for their interference with dyes, particularly in systems where redox state and oxygen levels change (4). But phenazines also enjoy rich applications as histological dyes and molecular indicators (5, 6). Based on unexpected observations during my work with these peculiar molecules, I propose two possible uses for phenazines as probes that I believe deserve further attention. First, in my abiotic partitioning experiments using octanol, I noticed that PCA reacts with octanol on time scales of days to form a purple compound. The reaction appeared to be oxygen and light dependent. When I placed a solution of PCA in octanol into our broad spectrum light box, it changed rapidly to a rich golden color, possibly due to semiquinone

radical reactions similar to those observed for unsubstituted phenazine in methanol (7). Characterizing the reaction(s) that result in these color changes and the parameters that control their rates and specificity may result in a useful lipid quantification tool. Assuming the reactions are well understood, adding small amounts of PCA to solutions of unknown lipids and then exposing the reaction mixtures to a known light/oxygen dose could provide relatively easy spectrophotometric measurements of lipid content, which could prove useful in contexts like biofilms or soils that contain a mixture of complex phases.

An additional and perhaps more promising idea for phenazines as molecular probes is to use pyocyanin to make absorbance measurements of the "energetic poise" of planktonic cells. I define this "energetic poise" as a measure of the approximately instantaneously available reducing equivalents in the cell. These available reducing equivalents could be in the form of NAD(P)H or FAD(P)H molecules or in the form of proteins harboring easily accessible electrons (e.g. as part of an Fe-S cluster). Given PYO's apparently promiscuous ability to enter cells and pull reducing equivalents from various cellular components (including NADH and dehydrogenase enzymes as well as unidentified cytosolic components), and the dramatic change in absorbance between the reduced and oxidized forms -- the peak at 690nm disappears upon reduction, and furthermore the reduced form of PYO appears to concentrate about 100x more strongly in the cell than in the supernatant, at least in *P. aeruginosa* PA14 cells -- it seems possible that by mixing a standard concentration of PYO with a suspension of cells of known density for a limited time (presumably quite a short time on the order of 1-5 minutes, depending on culture density) and then centrifuging the cells out rapidly, one could measure the absorbance of the residual supernatant at 690 nm and correlate the loss of absorbance with the amount of PYO that was reduced by cellular activity/easily accessible

reducing equivalents and/or retained by the cell (presumably in the reduced form). These measurements likely need to be made in an anaerobic chamber with an inert-gas-sparged PYO solution to avoid spontaneous reoxidation by dissolved oxygen. The time required to move dense cultures into the anaerobic chamber should provide them sufficient time to consume residual oxygen in their own supernatants before the measurement takes place. But even on a benchtop, our respirometry measurements described in Chapter 4 show that PYO is reduced more quickly by a culture of stationary PA14 cells than it is re-oxidized by oxygen.

This measurement may provide a method to qualitatively distinguish between the energetic poise of cells in various growth and non-growth states. When coupled with electrochemical measurements of cell specific metabolic rate like those made during the survival assay, it may be possible to make rapid, quantitative end point approximations of something like "instantaneous metabolic rate" for rapid hypothesis generation or in contexts that are relatively difficult to interrogate electrochemically. One could, for example, compare the "instantaneous metabolic rates" of planktonic stationary phase cultures starved for various macronutrients to determine quickly whether they differ substantially in their growth arrested metabolic poise. Given a calibrated PYO probe protocol, one could feasibly search for large phenotypic differences between several culture conditions in just a few minutes. Because PYO is relatively easy and cheap to synthesize (requiring approximately 3 days and $100 worth of reagents to make about 200 mg – enough for scores of experiments), developing a simple method like the one described here could be well worthwhile for screening large parameter spaces (carbon source, terminal electron acceptor, nutrient limitation, growth temperature, class and/or concentration of antibiotics or ETC inhibitors, etc.).

Closing remarks

In this thesis, I began by suggesting that abiotic chemical properties can offer new perspective on biological functions of microbial metabolites. I then put this idea into practice by examining phenazine lipophilicity across E_h and pH ranges, and discovered a physiologically relevant tuning mechanism that dictates phenazine biological retention. The results run counter to the dominant understanding that phenazines function outside the cell, and while we have not yet fully grasped the biological implications of this finding, the information we have gained from a strictly chemical angle appears profound even at this early stage. Although the vast problem of determining native secondary metabolite functions will inevitably require several orthogonal approaches, this thesis suggests careful examination of relevant physicochemical properties in environmentally relevant contexts can bring a measure of conceptual order to the universe of structurally diverse secondary metabolites.

References

1. Ciemniecki, J. A. (2024). The Bioenergetics of a Low-Power, Phenazine-Dependent Maintenance Metabolism in *Pseudomonas aeruginosa* [California Institute of Technology]. https://doi.org/10.7907/N992-EY51
2. Horak, R. D., Ciemniecki, J. A., & Newman, D. K. (2024). Bioenergetic suppression by redox-active metabolites promotes antibiotic tolerance in *Pseudomonas aeruginosa*. *Proceedings of the National Academy of Sciences*, 121(46). https://doi.org/10.1073/pnas.2406555121
3. Friedheim, E. A. (1931). Pyocyanine, an accessory respiratory enzyme. *The Journal of experimental medicine*, *54*(2), 207.
4. Flamholz, A. I., Saccomano, S., Cash, K., & Newman, D. K. (2022). Optical O_2 Sensors Also Respond to Redox Active Molecules Commonly Secreted by Bacteria. *mBio*, 13(6). https://doi.org/10.1128/mbio.02076-22

5. Min, K. A., Rajeswaran, W. G., Oldenbourg, R., Harris, G., Keswani, R. K., Chiang, M., Rzeczycki, P., Talattof, A., Hafeez, M., Horobin, R. W., Larsen, S. D., Stringer, K. A., & Rosania, G. R. (2015). Massive Bioaccumulation and Self-Assembly of Phenazine Compounds in Live Cells. *Advanced Science*, 2(8). https://doi.org/10.1002/advs.201500025
6. Stockert, J. C., Carou, M. C., Casas, A. G., Vior, M. C. G., Riega, S. D. E., Blanco, M. M., ... & Lombardo, D. M. (2020). Fluorescent redox-dependent labeling of lipid droplets in cultured cells by reduced phenazine methosulfate. *Heliyon*, *6*(6).
7. Bailey, D. N., Roe, D. K., & Hercules, D. M. (1968). Photoreduction of phenazine in acidic methanol. *Journal of the American Chemical Society*, *90*(23), 6291-6297.

Appendix A

SUPPLEMENTARY INFORMATION FOR CHAPTER 2

Supplement for:

Chapter 2: Redox-dependent lipophilicity of phenazine metabolites is modulated by intramolecular hydrogen bonds and controls their biological distribution

Korbinian O. Thalhammer[1], Matthew Scurria[2], Jinyang Li[3], Inês B. Trindade[3], Osvaldo Gutierrez[2], Stuart J. Conway[2,*], Dianne K. Newman[1,3,*]

[1]Division of Geological and Planetary Sciences, California Institute of Technology.

[2]Department of Chemistry & Biochemistry, University of California, Los Angeles.

[3]Division of Biology and Biological Engineering, California Institute of Technology.

*To whom correspondence should be addressed: Stuart J. Conway: stuartconway@ucla.edu; Dianne K. Newman: dkn@caltech.edu

Supplementary Information

Contents

Computational Details

All geometry optimizations of intermediates were achieved using the spin unrestricted uwb97xD [1]/cc-pvDZ [2] method, in water (dielectric constant: 78.35) and octanol (dielectric constant: 9.8629, EpsInf=2.0420) using the CPCM solvent model [3] as implemented in Gaussian16 [4]. Frequency calculations were also conducted at the same level of theory to obtain vibrational frequencies to determine the identity of the stationary points as intermediates (no imaginary frequencies), as well as obtaining the thermochemistry: enthalpy (ΔH) and free energy (ΔG) at the temperature of 298 K. All structural figures were generated with CYLview [5]. Distances in structural figures are shown in Å and energies are in kcal/mol. Single point energy corrections were carried out further with the following methods, using Truhlar's octanol solvent configuration. [6]

i) uwb97xD/6-311+g(d,p)-SMD(H_2O)//uwb97xD/cc-pvDZ-cpcm(H_2O)

ii) uwb97xD/6-311+g(d,p)-SMD(Octanol)//uwb97xD/cc-pvDZ-cpcm(Octanol)

Lipophilicity calculations (Log*D*) were done based on a previously established scheme, using the Gibbs free energies of the solvated molecules (Figure S2). [7, 8, 9] The energy of the intramolecular hydrogen-bond was calculated using the energy difference of the closed versus open form of each metabolite, values are given in kcal/mol. [10] The energy of the intramolecular hydrogen-bond was calculated only for structures that had defined closed versus open conformations, which were established based on the formation of a new intramolecular hydrogen-bond upon rotation of the substituent at the 1-position. The equilibrium constant (K_{eq}) at standard states and constant pressure was calculated to determine the isomeric ratio between open and closed forms. [11] Protonated forms of PCA and oxidized pyocyanin were used when analyzing the effects of an intramolecular

hydrogen-bond. *NBO* orbital analysis [12] was conducted to compare intramolecular hydrogen-bond capabilities of the redox forms of each metabolite. [13] The strength of the *NBO* interaction was used to rationalize the lipophilicity of the specific redox form.

$$E_{HB} = E_{closed} - E_{open}$$

Figure A1. Intramolecular hydrogen-bond calculation scheme. Electronic Energies were used, with all values reported in kcal/mol.

$$\text{Log}D = \frac{(\Delta G_{water} - \Delta G_{octanol})}{(2.303RT)}$$

Figure A2. Calculation scheme used to measure lipophilicity, using Gibbs free energy of the solvated metabolite, at room temperature. Value of *R* used was 1.987×10^{-3} kcal/mol.

$$\Delta \text{Log}D = \text{Log}D_{closed} - \text{Log}D_{open}$$

Figure A3. Differences in Log*D* due to the intramolecular hydrogen bond measured using the above scheme.

$$\Delta E_{HB} = E_{HB}\text{octanol} - E_{HB}\text{water}$$

Figure A4. Differences in intramolecular hydrogen bond strength due to changes in solvent.

$$K_{eq} = \frac{-(G^{o}_{closed} - G^{o}_{open})}{(RT)}$$

Figure A5. Calculation scheme used to measure equilibrium constant, using Gibbs free energy of the solvated metabolite, at room temperature. Value of *R* used was 1.987×10^{-3} kcal/mol.

Metabolite	E_{HB} (kcal/mol)	ΔE_{HB} (kcal/mol)	K_{eq}
$PCN_{oxidized}$ (water)	-1.588225	*xx*	2.373364
$PCN_{oxidized}$ (octanol)	-3.027731	-1.439506	25.862847
$PCN_{reduced}$ (water)	-2.491838	*xx*	95.368043
$PCN_{reduced}$ (octanol)	-2.574042	-0.082204	111.79018

$PCA_{reduced\text{-}protonated}$ (water)	-6.199789	*xx*	5755.5051
$PCA_{reduced\text{-}protonated}$ (octanol)	-7.518813	-1.319024	46376.067
$PCA_{oxidized\text{-}protonated}$ (water)	-5.312491	*xx*	1759.2903
$PCA_{oxidized\text{-}protonated}$ (octanol)	-5.706567	-0.394076	3339.1868
$Pyocyanin_{oxidized\text{-}protonated}$ (water)	-1.1401839	*xx*	5.951809
$Pyocyanin_{oxidized\text{-}protonated}$ (octanol)	-1.9189225	-0.7787386	21.807981
1-OH $Phenazine_{oxidized}$ (water)	-1.5386521	*xx*	8.920126

1-OH Phenazine$_{oxidized}$ (octanol)	-2.7227616	-1.1841095	63.430893

Table A1. Intramolecular hydrogen bond energies, ΔE_{HB}, and equilibrium constant (K_{eq}) calculated at the uwb97xD/6-311+g(d,p)-SMD(solvent)//uwb97xD/cc-pvDZ-cpcm(solvent) level of theory, according to the equations depicted above.

Metabolite	LogD	ΔLogD
PCN$_{oxidized}$ (open)	-1.002651	*xx*
PCN$_{oxidized}$ (closed)	0.0344949	1.03714598
PCN$_{reduced}$ (open)	0.596071	*xx*
PCN$_{reduced}$ (closed)	0.665601	0.06898975
PCA$_{reduced\text{-}protonated}$ (open)	0.375764	*xx*
PCA$_{reduced\text{-}protonated}$ (closed)	1.28183	0.90606544

$PCA_{reduced}$	-4.235971	*xx*
$PCA_{oxidized\text{-}protonated}$ (open)	-0.321952	*xx*
$PCA_{oxidized\text{-}protonated}$ (closed)	-0.043694	0.27825868
$PCA_{oxidized}$	-6.372354	*xx*
$Pyocyanin_{reduced}$	1.74498086	*xx*
$Pyocyanin_{oxidized\text{-}protonated}$ (open)	-1.1866238	*xx*
$Pyocyanin_{oxidized\text{-}protonated}$ (closed)	-0.6227475	0.56387626
$Pyocyanin_{oxidized}$	-0.0625507	*xx*
1-OH $Phenazine_{reduced}$	1.11855389	*xx*
1-OH $Phenazine_{oxidized}$ (open)	-0.2000703	*xx*

1-OH Phenazine$_{oxidized}$ (closed)	0.651722321	0.8517935

Table A2. LogD and ΔLogD calculated at the uwb97xD/6-311+g(d,p)-SMD(solvent)//uwb97xD/cc-pvDZ-cpcm(solvent) level of theory, according to the equations depicted above at neutral pH.

Metabolite	NBO Interaction Energy (kcal/mol)
PCN$_{oxidized}$	7.36
PCN$_{reduced}$	7.67
PCA$_{reduced}$	15.66
PCA$_{oxidized}$	*no interaction*
Pyocyanin$_{reduced}$	0.71
Pyocyanin$_{oxidized}$	*no interaction*
1-OH Phenazine$_{reduced}$	0.65
1-OH Phenazine$_{oxidized}$	3.05

Table A3. Intramolecular hydrogen bonding strength calculated using *NBO* analysis at the uwb97xD/cc-pvDZ-cpcm(H_2O) level of theory.

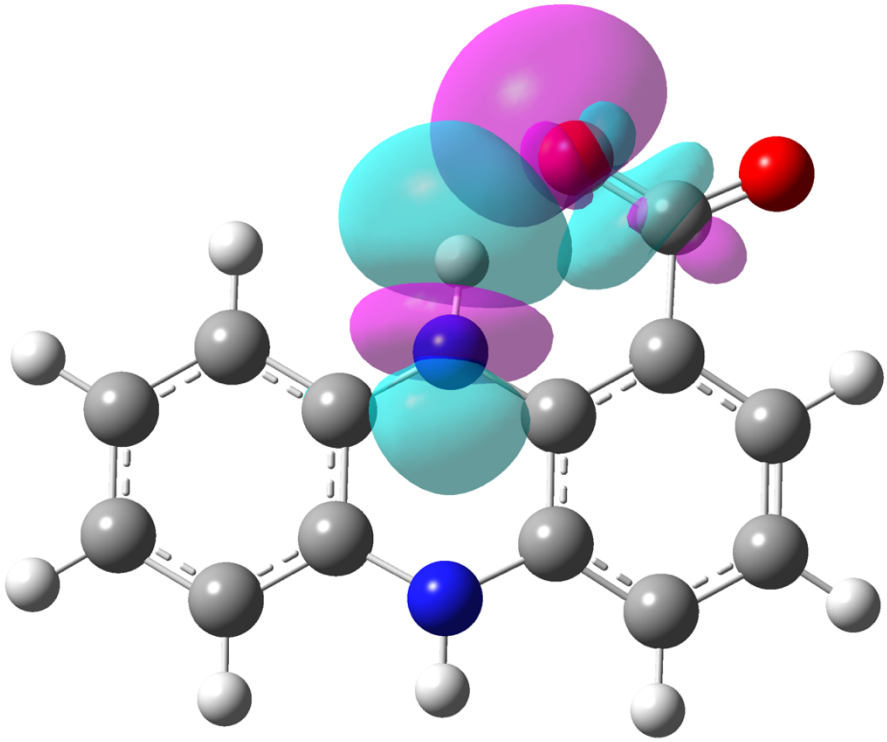

Figure A6. Intramolecular hydrogen bonding within $PCA_{reduced}$ shown using *NBO* orbitals, generated from the oxygen lone pair, calculated at the uwb97xD/cc-pvDZ-cpcm(H_2O) level of theory.

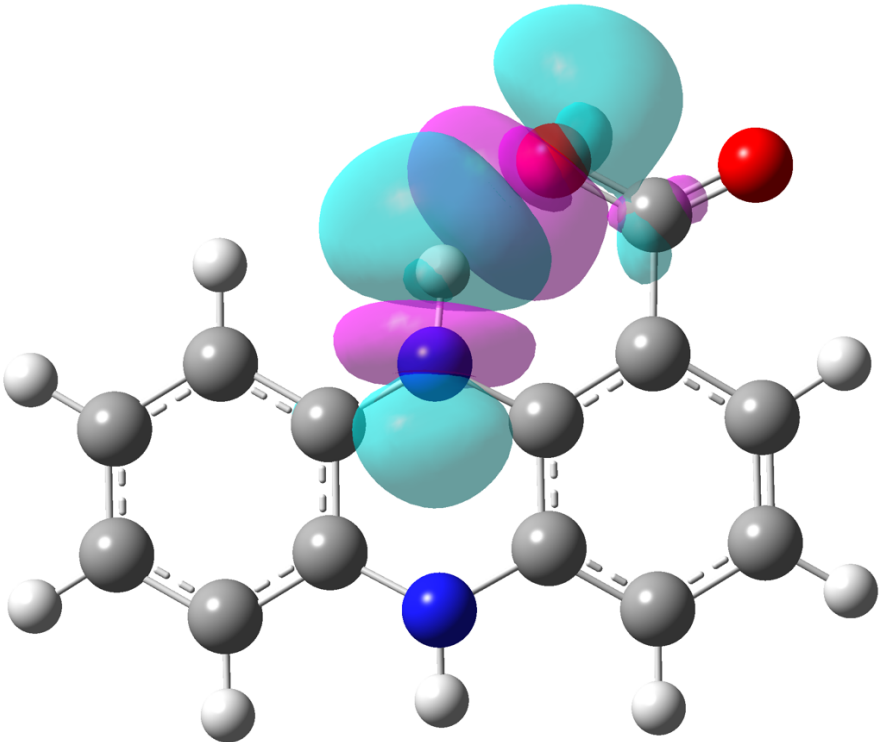

Figure A7. Intramolecular hydrogen bonding within $PCA_{reduced}$ shown using *NBO* orbitals, generated from the carbonyl π-bond, calculated at the uwb97xD/cc-pvDZ-cpcm(H_2O) level of theory.

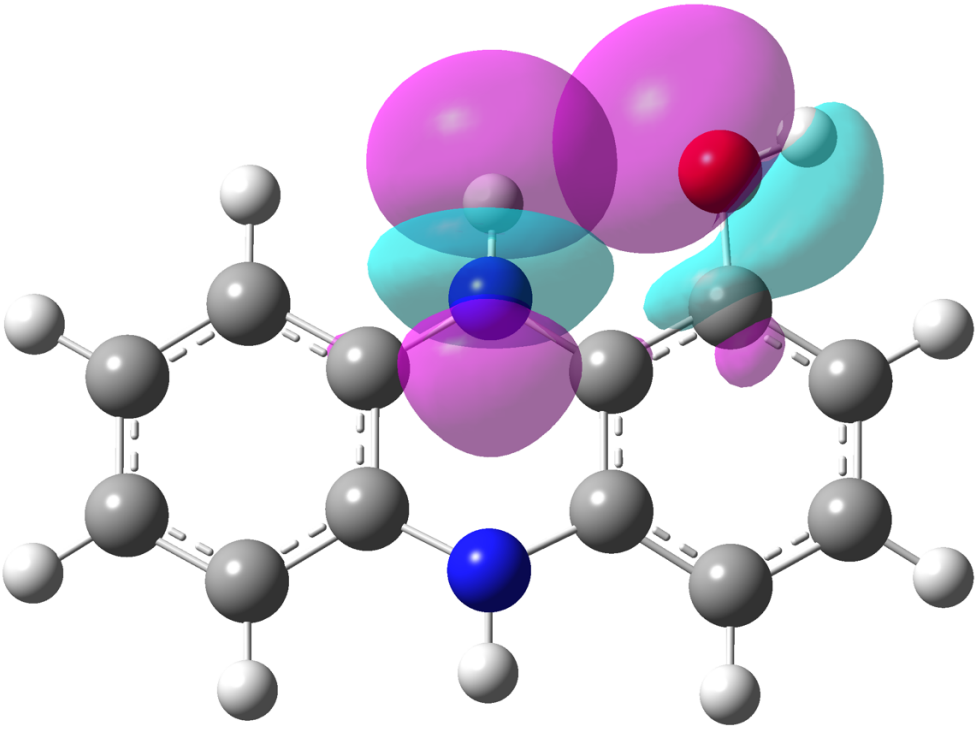

Figure A8. Intramolecular hydrogen bonding within OH-Phenazine$_{reduced}$ shown using *NBO* orbitals, calculated at the uwb97xD/cc-pvDZ-cpcm(H_2O) level of theory.

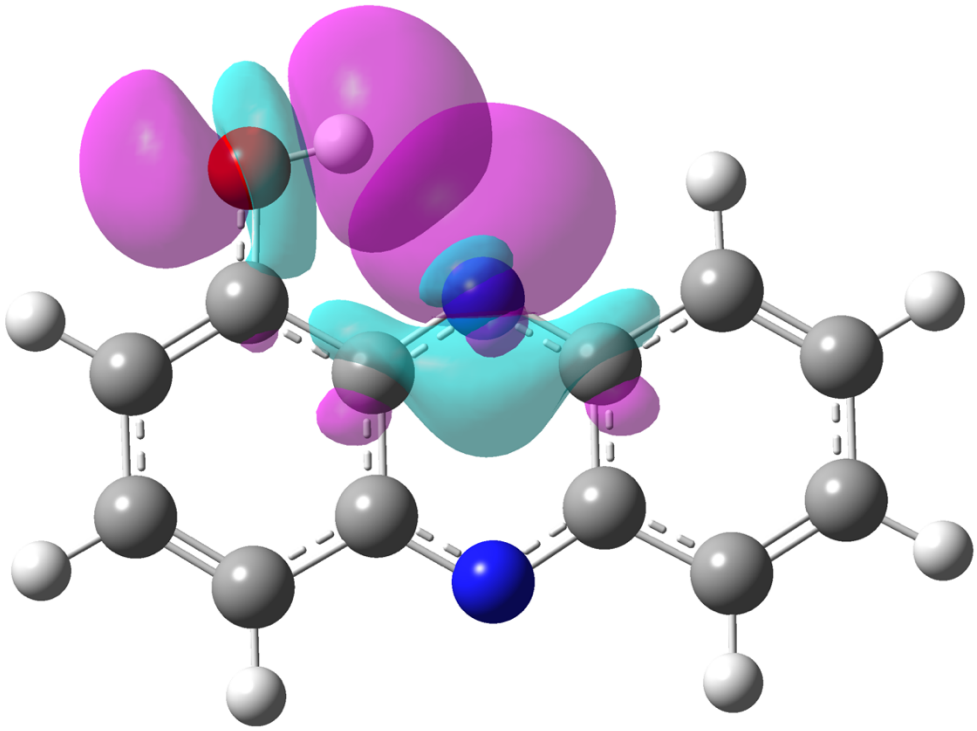

Figure A9. Intramolecular hydrogen bonding within OH-Phenazine$_{oxidized}$ shown using *NBO* orbitals, calculated at the uwb97xD/cc-pvDZ-cpcm(H_2O) level of theory.

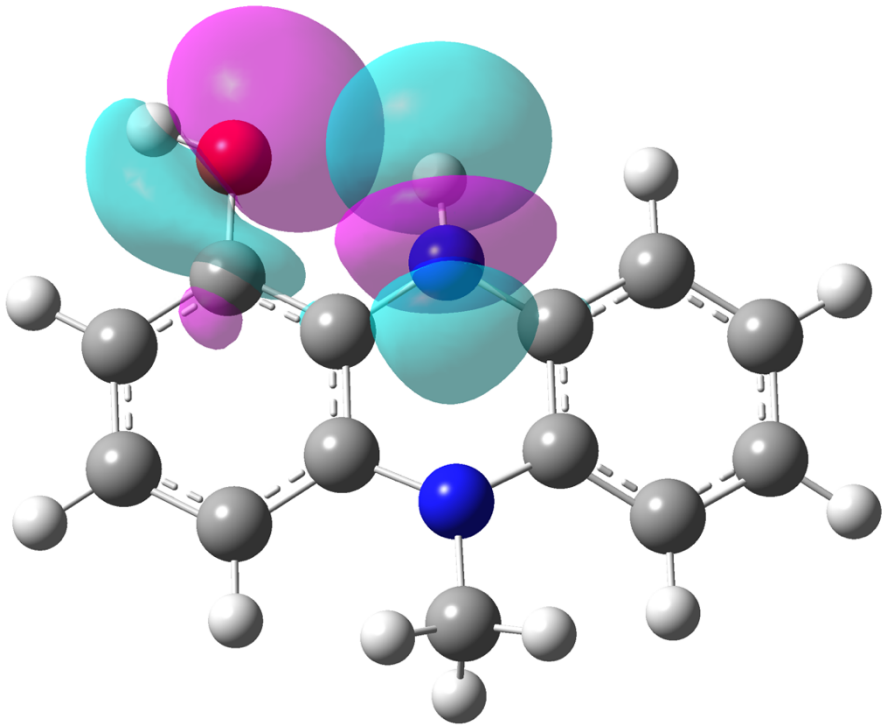

Figure A10. Intramolecular hydrogen bonding within Pyocyanin$_{reduced}$ shown using *NBO* orbitals, calculated at the uwb97xD/cc-pvDZ-cpcm(H_2O) level of theory.

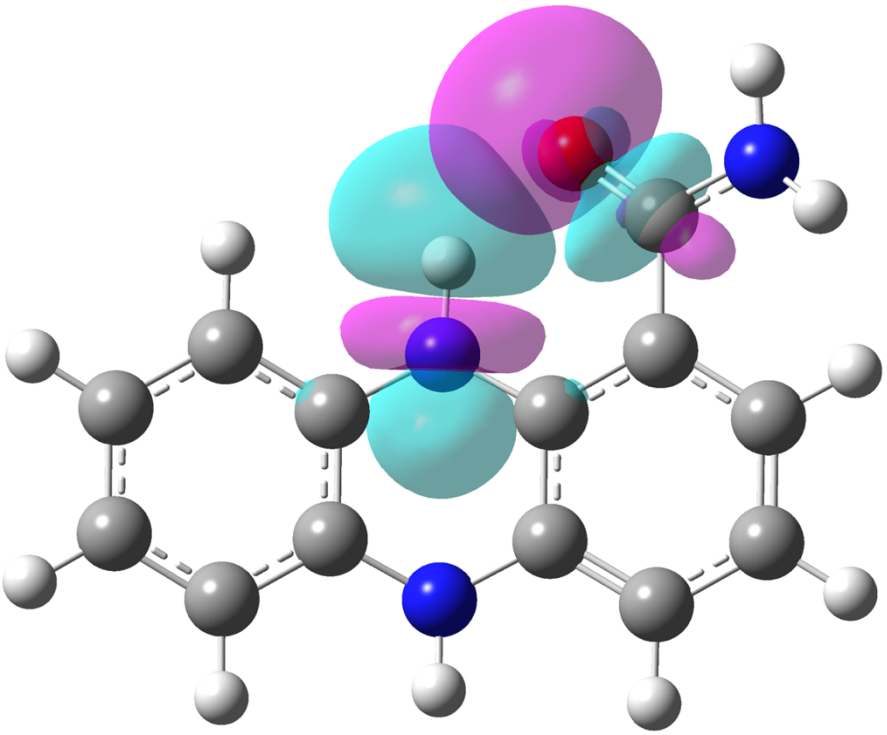

Figure A11. Intramolecular hydrogen bonding within $PCN_{reduced}$ shown using *NBO* orbitals, generated from the oxygen lone pair, calculated at the uwb97xD/cc-pvDZ-cpcm(H_2O) level of theory.

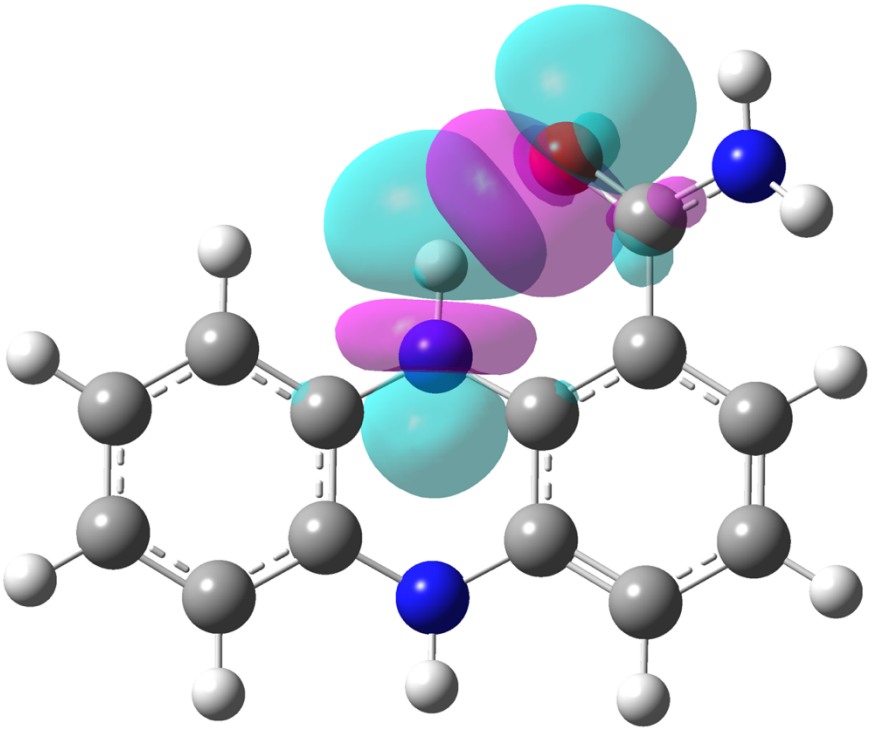

Figure A12. Intramolecular hydrogen bonding within $PCN_{reduced}$ shown using *NBO* orbitals, generated from the carbonyl π-bond, calculated at the uwb97xD/cc-pvDZ-cpcm(H_2O) level of theory.

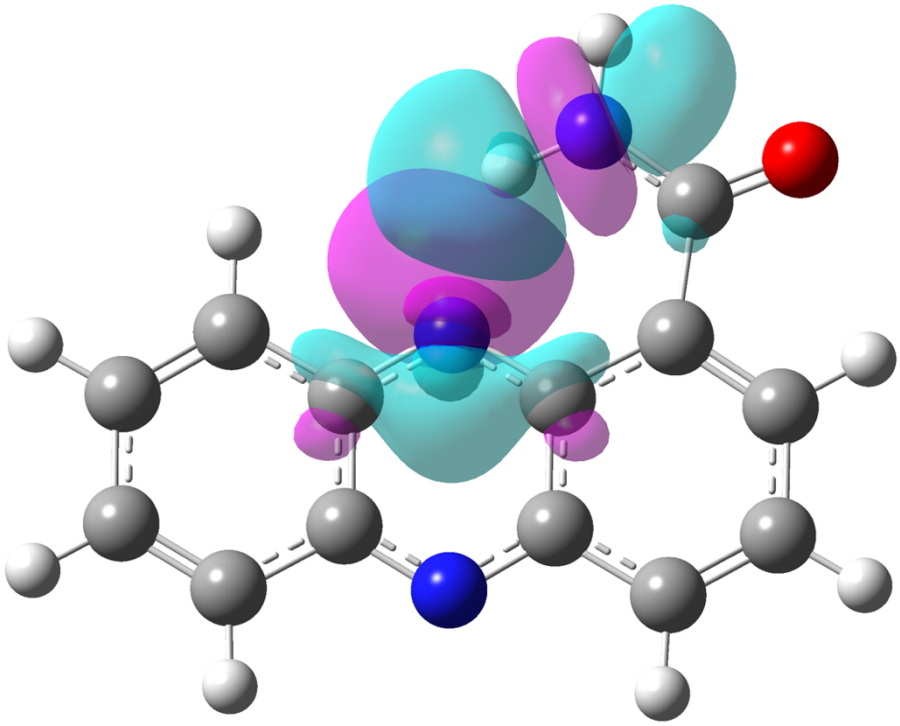

Figure A13. Intramolecular hydrogen bonding within $PCN_{oxidized}$ shown using *NBO* orbitals, calculated at the uwb97xD/cc-pvDZ-cpcm(H_2O) level of theory.

Table A4. Cartesian coordinates (xyz format) and energies of all the structures involved in each reaction mechanism studied calculated at the uwb97xD//cc-pvDZ-cpcm(solvent) level of theory.

PCN_reduced_open

E(scf) = -741.344857226 a.u.

C	4.265822	-0.133093	0.340205	C	3.786399	-1.436961	0.389139
C	3.389019	0.924961	0.073929	H	5.322723	0.075121	0.512800
C	2.426911	-1.688854	0.170160	H	3.755852	1.953264	0.042483

H	2.040146	-2.709517	0.212753	H	-0.688131	3.583336	-0.010593
H	4.460565	-2.267972	0.600920	H	-3.121051	3.201360	0.388692
C	2.040658	0.676385	-0.164317	H	-4.003768	0.861611	0.436758
C	1.556077	-0.642874	-0.116658	N	0.195316	-0.860491	-0.394234
C	-0.231976	1.498480	-0.207046	N	1.128684	1.690304	-0.484629
C	-1.090898	2.568235	0.004977	H	-0.142493	-1.793648	-0.182225
C	-2.456396	2.351576	0.230176	H	1.466877	2.636903	-0.359613
C	-2.947864	1.060149	0.254109	C	-2.741660	-1.393823	0.080776
C	-2.096846	-0.039801	0.034268	O	-3.703161	-1.622773	0.801994
C	-0.726498	0.172012	-0.184989	N	-2.189927	-2.365130	-0.712545

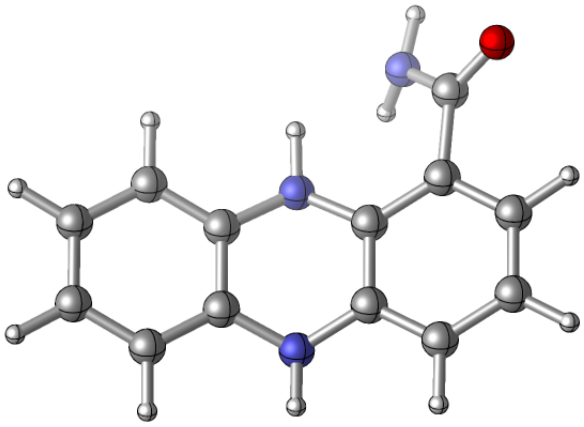

Zero-point correction= 0.222875 (Hartree/Particle)

Thermal correction to Energy= 0.235843

Thermal correction to Enthalpy= 0.236787

Thermal correction to Gibbs Free Energy= 0.183369

Sum of electronic and zero-point Energies= -741.121982

Sum of electronic and thermal Energies= -741.109014

Sum of electronic and thermal Enthalpies= -741.108070

Sum of electronic and thermal Free Energies= -741.161489

PCN_reduced_closed

E(scf) = -741.350279331 a.u.

C	4.271787	-0.145413	0.354472	C	-2.965827	1.027005	0.131204
C	3.391967	0.929385	0.173050	C	-2.081468	-0.065234	-0.027110
C	2.441989	-1.688515	0.027962	C	-0.710059	0.186012	-0.215425
C	3.798778	-1.450056	0.280834	H	-0.732275	3.590127	0.087019
H	5.325847	0.051139	0.555935	H	-3.182778	3.158784	0.284093
H	3.755125	1.957840	0.232459	H	-4.039620	0.852101	0.201404
H	2.058485	-2.709739	-0.023069	N	0.214556	-0.813612	-0.468596
H	4.476039	-2.293488	0.422821	N	1.137292	1.730039	-0.354673
C	2.048551	0.696658	-0.102001	H	-0.180227	-1.753239	-0.474568
C	1.567578	-0.625031	-0.171959	H	1.470185	2.669043	-0.173273
C	-0.231908	1.520595	-0.154592	C	-2.578933	-1.472480	-0.005937
C	-1.115625	2.568270	0.047005	O	-1.901711	-2.427305	-0.406402
C	-2.492721	2.322897	0.166460	N	-3.835571	-1.673839	0.463875

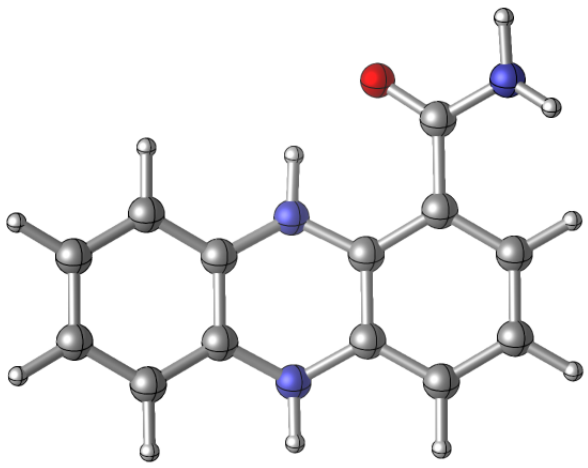

Zero-point correction= 0.222637 (Hartree/Particle)

Thermal correction to Energy= 0.235668

Thermal correction to Enthalpy= 0.236612

Thermal correction to Gibbs Free Energy= 0.183037

Sum of electronic and zero-point Energies= -741.127643

Sum of electronic and thermal Energies= -741.114611

Sum of electronic and thermal Enthalpies= -741.113667

Sum of electronic and thermal Free Energies= -741.167242

PCN_reduced_open_octanol

E(scf) = -741.343252018 a.u.

C	4.266249	-0.132813	0.339122	C	3.389359	0.924834	0.072322

C	2.427298	-1.688224	0.171316	C	-2.096826	-0.039698	0.035043
C	3.786764	-1.436441	0.389526	C	-0.726489	0.172047	-0.184274
H	5.323217	0.075440	0.511061	H	-0.688351	3.583098	-0.011319
H	3.756466	1.953048	0.039799	H	-3.120785	3.201125	0.390088
H	2.040517	-2.708852	0.215237	H	-4.003182	0.860831	0.439111
H	4.460926	-2.267257	0.601926	N	0.195387	-0.860931	-0.392746
C	2.040914	0.676366	-0.164856	N	1.128755	1.690227	-0.485153
C	1.556279	-0.642675	-0.116010	H	-0.142689	-1.792873	-0.175788
C	-0.232087	1.498275	-0.207066	H	1.466690	2.636588	-0.358573
C	-1.091009	2.567905	0.004758	C	-2.742847	-1.393074	0.080304
C	-2.456224	2.351409	0.230973	O	-3.710140	-1.620595	0.792477
C	-2.947672	1.060104	0.255271	N	-2.183770	-2.368368	-0.706543

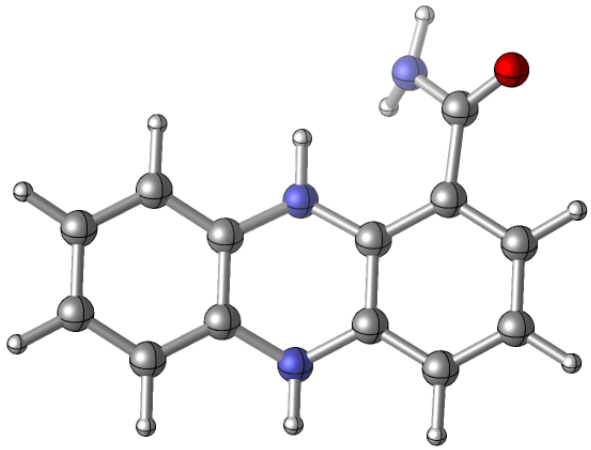

Zero-point correction= 0.222925 (Hartree/Particle)

Thermal correction to Energy= 0.235885

Thermal correction to Enthalpy= 0.236829

Thermal correction to Gibbs Free Energy= 0.183435

Sum of electronic and zero-point Energies= -741.120327

Sum of electronic and thermal Energies= -741.107367

Sum of electronic and thermal Enthalpies= -741.106423

Sum of electronic and thermal Free Energies= -741.159817

PCN_reduced_closed_octanol

E(scf) = -741.348848925 a.u.

C	4.274051	-0.144341	0.348602	C	-2.495249	2.322250	0.161805
C	3.393058	0.930094	0.171457	C	-2.967497	1.026370	0.125983
C	2.444131	-1.687691	0.025565	C	-2.082095	-0.065798	-0.028023
C	3.801461	-1.448927	0.274436	C	-0.710129	0.185518	-0.211966
H	5.328641	0.052440	0.546852	H	-0.734993	3.589978	0.086706
H	3.756130	1.958619	0.230817	H	-3.185902	3.158143	0.275785
H	2.060902	-2.708954	-0.025912	H	-4.041483	0.850700	0.191334
H	4.479601	-2.292202	0.412830	N	0.214580	-0.813973	-0.460438
C	2.048979	0.697134	-0.099261	N	1.136565	1.730677	-0.346972
C	1.568394	-0.624565	-0.169557	H	-0.180011	-1.753662	-0.470509
C	-0.232784	1.520685	-0.150992	H	1.469130	2.669571	-0.165572
C	-1.117649	2.567820	0.046771	C	-2.578317	-1.472963	-0.005634

O	-1.898674	-2.429172	-0.396416	N	-3.840234	-1.673359	0.454903

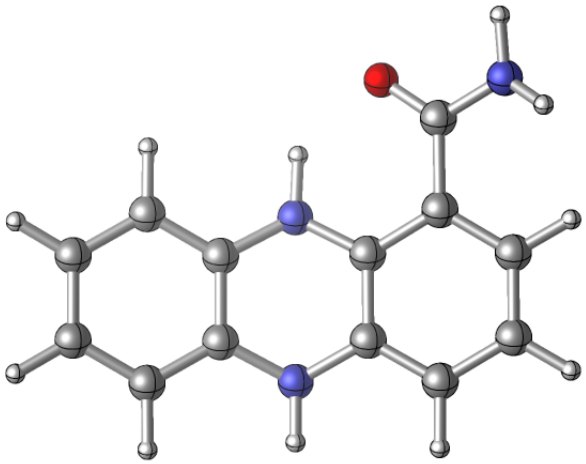

Zero-point correction= 0.222673 (Hartree/Particle)

Thermal correction to Energy= 0.235698

Thermal correction to Enthalpy= 0.236643

Thermal correction to Gibbs Free Energy= 0.183084

Sum of electronic and zero-point Energies= -741.126176

Sum of electronic and thermal Energies= -741.113150

Sum of electronic and thermal Enthalpies= -741.112206

Sum of electronic and thermal Free Energies= -741.165764

PCN_oxidized_open

E(scf) = -740.117781549 a.u.

C	4.268597	-0.149452	-0.057849	C	-2.902959	1.040718	0.022377
C	3.418177	0.917723	-0.016329	C	-2.065135	-0.042198	0.035074
C	2.419715	-1.728407	-0.081988	C	-0.640245	0.163139	0.028671
C	3.763577	-1.488011	-0.092264	H	-0.636280	3.615611	0.053943
H	5.347645	0.011511	-0.066259	H	-3.098568	3.209574	0.034698
H	3.780517	1.946314	0.008074	H	-3.983520	0.886673	0.022691
H	2.011973	-2.739829	-0.106099	N	0.181388	-0.890543	-0.019334
H	4.467787	-2.320652	-0.126566	N	1.180302	1.763172	0.022955
C	2.002308	0.707369	-0.005385	C	-2.625609	-1.439817	0.130561
C	1.495221	-0.636637	-0.034648	O	-2.359024	-2.185444	1.062767
C	-0.134069	1.508387	0.035333	N	-3.481903	-1.767981	-0.863254
C	-1.051504	2.607128	0.044139	H	-3.895894	-2.692300	-0.867740
C	-2.395302	2.375964	0.032432	H	-3.596606	-1.181321	-1.678176

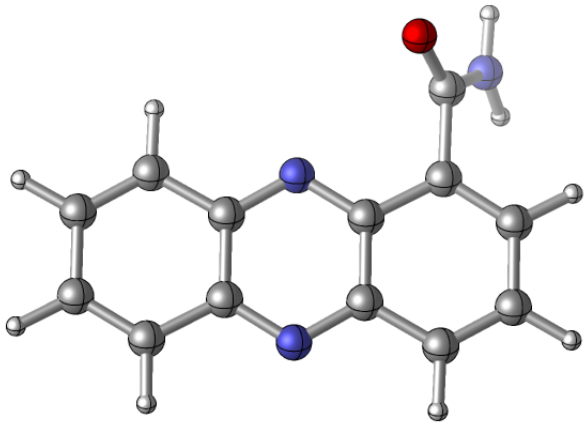

Zero-point correction= 0.198600 (Hartree/Particle)

Thermal correction to Energy= 0.211223

Thermal correction to Enthalpy= 0.212167

Thermal correction to Gibbs Free Energy= 0.159034

Sum of electronic and zero-point Energies= -739.919182

Sum of electronic and thermal Energies= -739.906558

Sum of electronic and thermal Enthalpies= -739.905614

Sum of electronic and thermal Free Energies= -739.958748

PCN_oxidized_closed

E(scf) = -740.126441754 a.u.

C	4.274329	-0.080236	-0.000040	C	-1.078581	2.597968	-0.000020
C	3.405623	0.972809	-0.000105	C	-2.420738	2.360587	0.000053
C	2.451906	-1.692672	0.000151	C	-2.913119	1.024198	0.000075
C	3.791522	-1.427083	0.000094	C	-2.086065	-0.069045	0.000015
H	5.350509	0.098160	-0.000088	C	-0.655906	0.148648	0.000018
H	3.748822	2.008072	-0.000203	H	-0.663274	3.606340	-0.000059
H	2.066064	-2.712973	0.000247	H	-3.129852	3.189046	0.000082
H	4.510003	-2.248099	0.000147	H	-3.987589	0.839869	0.000126
C	1.994351	0.735985	-0.000043	N	0.200789	-0.880145	0.000102
C	1.512233	-0.614895	0.000073	N	1.150390	1.773560	-0.000080
C	-0.159736	1.501576	-0.000032	C	-2.777180	-1.420415	-0.000001

O	-4.005661	-1.484062	0.000089	H	-2.432034	-3.419644	-0.000376
N	-1.990017	-2.509700	-0.000277	H	-0.977340	-2.398828	-0.000227

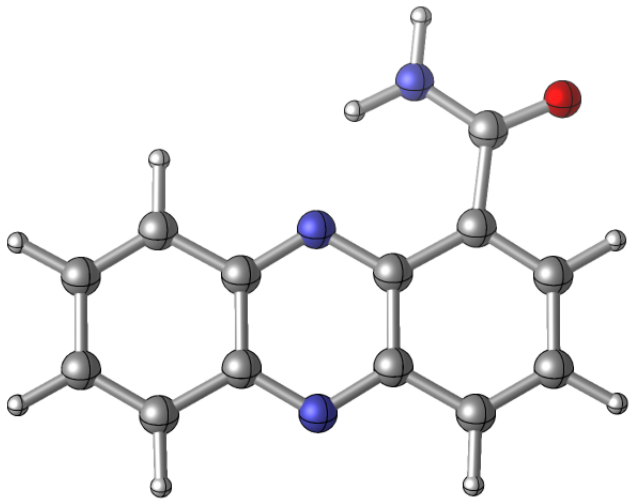

Zero-point correction= 0.199481 (Hartree/Particle)

Thermal correction to Energy= 0.211626

Thermal correction to Enthalpy= 0.212570

Thermal correction to Gibbs Free Energy= 0.160749

Sum of electronic and zero-point Energies= -739.926961

Sum of electronic and thermal Energies= -739.914816

Sum of electronic and thermal Enthalpies= -739.913872

Sum of electronic and thermal Free Energies= -739.965693

PCN_oxidized_open_octanol

E(scf) = -740.116075096 a.u.

C	4.267756	-0.150208	0.057228	C	-2.902790	1.041062	-0.021913
C	3.417806	0.917255	0.015963	C	-2.064909	-0.041713	-0.034938
C	2.418525	-1.728594	0.081733	C	-0.640150	0.163769	-0.028284
C	3.762360	-1.488591	0.091631	H	-0.635517	3.615748	-0.053518
H	5.346877	0.010451	0.065289	H	-3.098166	3.210021	-0.034164
H	3.779943	1.945870	-0.008593	H	-3.983261	0.886324	-0.022942
H	2.009676	-2.739514	0.105364	N	0.180803	-0.890228	0.020080
H	4.466300	-2.321497	0.125401	N	1.180502	1.763572	-0.022629
C	2.001887	0.707407	0.005304	C	-2.624526	-1.439793	-0.131907
C	1.494464	-0.636481	0.034743	O	-2.361952	-2.182750	-1.065576
C	-0.133809	1.508827	-0.034985	N	-3.482142	-1.768677	0.863265
C	-1.051239	2.607508	-0.043547	H	-3.876435	-2.701520	0.875113
C	-2.395024	2.376248	-0.031721	H	-3.570053	-1.196723	1.691812

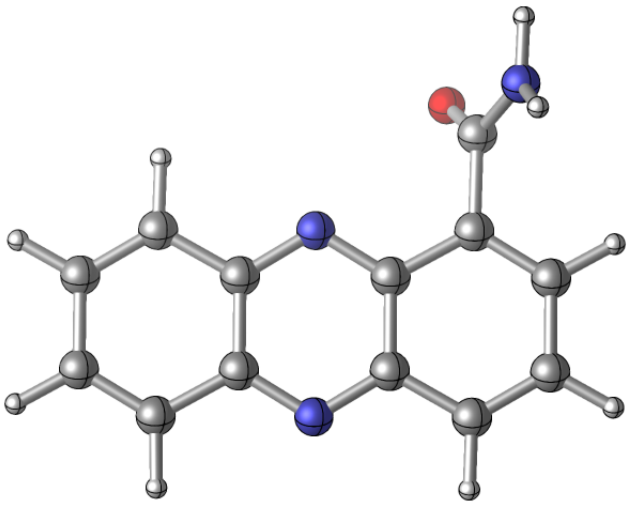

Zero-point correction= 0.198606 (Hartree/Particle)

Thermal correction to Energy= 0.211228

Thermal correction to Enthalpy= 0.212172

Thermal correction to Gibbs Free Energy= 0.159018

Sum of electronic and zero-point Energies= -739.917469

Sum of electronic and thermal Energies= -739.904847

Sum of electronic and thermal Enthalpies= -739.903903

Sum of electronic and thermal Free Energies= -739.957057

PCN_oxidized_closed_octanol

E(scf) = -740.125300697 a.u.

C	4.274595	-0.080572	-0.000088	C	2.452154	-1.692772	-0.000106
C	3.405751	0.972320	-0.000033	C	3.791772	-1.427300	-0.000125

H	5.350784	0.097963	-0.000102	C	-0.655772	0.148320	0.000065
H	3.748259	2.007798	-0.000003	H	-0.661399	3.605951	0.000073
H	2.066248	-2.713055	-0.000134	H	-3.128678	3.189446	0.000020
H	4.510135	-2.248469	-0.000170	H	-3.987013	0.839586	0.000025
C	1.994521	0.735469	-0.000012	N	0.200828	-0.880606	-0.000010
C	1.512307	-0.615154	-0.000041	N	1.150841	1.773244	0.000035
C	-0.159106	1.501308	0.000065	C	-2.778760	-1.419709	0.000007
C	-1.077623	2.597972	0.000076	O	-4.006391	-1.482046	-0.000794
C	-2.419725	2.360793	0.000057	N	-1.991868	-2.510076	0.000841
C	-2.912600	1.024532	0.000054	H	-2.436049	-3.418845	-0.000017
C	-2.085925	-0.068845	0.000093	H	-0.979303	-2.400113	0.000510

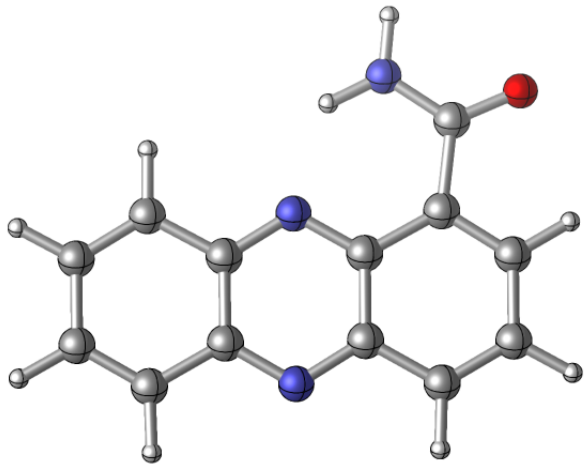

Zero-point correction= 0.199512 (Hartree/Particle)

Thermal correction to Energy= 0.211659

Thermal correction to Enthalpy= 0.212603

Thermal correction to Gibbs Free Energy= 0.160772

Sum of electronic and zero-point Energies= -739.925789

Sum of electronic and thermal Energies= -739.913642

Sum of electronic and thermal Enthalpies= -739.912698

Sum of electronic and thermal Free Energies= -739.964528

PCA_reduced_open

E(scf) = -761.201341105 a.u.

C	-4.259925	-0.088303	0.255285	C	3.011883	0.981990	0.192962
C	-3.356999	0.973941	0.126341	C	2.108781	-0.085982	0.015653
C	-2.454687	-1.657321	-0.078580	C	0.744306	0.172370	-0.179179
C	-3.811877	-1.399637	0.150225	H	0.805651	3.566147	0.185254
H	-5.314097	0.122902	0.440183	H	3.244749	3.107639	0.421218
H	-3.702333	2.006789	0.207980	H	4.071840	0.751575	0.298147
H	-2.090671	-2.684367	-0.151800	N	-0.196474	-0.806090	-0.494327
H	-4.508306	-2.233158	0.250193	N	-1.077419	1.746331	-0.332748
C	-2.012237	0.723921	-0.128104	C	2.689585	-1.460518	0.020798
C	-1.559125	-0.604380	-0.225785	O	3.781918	-1.730642	-0.415763
C	0.282712	1.509525	-0.109398	O	1.942298	-2.446330	0.570087
C	1.179447	2.541682	0.128672	H	1.223262	-2.067673	1.098089
C	2.551178	2.281831	0.261223	H	0.113571	-1.757666	-0.635296

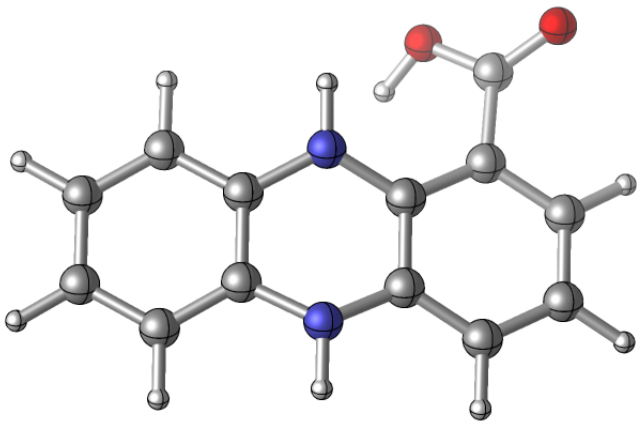

Zero-point correction= 0.209784 (Hartree/Particle)

Thermal correction to Energy= 0.222886

Thermal correction to Enthalpy= 0.223830

Thermal correction to Gibbs Free Energy= 0.169523

Sum of electronic and zero-point Energies= -760.991557

Sum of electronic and thermal Energies= -760.978455

Sum of electronic and thermal Enthalpies= -760.977511

Sum of electronic and thermal Free Energies= -761.031818

PCA_reduced_closed

E(scf) = -761.215996897 a.u.

C	4.298767	-0.126822	-0.257468	C	-2.976924	1.017332	-0.174335
C	3.406658	0.939664	-0.090769	C	-2.086331	-0.070028	-0.007978
C	2.465527	-1.684020	-0.044680	C	-0.708871	0.169411	0.155239
C	3.830515	-1.434971	-0.233802	H	-0.742647	3.576494	-0.081894
H	5.359467	0.079086	-0.408113	H	-3.186421	3.148688	-0.332177
H	3.766727	1.970597	-0.111561	H	-4.040248	0.812877	-0.284817
H	2.085666	-2.707797	-0.031892	N	0.212111	-0.838047	0.360457
H	4.517411	-2.272187	-0.364867	N	1.129272	1.722215	0.344869
C	2.052725	0.696330	0.117305	C	-2.596686	-1.453629	-0.007818
C	1.578066	-0.628787	0.137250	O	-1.917281	-2.461508	0.131264
C	-0.235963	1.508374	0.130144	O	-3.921116	-1.536058	-0.183638
C	-1.124180	2.553374	-0.058754	H	-4.146620	-2.479924	-0.168227
C	-2.502192	2.310148	-0.200657				

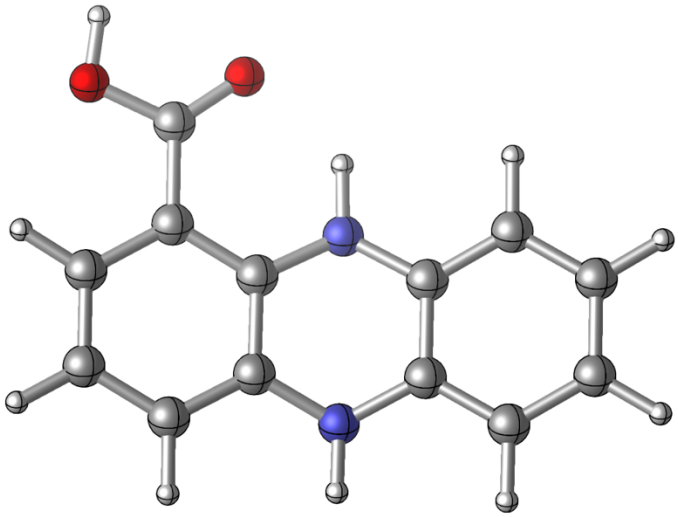

Zero-point correction= 0.210624 (Hartree/Particle)

Thermal correction to Energy= 0.223276

Thermal correction to Enthalpy= 0.224220

Thermal correction to Gibbs Free Energy= 0.171229

Sum of electronic and zero-point Energies= -761.005373

Sum of electronic and thermal Energies= -760.992721

Sum of electronic and thermal Enthalpies= -760.991777

Sum of electronic and thermal Free Energies= -761.044768

PCA_oxidized_open

E(scf) = -759.980243658 a.u.

C	-4.289817	-0.130663	0.032770	C	0.125842	1.489812	-0.041310
C	-3.432029	0.929998	-0.019327	C	1.042480	2.588707	-0.050934
C	-2.451764	-1.721637	0.105607	C	2.386282	2.361274	-0.017863
C	-3.793921	-1.471652	0.097513	C	2.890471	1.028428	0.010995
H	-5.367807	0.037166	0.026967	C	2.055414	-0.060240	-0.006310
H	-3.786675	1.960467	-0.065868	C	0.625712	0.140980	-0.013633
H	-2.051261	-2.735102	0.152446	H	0.624540	3.595786	-0.077690
H	-4.504268	-2.298687	0.140068	H	3.089663	3.194336	-0.018449
C	-2.017925	0.708516	-0.011540	H	3.968632	0.871511	0.027402
C	-1.519557	-0.637049	0.046404	N	-0.207960	-0.901439	0.047524

N	-1.186134	1.755522	-0.045986	O	3.839543	-1.490059	0.533282
C	2.645772	-1.431828	-0.080194	H	4.189200	-2.383375	0.381730
O	2.159816	-2.383511	-0.644587				

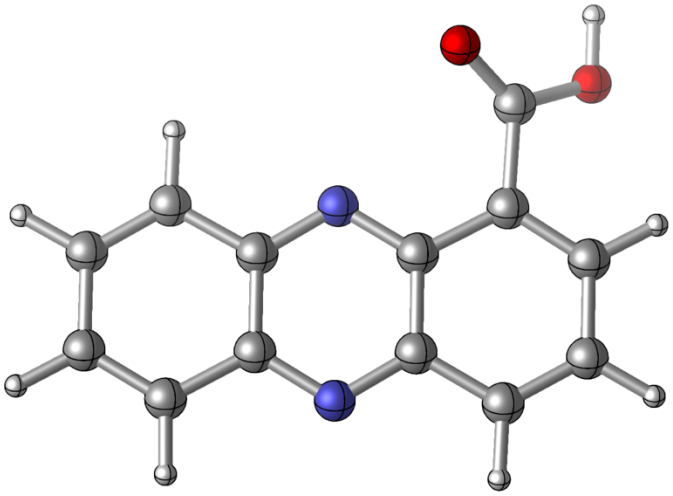

Zero-point correction= 0.186892 (Hartree/Particle)

Thermal correction to Energy= 0.198931

Thermal correction to Enthalpy= 0.199875

Thermal correction to Gibbs Free Energy= 0.147772

Sum of electronic and zero-point Energies= -759.793352

Sum of electronic and thermal Energies= -759.781313

Sum of electronic and thermal Enthalpies= -759.780369

Sum of electronic and thermal Free Energies= -759.832472

PCA_oxidized_closed

E(scf) = -759.992882352 a.u.

C	-4.246355	-0.041451	0.000047	C	2.953185	0.977558	-0.000027
C	-3.368867	1.003913	0.000027	C	2.096482	-0.092601	-0.000021
C	-2.439176	-1.672719	0.000055	C	0.677969	0.155792	0.000000
C	-3.775870	-1.392602	0.000062	H	0.749435	3.602620	-0.000004
H	-5.320797	0.146200	0.000052	H	3.203105	3.137897	-0.000018
H	-3.702591	2.042056	0.000016	H	4.025052	0.778381	-0.000043
H	-2.063739	-2.696645	0.000064	N	-0.181579	-0.870138	0.000022
H	-4.502095	-2.206630	0.000079	N	-1.109233	1.788058	0.000005
C	-1.959629	0.755414	0.000020	C	2.693398	-1.477027	-0.000061
C	-1.492803	-0.603224	0.000033	O	3.893851	-1.652525	-0.000135
C	0.199130	1.508722	-0.000001	O	1.852795	-2.503169	0.000002
C	1.141292	2.584980	-0.000007	H	0.918551	-2.153510	0.000049
C	2.480509	2.321535	-0.000015				

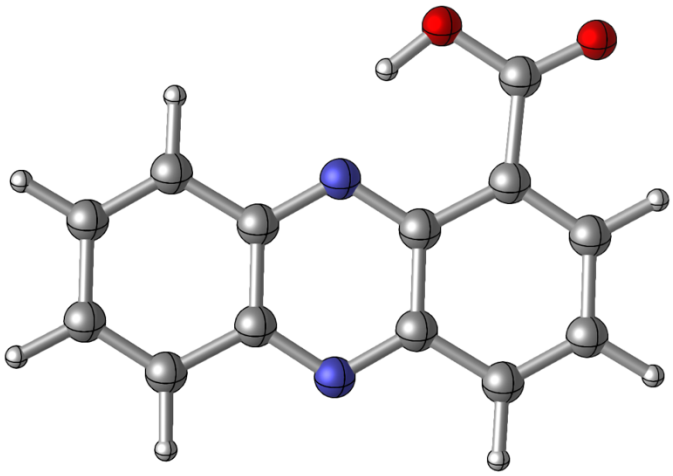

Zero-point correction= 0.187337 (Hartree/Particle)

Thermal correction to Energy= 0.198982

Thermal correction to Enthalpy= 0.199926

Thermal correction to Gibbs Free Energy= 0.149183

Sum of electronic and zero-point Energies= -759.805546

Sum of electronic and thermal Energies= -759.793900

Sum of electronic and thermal Enthalpies= -759.792956

Sum of electronic and thermal Free Energies= -759.843699

PCA_reduced_open_octanol

E(scf) = -761.199691694 a.u.

C	-4.261289	-0.087140	0.251274	C	3.013527	0.981461	0.189518
C	-3.357376	0.974508	0.125126	C	2.109865	-0.086167	0.015226
C	-2.456185	-1.656489	-0.079256	C	0.745131	0.172405	-0.176806
C	-3.813766	-1.398443	0.146331	H	0.808192	3.566227	0.183726
H	-5.315783	0.124526	0.433564	H	3.247466	3.107219	0.415032
H	-3.702675	2.007456	0.206175	H	4.073619	0.750328	0.291481
H	-2.092720	-2.683764	-0.152714	N	-0.196446	-0.807032	-0.487416
H	-4.510897	-2.231637	0.243708	N	-1.076782	1.746509	-0.327862
C	-2.012194	0.724266	-0.126082	C	2.689993	-1.461532	0.020020
C	-1.559450	-0.604228	-0.223327	O	3.780680	-1.733342	-0.417137
C	0.283862	1.509455	-0.107513	O	1.939803	-2.445492	0.571470
C	1.181434	2.541471	0.127701	H	1.224197	-2.061727	1.099993
C	2.553265	2.281455	0.257647				

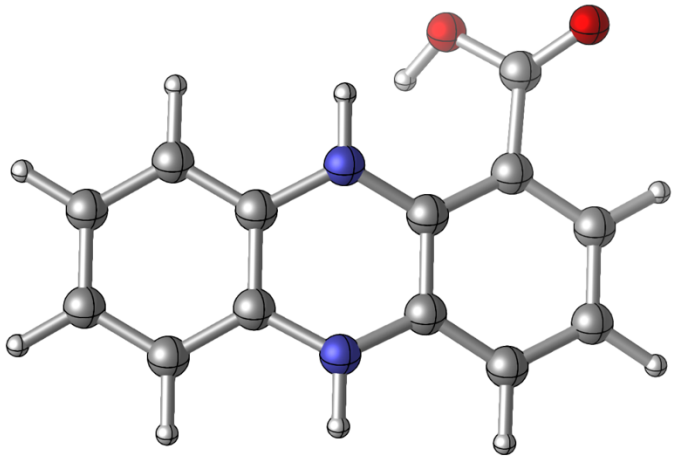

Zero-point correction= 0.209795 (Hartree/Particle)

Thermal correction to Energy= 0.222919

Thermal correction to Enthalpy= 0.223863

Thermal correction to Gibbs Free Energy= 0.169449

Sum of electronic and zero-point Energies= -760.989896

Sum of electronic and thermal Energies= -760.976773

Sum of electronic and thermal Enthalpies= -760.975828

Sum of electronic and thermal Free Energies= -761.030243

PCA_reduced_closed_octanol

E(scf) = -761.214907541 a.u.

C	4.299660	-0.126425	-0.254270	C	-0.236539	1.508512	0.128449
C	3.407050	0.939837	-0.089576	C	-1.125355	2.553150	-0.058305
C	2.466329	-1.683501	-0.043958	C	-2.503573	2.309861	-0.198385
C	3.831505	-1.434433	-0.230742	C	-2.977831	1.017053	-0.172076
H	5.360588	0.079503	-0.403062	C	-2.086642	-0.070063	-0.007772
H	3.767215	1.970791	-0.109978	C	-0.708979	0.169353	0.153258
H	2.086511	-2.707277	-0.031342	H	-0.744205	3.576476	-0.081127
H	4.518726	-2.271607	-0.360112	H	-3.188194	3.148308	-0.328328
C	2.052901	0.696525	0.115969	H	-4.041186	0.812023	-0.281006
C	1.578289	-0.628509	0.135651	N	0.212091	-0.838054	0.355429

N	1.128948	1.722568	0.341134	O	-3.921425	-1.537092	-0.180568
C	-2.596086	-1.453682	-0.007716	H	-4.143879	-2.481522	-0.165145
O	-1.916580	-2.461616	0.128687				

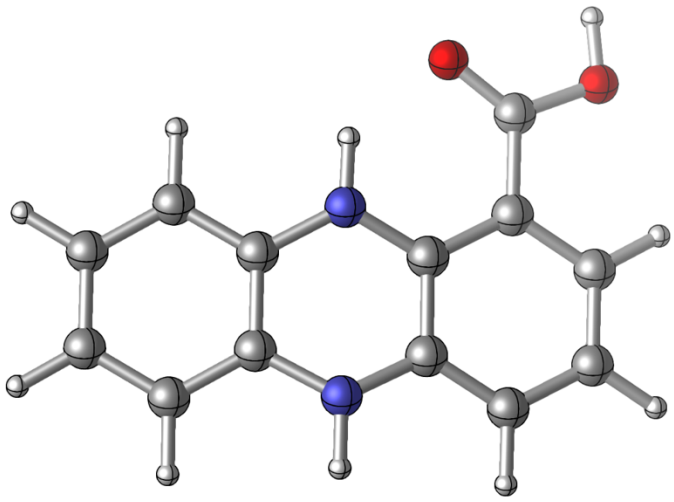

Zero-point correction= 0.210677 (Hartree/Particle)

Thermal correction to Energy= 0.223327

Thermal correction to Enthalpy= 0.224271

Thermal correction to Gibbs Free Energy= 0.171287

Sum of electronic and zero-point Energies= -761.004230

Sum of electronic and thermal Energies= -760.991580

Sum of electronic and thermal Enthalpies= -760.990636

Sum of electronic and thermal Free Energies= -761.043621

PCA_oxidized_open_octanol

E(scf) = -759.979014688 a.u.

C	-4.289349	-0.131025	0.032079	C	2.890165	1.028462	0.011327
C	-3.431899	0.929830	-0.019962	C	2.055153	-0.060132	-0.005938
C	-2.451119	-1.721641	0.105826	C	0.625483	0.141233	-0.013077
C	-3.793225	-1.471912	0.097211	H	0.623646	3.595662	-0.077573
H	-5.367408	0.036631	0.025858	H	3.089245	3.194447	-0.017934
H	-3.786246	1.960365	-0.066861	H	3.968262	0.871086	0.027926
H	-2.049545	-2.734635	0.152682	N	-0.207844	-0.901247	0.048414
H	-4.503406	-2.299141	0.139537	N	-1.186366	1.755883	-0.046069
C	-2.017753	0.708672	-0.011717	C	2.644806	-1.432050	-0.080187
C	-1.519207	-0.636785	0.046715	O	2.157326	-2.384676	-0.640315
C	0.125518	1.489969	-0.041126	O	3.842326	-1.489228	0.528434
C	1.042137	2.588818	-0.050699	H	4.188007	-2.383925	0.377014
C	2.385905	2.361275	-0.017454				

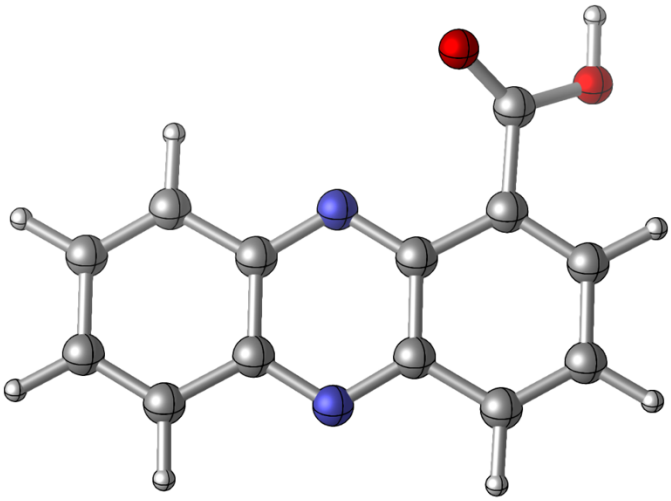

Zero-point correction= 0.186912 (Hartree/Particle)

Thermal correction to Energy= 0.198950

Thermal correction to Enthalpy= 0.199894

Thermal correction to Gibbs Free Energy= 0.147789

Sum of electronic and zero-point Energies= -759.792102

Sum of electronic and thermal Energies= -759.780065

Sum of electronic and thermal Enthalpies= -759.779120

Sum of electronic and thermal Free Energies= -759.831226

PCA_oxidized_closed_octanol

E(scf) = -759.991601693 a.u.

C	-4.247046	-0.042524	0.000073	C	2.952011	0.978030	-0.000105
C	-3.369700	1.002951	0.000093	C	2.095996	-0.092548	-0.000047
C	-2.439530	-1.673216	-0.000045	C	0.677332	0.155435	-0.000025
C	-3.776283	-1.393520	0.000002	H	0.746783	3.602397	-0.000030
H	-5.321555	0.145029	0.000104	H	3.201170	3.138567	-0.000170
H	-3.703084	2.041213	0.000135	H	4.023779	0.777977	-0.000120
H	-2.063568	-2.696979	-0.000112	N	-0.182012	-0.870638	-0.000053
H	-4.502233	-2.207855	-0.000009	N	-1.110386	1.787701	0.000034
C	-1.960425	0.754738	0.000041	C	2.695976	-1.475705	0.000055
C	-1.493239	-0.603555	-0.000019	O	3.895975	-1.647784	0.000171
C	0.197864	1.508465	-0.000006	O	1.858179	-2.504207	-0.000003
C	1.139605	2.585118	-0.000050	H	0.924140	-2.157386	-0.000080
C	2.478791	2.321916	-0.000122				

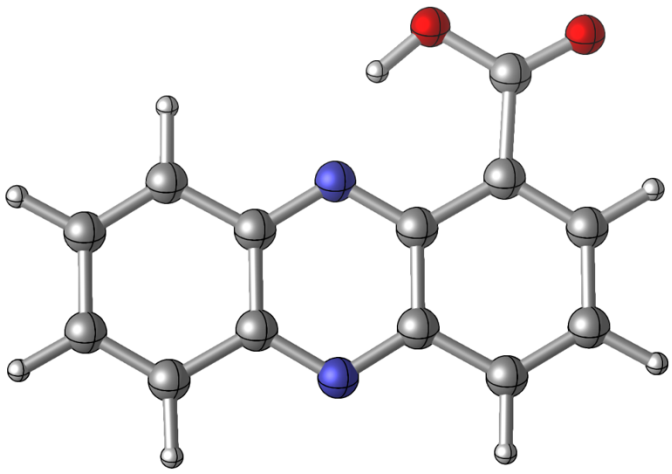

Zero-point correction= 0.187403 (Hartree/Particle)

Thermal correction to Energy= 0.199054

Thermal correction to Enthalpy= 0.199998

Thermal correction to Gibbs Free Energy= 0.149223

Sum of electronic and zero-point Energies= -759.804199

Sum of electronic and thermal Energies= -759.792548

Sum of electronic and thermal Enthalpies= -759.791604

Sum of electronic and thermal Free Energies= -759.842378

PCA_reduced_negative_closed

E(scf) = -760.737927513 a.u.

C	4.228089	-0.080592	-0.331218	C	-0.298591	1.501650	0.173327
C	3.328840	0.974091	-0.120281	C	-1.191459	2.535166	-0.075127
C	2.420506	-1.658916	-0.045872	C	-2.552249	2.253938	-0.269527
C	3.773949	-1.393116	-0.292929	C	-2.994831	0.941148	-0.238223
H	5.278901	0.138334	-0.527533	C	-2.107443	-0.127220	-0.016046
H	3.675549	2.009876	-0.153210	C	-0.752626	0.163867	0.206591
H	2.053636	-2.687509	-0.022382	H	-0.826322	3.564790	-0.105151
H	4.463810	-2.222445	-0.458446	H	-3.251654	3.072727	-0.448414
C	1.989619	0.715024	0.150943	H	-4.044491	0.691034	-0.392725
C	1.523711	-0.617938	0.185853	N	0.180439	-0.836966	0.483792

N	1.065035	1.731446	0.437145	O	-3.880254	-1.698651	-0.186800
C	-2.649268	-1.561069	-0.033145	H	-0.248397	-1.766557	0.344832
O	-1.809279	-2.502678	0.099870	H	1.387433	2.672824	0.245840

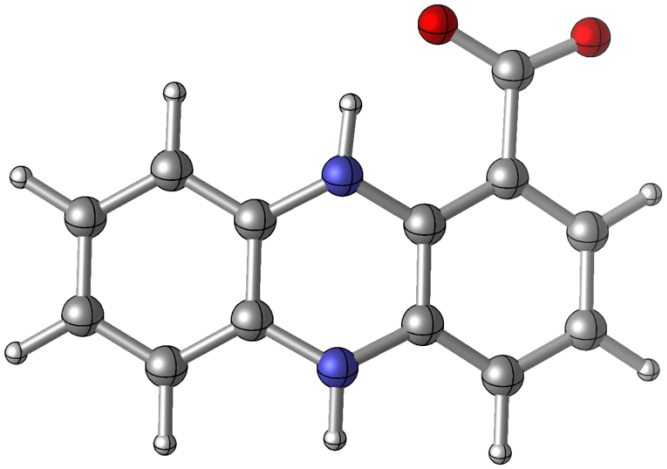

Zero-point correction= 0.197392 (Hartree/Particle)

Thermal correction to Energy= 0.209658

Thermal correction to Enthalpy= 0.210603

Thermal correction to Gibbs Free Energy= 0.158373

Sum of electronic and zero-point Energies= -760.540536

Sum of electronic and thermal Energies= -760.528269

Sum of electronic and thermal Enthalpies= -760.527325

Sum of electronic and thermal Free Energies= -760.579554

PCA_oxidized_negative

E(scf) = -759.498515862 a.u.

C	-4.246396	-0.096328	0.027940	C	2.457872	2.311626	-0.008023
C	-3.375913	0.954335	-0.033302	C	2.941461	0.969543	0.045500
C	-2.424514	-1.701425	0.127911	C	2.103719	-0.115551	0.013985
C	-3.765041	-1.440946	0.111767	C	0.680039	0.125624	-0.004984
H	-5.322587	0.083645	0.014849	H	0.719007	3.583491	-0.101789
H	-3.720600	1.987766	-0.094157	H	3.174383	3.135556	-0.007058
H	-2.033432	-2.718202	0.188676	H	4.017685	0.795292	0.101943
H	-4.483192	-2.260970	0.161973	N	-0.170309	-0.906253	0.064589
C	-1.963614	0.720720	-0.016302	N	-1.121647	1.760867	-0.058788
C	-1.479599	-0.627519	0.058618	C	2.706251	-1.530944	-0.046480
C	0.188939	1.482782	-0.045709	O	2.303707	-2.253309	-0.983421
C	1.118846	2.569418	-0.060416	O	3.576308	-1.786302	0.817412

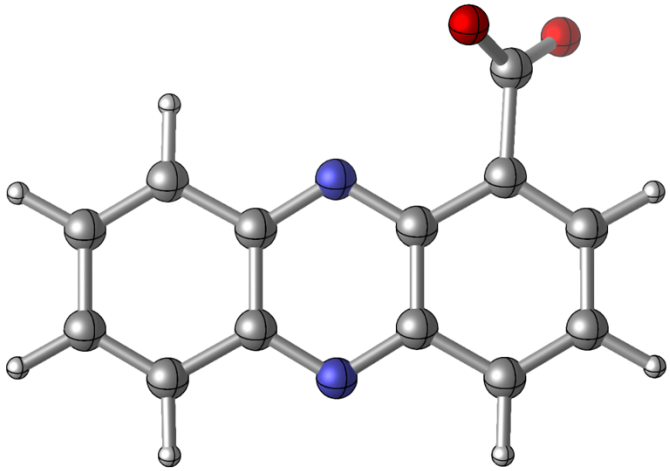

Zero-point correction= 0.173632 (Hartree/Particle)

Thermal correction to Energy= 0.185528

Thermal correction to Enthalpy= 0.186472

Thermal correction to Gibbs Free Energy= 0.134397

Sum of electronic and zero-point Energies= -759.324884

Sum of electronic and thermal Energies= -759.312988

Sum of electronic and thermal Enthalpies= -759.312044

Sum of electronic and thermal Free Energies= -759.364119

PCA_reduced_negative_octanol

E(scf) = -760.729175798 a.u.

C	4.228125	-0.079914	-0.329975	C	-2.554966	2.252764	-0.267270
C	3.327825	0.974602	-0.121144	C	-2.995915	0.939194	-0.235921
C	2.420123	-1.657814	-0.044340	C	-2.107379	-0.127666	-0.014871
C	3.773795	-1.392073	-0.290168	C	-0.753112	0.165284	0.206512
H	5.279128	0.139023	-0.525581	H	-0.830168	3.565765	-0.104134
H	3.674346	2.010582	-0.154725	H	-3.255697	3.070748	-0.445227
H	2.052825	-2.686170	-0.020528	H	-4.045012	0.685909	-0.389617
H	4.463772	-2.221759	-0.453937	N	0.179882	-0.836399	0.480121
C	1.988544	0.716104	0.149162	N	1.064552	1.733309	0.434600
C	1.521852	-0.617306	0.185083	C	-2.646592	-1.564173	-0.033284
C	-0.300376	1.502805	0.172836	O	-1.802336	-2.501786	0.101190
C	-1.194305	2.535608	-0.074153	O	-3.876152	-1.702520	-0.189234

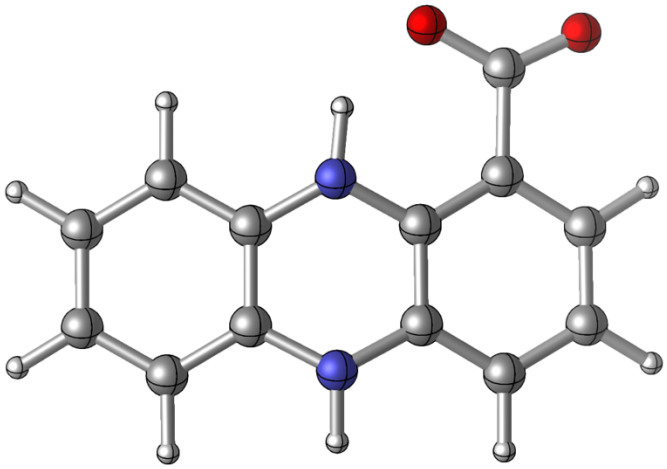

Zero-point correction= 0.197300 (Hartree/Particle)

Thermal correction to Energy= 0.209571

Thermal correction to Enthalpy= 0.210515

Thermal correction to Gibbs Free Energy= 0.158285

Sum of electronic and zero-point Energies= -760.531876

Sum of electronic and thermal Energies= -760.519605

Sum of electronic and thermal Enthalpies= -760.518661

Sum of electronic and thermal Free Energies= -760.570891

PCA_oxidized_negative_octanol

E(scf) = -759.488860169 a.u.

C	-4.247441	-0.097964	0.028371	C	0.187063	1.482584	-0.046890
C	-3.377257	0.953063	-0.033924	C	1.116632	2.569336	-0.062262
C	-2.424698	-1.701368	0.129655	C	2.455547	2.311039	-0.008391
C	-3.765526	-1.442137	0.113259	C	2.939584	0.969387	0.047030
H	-5.323804	0.081805	0.015193	C	2.103121	-0.116653	0.015456
H	-3.721876	1.986528	-0.095683	C	0.679145	0.124857	-0.004679
H	-2.031307	-2.717206	0.190861	H	0.716043	3.583088	-0.104890
H	-4.483015	-2.262831	0.163947	H	3.171969	3.135293	-0.007593
C	-1.964858	0.720416	-0.016872	H	4.015283	0.793337	0.106301
C	-1.480439	-0.626969	0.059495	N	-0.171378	-0.906166	0.066322

N	-1.123344	1.761128	-0.060244	O	2.292839	-2.259368	-0.971763
C	2.710981	-1.532125	-0.046678	O	3.598240	-1.773825	0.802750

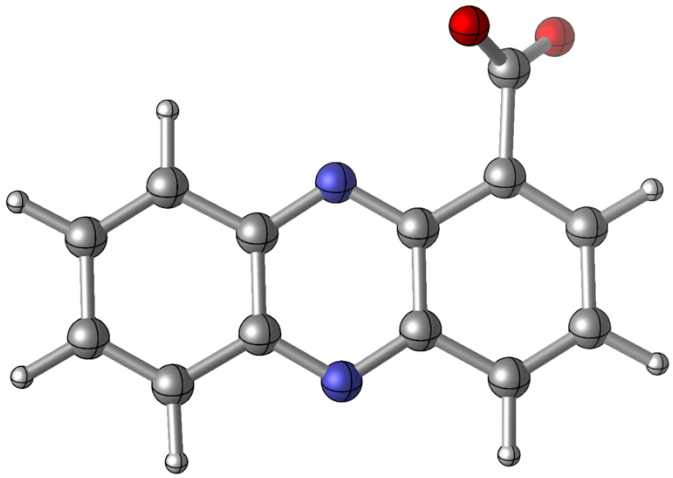

Zero-point correction= 0.173589 (Hartree/Particle)

Thermal correction to Energy= 0.185485

Thermal correction to Enthalpy= 0.186429

Thermal correction to Gibbs Free Energy= 0.134403

Sum of electronic and zero-point Energies= -759.315271

Sum of electronic and thermal Energies= -759.303376

Sum of electronic and thermal Enthalpies= -759.302431

Sum of electronic and thermal Free Energies= -759.354457

Pyocyanin_reduced_closed

E(scf) = -687.172803951 a.u.

C	3.769293	0.059908	0.475917	C	-2.372023	-1.064893	0.026112
C	2.716227	0.959781	0.260445	C	-1.116365	-0.511874	-0.227138
C	2.282851	-1.780057	0.010883	H	-1.847965	2.764622	0.384444
C	3.555878	-1.305627	0.349036	H	-4.079224	1.774243	0.770505
H	4.752989	0.444405	0.749596	H	-4.431181	-0.683846	0.553032
H	2.895657	2.027514	0.382930	N	-0.036495	-1.321916	-0.618450
H	2.097562	-2.852656	-0.080861	N	0.371841	1.355165	-0.410096
H	4.368683	-2.013680	0.517639	O	-2.458876	-2.418936	-0.106403
C	1.454301	0.500371	-0.114814	C	0.595776	2.782472	-0.459862
C	1.240241	-0.891871	-0.229427	H	0.679480	3.248050	0.539960
C	-0.917564	0.872805	-0.113498	H	1.518685	2.985715	-1.018515
C	-1.986974	1.691275	0.265376	H	-0.230804	3.260748	-1.000674
C	-3.245660	1.128153	0.491517	H	-3.354180	-2.707347	0.108697
C	-3.448422	-0.242876	0.373391	H	-0.211473	-2.314414	-0.503344

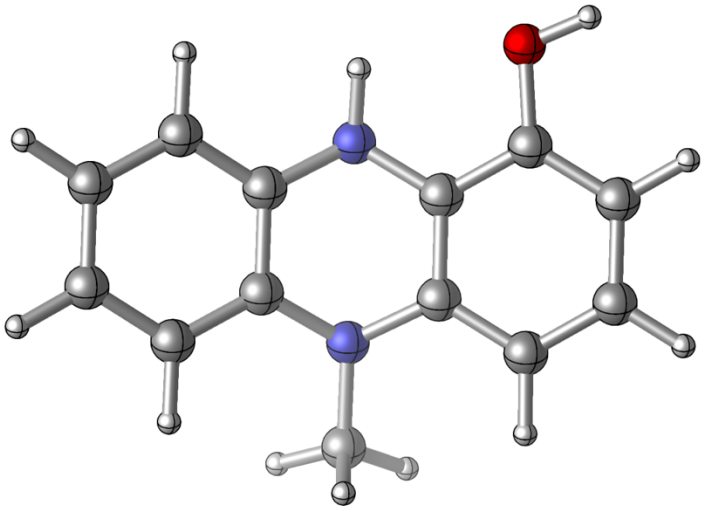

Zero-point correction= 0.228000 (Hartree/Particle)

Thermal correction to Energy= 0.240437

Thermal correction to Enthalpy= 0.241382

Thermal correction to Gibbs Free Energy= 0.189938

Sum of electronic and zero-point Energies= -686.944804

Sum of electronic and thermal Energies= -686.932367

Sum of electronic and thermal Enthalpies= -686.931422

Sum of electronic and thermal Free Energies= -686.982866

Pyocyanin_reduced_closed_octanol

E(scf) = -687.171721153 a.u.

C	3.769989	0.060489	0.474777	C	2.716408	0.959956	0.260703

C	2.283840	-1.779467	0.010081	C	-1.116258	-0.512090	-0.226103
C	3.556946	-1.304864	0.347248	H	-1.848770	2.764174	0.384585
H	4.753781	0.445118	0.747820	H	-4.080510	1.774084	0.767895
H	2.895434	2.027687	0.383813	H	-4.431934	-0.683853	0.550474
H	2.098967	-2.852099	-0.082209	N	-0.036296	-1.322003	-0.615839
H	4.370182	-2.012686	0.514583	N	0.371550	1.355021	-0.407706
C	1.454471	0.500396	-0.113679	O	-2.458907	-2.419334	-0.105932
C	1.240645	-0.891734	-0.228592	C	0.595191	2.781786	-0.460615
C	-0.917853	0.872604	-0.112434	H	0.679120	3.249921	0.538149
C	-1.987728	1.690870	0.265174	H	1.518003	2.983833	-1.019987
C	-3.246631	1.128008	0.489929	H	-0.231625	3.258725	-1.002387
C	-3.448911	-0.242964	0.371776	H	-3.355069	-2.706277	0.106454
C	-2.372054	-1.064754	0.025963	H	-0.211429	-2.314495	-0.502288

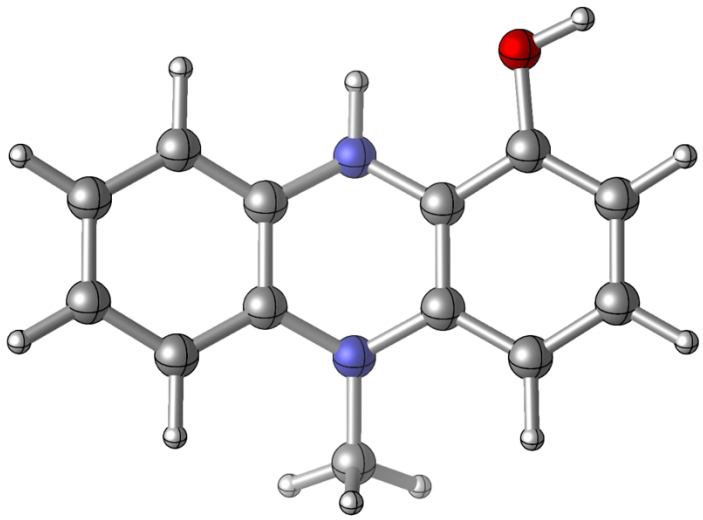

Zero-point correction= 0.228019 (Hartree/Particle)

Thermal correction to Energy= 0.240462

Thermal correction to Enthalpy= 0.241406

Thermal correction to Gibbs Free Energy= 0.189954

Sum of electronic and zero-point Energies= -686.943702

Sum of electronic and thermal Energies= -686.931260

Sum of electronic and thermal Enthalpies= -686.930315

Sum of electronic and thermal Free Energies= -686.981767

Pyocyanin_oxidized

E(scf) = -685.939462987 a.u.

C	3.816581	0.076282	0.085863	C	-2.066474	1.625696	0.099520
C	2.767988	0.977394	0.056406	C	-3.348049	1.003158	0.122644
C	2.302339	-1.782974	0.001714	C	-3.553944	-0.347071	0.059604
C	3.596371	-1.312816	0.051996	C	-2.441816	-1.262214	-0.027344
H	4.836009	0.460586	0.144345	C	-1.070620	-0.619298	-0.026090
H	2.989692	2.040612	0.109384	H	-2.010356	2.708822	0.164917
H	2.075029	-2.849528	-0.015046	H	-4.216751	1.662708	0.194897
H	4.439006	-2.003783	0.074434	H	-4.558815	-0.771019	0.074068
C	1.438238	0.509814	-0.012440	N	-0.051314	-1.421899	-0.055431
C	1.210753	-0.889384	-0.023554	N	0.341938	1.347828	-0.061319
C	-0.938409	0.839731	0.012720	O	-2.551125	-2.486980	-0.088933

C	0.494138	2.793403	-0.167434	H	1.488875	3.045335	-0.538599
H	0.329261	3.276051	0.806861	H	-0.239888	3.174233	-0.888173

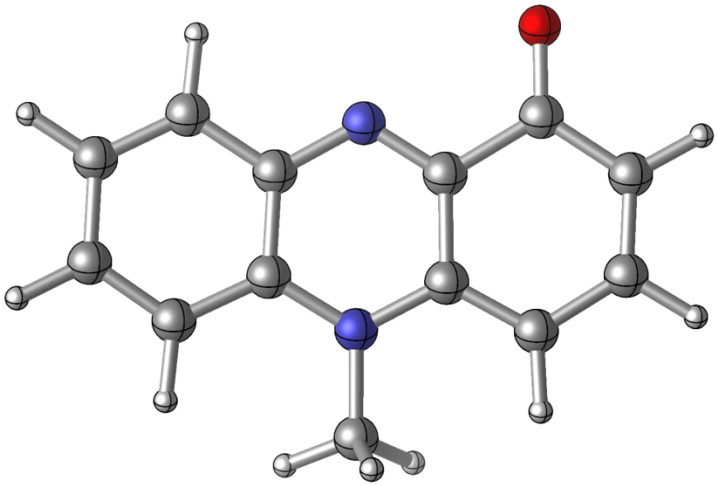

Zero-point correction= 0.204471 (Hartree/Particle)

Thermal correction to Energy= 0.216363

Thermal correction to Enthalpy= 0.217307

Thermal correction to Gibbs Free Energy= 0.166121

Sum of electronic and zero-point Energies= -685.734992

Sum of electronic and thermal Energies= -685.723100

Sum of electronic and thermal Enthalpies= -685.722156

Sum of electronic and thermal Free Energies= -685.773342

Pyocyanin_oxidized_octanol

E(scf) = -685.937499895 a.u.

C	3.817491	0.074970	0.088843	C	-3.556081	-0.345610	0.062926
C	2.768537	0.976521	0.057548	C	-2.442826	-1.261943	-0.029331
C	2.301710	-1.782749	0.003427	C	-1.070148	-0.619451	-0.027345
C	3.596644	-1.313236	0.055302	H	-2.009334	2.707978	0.172718
H	4.836978	0.459084	0.148760	H	-4.217211	1.663211	0.204939
H	2.990010	2.039899	0.111023	H	-4.560350	-0.770686	0.077997
H	2.073224	-2.849041	-0.013171	N	-0.052087	-1.422053	-0.057329
H	4.438610	-2.005007	0.079285	N	0.342794	1.348216	-0.064378
C	1.439242	0.509402	-0.013168	O	-2.553055	-2.484462	-0.095274
C	1.211213	-0.889254	-0.023846	C	0.496274	2.792371	-0.175068
C	-0.938392	0.840242	0.013582	H	0.343459	3.279379	0.799349
C	-2.065535	1.624893	0.104689	H	1.487518	3.041161	-0.558500
C	-3.349514	1.002723	0.129136	H	-0.245109	3.173310	-0.888442

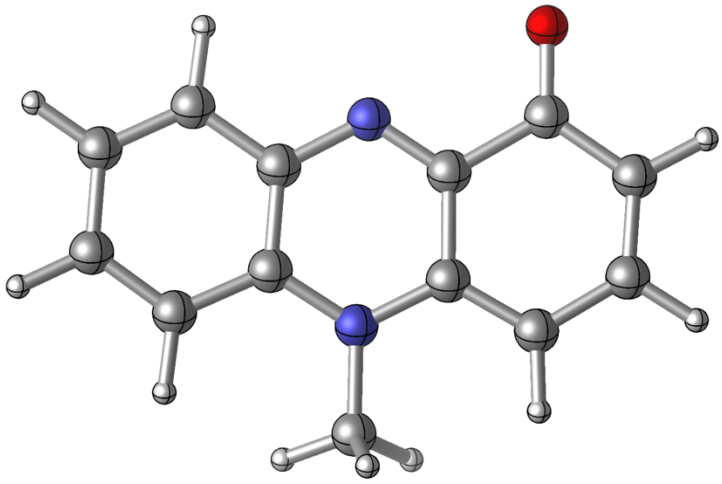

Zero-point correction= 0.204450 (Hartree/Particle)

Thermal correction to Energy= 0.216357

Thermal correction to Enthalpy= 0.217301

Thermal correction to Gibbs Free Energy= 0.166097

Sum of electronic and zero-point Energies= -685.733050

Sum of electronic and thermal Energies= -685.721143

Sum of electronic and thermal Enthalpies= -685.720199

Sum of electronic and thermal Free Energies= -685.771403

Pyocyanin_oxidized_protonated_closed

E(scf) = -686.399216694 a.u.

C	3.795705	0.081443	0.078293	C	-3.492922	-0.334325	0.039920
C	2.765322	0.988548	0.058985	C	-2.388366	-1.148490	-0.008160
C	2.290994	-1.796676	-0.017522	C	-1.070370	-0.553340	-0.018980
C	3.569320	-1.320492	0.030173	H	-2.016607	2.763922	0.121293
H	4.819069	0.453020	0.138981	H	-4.200045	1.695550	0.140181
H	2.991872	2.049216	0.121360	H	-4.490839	-0.769689	0.053983
H	2.062616	-2.861875	-0.041950	N	-0.048953	-1.389964	-0.047784
H	4.417098	-2.004659	0.041735	N	0.350334	1.364088	-0.046081
C	1.428158	0.523352	-0.007435	O	-2.483903	-2.473173	-0.037001
C	1.190980	-0.890441	-0.025981	C	0.549850	2.818425	-0.124026
C	-0.923403	0.875137	-0.000319	H	0.558954	3.246773	0.886221
C	-2.076009	1.681369	0.063076	H	1.488988	3.031486	-0.636583
C	-3.311883	1.064777	0.083234	H	-0.257799	3.256015	-0.715100

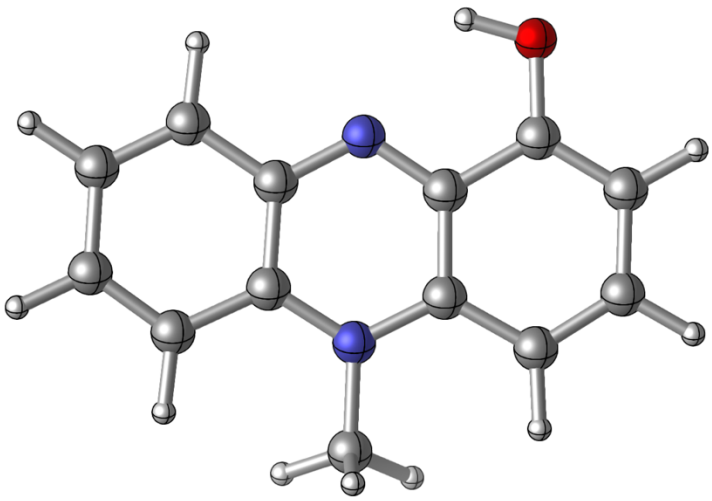

Zero-point correction= 0.218585 (Hartree/Particle)

Thermal correction to Energy= 0.230417

Thermal correction to Enthalpy= 0.231361

Thermal correction to Gibbs Free Energy= 0.180725

Sum of electronic and zero-point Energies= -686.180632

Sum of electronic and thermal Energies= -686.168800

Sum of electronic and thermal Enthalpies= -686.167855

Sum of electronic and thermal Free Energies= -686.218491

Pyocyanin_oxidized_protonated_open

E(scf) = -686.393711483 a.u.

C	3.812853	0.047861	0.081289	C	-0.900440	0.866881	-0.001226
C	2.790024	0.963508	0.060682	C	-2.035183	1.700795	0.066074
C	2.292140	-1.815848	-0.017345	C	-3.282321	1.116096	0.089539
C	3.574776	-1.352090	0.032304	C	-3.483875	-0.279570	0.043777
H	4.839206	0.411031	0.143814	C	-2.399999	-1.122517	-0.009372
H	3.026432	2.021947	0.124416	C	-1.063937	-0.563881	-0.021262
H	2.052835	-2.878639	-0.042488	H	-1.949260	2.781303	0.125715
H	4.416599	-2.043656	0.044828	H	-4.158880	1.762179	0.150622
C	1.449179	0.508352	-0.007652	H	-4.495863	-0.685159	0.060281
C	1.197223	-0.901349	-0.026731	N	-0.041277	-1.402675	-0.050948

N	0.375115	1.351916	-0.047935	H	0.548724	3.243887	0.874596
O	-2.466789	-2.452523	-0.044116	H	1.537803	3.013702	-0.606739
C	0.578990	2.805473	-0.130888	H	-0.203478	3.238454	-0.758547

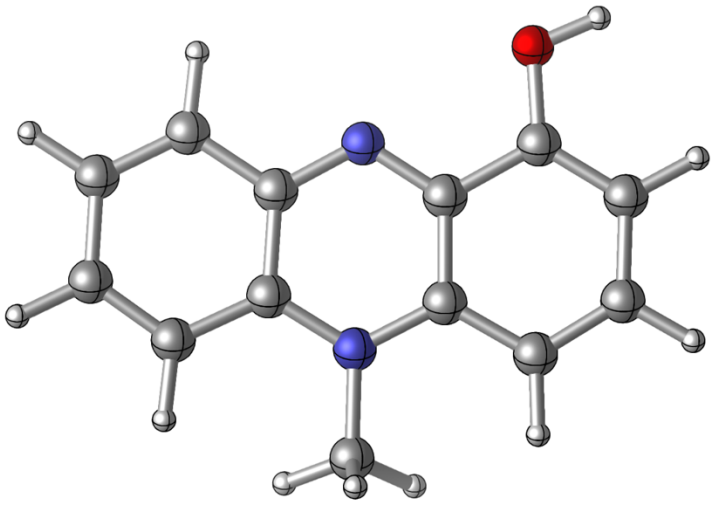

Zero-point correction= 0.218397 (Hartree/Particle)

Thermal correction to Energy= 0.230302

Thermal correction to Enthalpy= 0.231246

Thermal correction to Gibbs Free Energy= 0.180592

Sum of electronic and zero-point Energies= -686.175314

Sum of electronic and thermal Energies= -686.163410

Sum of electronic and thermal Enthalpies= -686.162466

Sum of electronic and thermal Free Energies= -686.213120

Pyocyanin_oxidized_protonated_closed_octanol

E(scf) = -686.393003486 a.u.

C	3.796316	0.080601	0.078611	C	-3.493461	-0.334190	0.040075
C	2.765948	0.988144	0.059396	C	-2.388705	-1.148734	-0.008282
C	2.291025	-1.796733	-0.017612	C	-1.070486	-0.553293	-0.019040
C	3.569676	-1.321055	0.030206	H	-2.017213	2.764042	0.122065
H	4.819823	0.451918	0.139487	H	-4.200381	1.695094	0.140829
H	2.993141	2.048733	0.122149	H	-4.491202	-0.769906	0.054157
H	2.062380	-2.861899	-0.042198	N	-0.048983	-1.389478	-0.047997
H	4.417205	-2.005551	0.041695	N	0.350649	1.364405	-0.046076
C	1.428819	0.523436	-0.007249	O	-2.485212	-2.472410	-0.037305
C	1.191357	-0.890229	-0.026022	C	0.550178	2.818512	-0.124978
C	-0.923660	0.875696	-0.000081	H	0.559228	3.248464	0.884760
C	-2.075885	1.681405	0.063496	H	1.489476	3.031438	-0.637605
C	-3.312211	1.064256	0.083649	H	-0.257541	3.255919	-0.716359

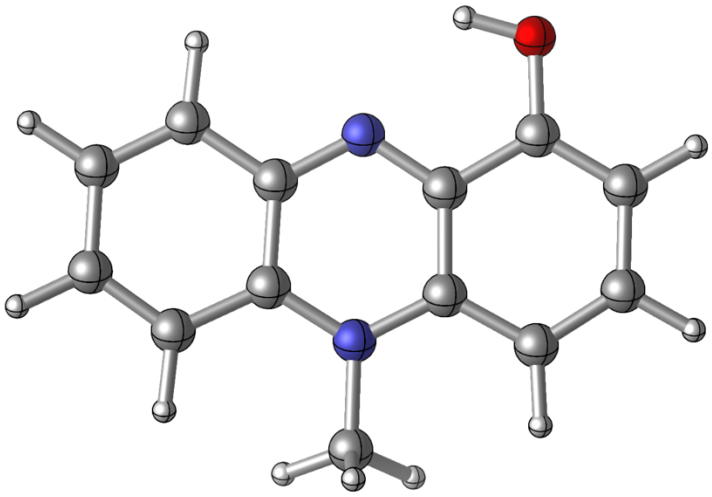

Zero-point correction= 0.218567 (Hartree/Particle)

Thermal correction to Energy= 0.230412

Thermal correction to Enthalpy= 0.231356

Thermal correction to Gibbs Free Energy= 0.180667

Sum of electronic and zero-point Energies= -686.174437

Sum of electronic and thermal Energies= -686.162592

Sum of electronic and thermal Enthalpies= -686.161648

Sum of electronic and thermal Free Energies= -686.212337

Pyocyanin_oxidized_protonated_open_octanol

E(scf) = -686.387409115 a.u.

C	3.813018	0.047650	0.081493	C	-3.484166	-0.280434	0.043878
C	2.790221	0.963764	0.060966	C	-2.399753	-1.123247	-0.009445
C	2.292109	-1.815624	-0.017418	C	-1.063843	-0.563717	-0.021281
C	3.574917	-1.352087	0.032318	H	-1.950855	2.781020	0.126351
H	4.839480	0.410651	0.144132	H	-4.159856	1.760755	0.151068
H	3.027253	2.022114	0.124990	H	-4.496170	-0.686111	0.060362
H	2.052163	-2.878270	-0.042682	N	-0.041010	-1.402035	-0.051080
H	4.416647	-2.043763	0.044796	N	0.374890	1.352451	-0.047880
C	1.449530	0.508940	-0.007474	O	-2.465147	-2.452554	-0.044389
C	1.197510	-0.900836	-0.026755	C	0.578046	2.805883	-0.131587
C	-0.900946	0.867143	-0.001044	H	0.545271	3.246013	0.873217
C	-2.035849	1.700394	0.066392	H	1.537864	3.014591	-0.605437
C	-3.283050	1.114931	0.089827	H	-0.203411	3.238012	-0.761370

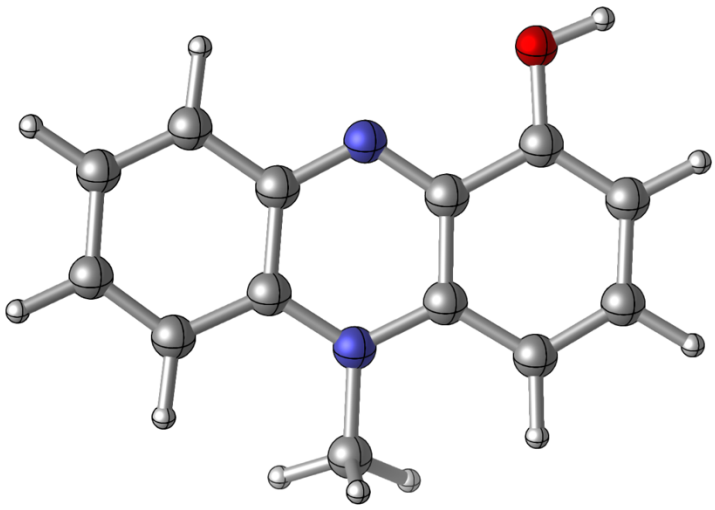

Zero-point correction= 0.218367 (Hartree/Particle)

Thermal correction to Energy= 0.230286

Thermal correction to Enthalpy= 0.231230

Thermal correction to Gibbs Free Energy= 0.180519

Sum of electronic and zero-point Energies= -686.169042

Sum of electronic and thermal Energies= -686.157123

Sum of electronic and thermal Enthalpies= -686.156179

Sum of electronic and thermal Free Energies= -686.206890

OH-phenazine_reduced_closed

E(scf) = -647.878437189 a.u.

C	-3.835848	-0.473704	-0.323529	C	0.914744	-1.042687	0.184973
C	-2.732907	-1.304385	-0.090556	C	2.014320	-1.860927	-0.080611
C	-2.415767	1.462222	-0.064706	C	3.264118	-1.283799	-0.312231
C	-3.677183	0.906866	-0.311290	C	3.422001	0.099789	-0.300612
H	-4.812860	-0.918262	-0.518679	C	2.314014	0.916031	-0.051649
H	-2.847157	-2.390734	-0.107917	C	1.063024	0.350245	0.202036
H	-2.280429	2.546183	-0.060923	H	1.888303	-2.944977	-0.098020
H	-4.527849	1.564368	-0.496849	H	4.125889	-1.923276	-0.508342
C	-1.481475	-0.758493	0.177972	H	4.397173	0.555021	-0.485711
C	-1.320486	0.642795	0.191924	N	-0.051261	1.155408	0.503810

N	-0.360366	-1.555355	0.468914	H	-0.476967	-2.545127	0.285199
O	2.362705	2.277764	-0.026095	H	3.257621	2.572303	-0.235054
H	0.084690	2.138293	0.295666				

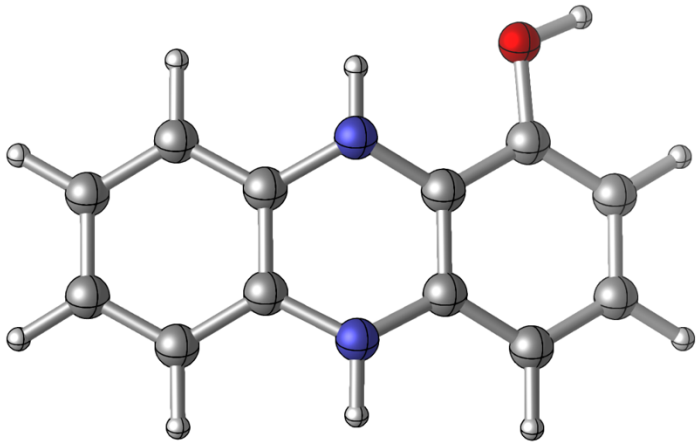

Zero-point correction= 0.199668 (Hartree/Particle)

Thermal correction to Energy= 0.210780

Thermal correction to Enthalpy= 0.211724

Thermal correction to Gibbs Free Energy= 0.162997

Sum of electronic and zero-point Energies= -647.678770

Sum of electronic and thermal Energies= -647.667658

Sum of electronic and thermal Enthalpies= -647.666713

Sum of electronic and thermal Free Energies= -647.715440

OH-phenazine_reduced_closed_octanol

E(scf) = -647.877216847 a.u.

C	-3.836716	-0.473875	-0.321460	C	3.422701	0.099901	-0.298279
C	-2.733325	-1.304293	-0.090188	C	2.314201	0.915838	-0.051344
C	-2.416575	1.461826	-0.063908	C	1.063013	0.350361	0.200741
C	-3.678193	0.906511	-0.308939	H	1.889517	-2.944611	-0.097174
H	-4.813936	-0.918471	-0.515293	H	4.127390	-1.923055	-0.504194
H	-2.847661	-2.390665	-0.107465	H	4.398249	0.555060	-0.481854
H	-2.281512	2.545824	-0.059748	N	-0.051364	1.155344	0.500348
H	-4.529202	1.563947	-0.492957	N	-0.360147	-1.555382	0.465588
C	-1.481715	-0.758487	0.176647	O	2.362807	2.278025	-0.026756
C	-1.320805	0.642705	0.190750	H	0.084845	2.138593	0.294407
C	0.915067	-1.042568	0.183683	H	-0.476610	-2.544893	0.282073
C	2.015169	-1.860497	-0.080016	H	3.258509	2.571410	-0.232765
C	3.265267	-1.283600	-0.309776				

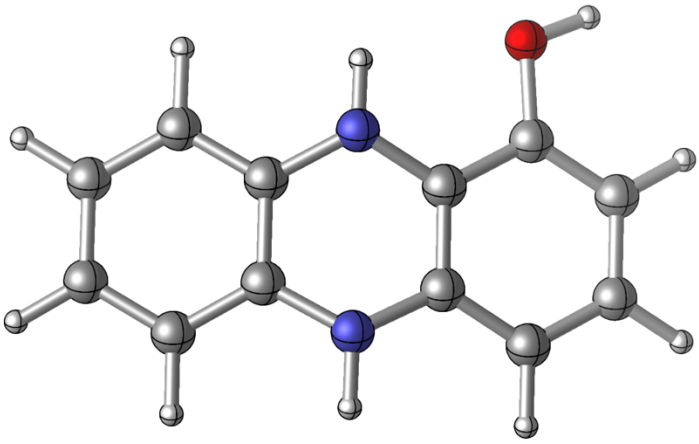

Zero-point correction= 0.199664 (Hartree/Particle)

Thermal correction to Energy= 0.210788

Thermal correction to Enthalpy= 0.211732

Thermal correction to Gibbs Free Energy= 0.162980

Sum of electronic and zero-point Energies= -647.677552

Sum of electronic and thermal Energies= -647.666429

Sum of electronic and thermal Enthalpies= -647.665484

Sum of electronic and thermal Free Energies= -647.714237

OH-phenazine_oxidized_closed

E(scf) = -646.663074024 a.u.

C	3.815118	-0.525115	0.000043	C	-3.272275	-1.265953	-0.000041
C	2.725707	-1.348930	0.000029	C	-3.426319	0.153139	-0.000039
C	2.416814	1.462709	0.000031	C	-2.319775	0.959691	-0.000025
C	3.659748	0.896394	0.000044	C	-1.007332	0.362463	-0.000011
H	4.820217	-0.949481	0.000054	H	-1.932539	-2.955674	-0.000028
H	2.822682	-2.435374	0.000028	H	-4.174867	-1.879652	-0.000052
H	2.273882	2.544115	0.000031	H	-4.420633	0.600290	-0.000050
H	4.548724	1.528743	0.000055	N	0.035546	1.191033	0.000003
C	1.405106	-0.797445	0.000015	N	0.349833	-1.624652	0.000001
C	1.253618	0.632425	0.000016	O	-2.399072	2.300025	-0.000023
C	-0.866359	-1.063936	-0.000012	H	-1.476937	2.618587	-0.000011
C	-2.044987	-1.871513	-0.000027				

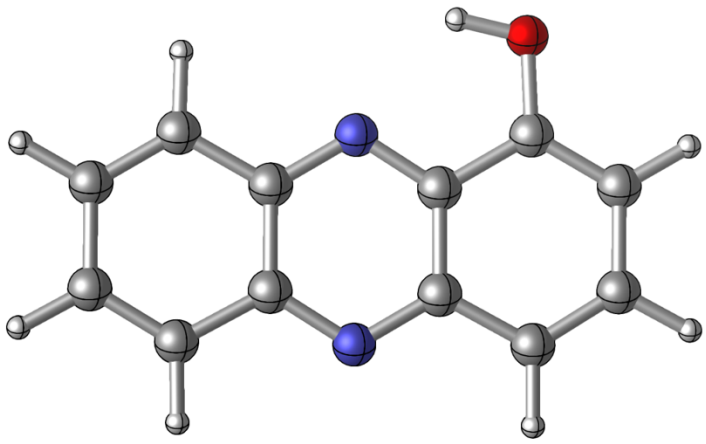

Zero-point correction= 0.176682 (Hartree/Particle)

Thermal correction to Energy= 0.186739

Thermal correction to Enthalpy= 0.187683

Thermal correction to Gibbs Free Energy= 0.140997

Sum of electronic and zero-point Energies= -646.486392

Sum of electronic and thermal Energies= -646.476335

Sum of electronic and thermal Enthalpies= -646.475391

Sum of electronic and thermal Free Energies= -646.522077

OH-phenazine_oxidized_closed_octanol

E(scf) = -646.662458149 a.u.

C	3.814895	-0.525183	0.000043	C	-0.866180	-1.063949	-0.000012
C	2.725411	-1.348802	0.000029	C	-2.044713	-1.871578	-0.000027
C	2.416695	1.462612	0.000031	C	-3.271888	-1.266000	-0.000040
C	3.659578	0.896263	0.000044	C	-3.426141	0.153058	-0.000039
H	4.819960	-0.949704	0.000054	C	-2.319787	0.959764	-0.000025
H	2.821551	-2.435292	0.000028	C	-1.007339	0.362510	-0.000011
H	2.273560	2.543986	0.000031	H	-1.931605	-2.955615	-0.000028
H	4.548538	1.528697	0.000055	H	-4.174429	-1.879806	-0.000052
C	1.404869	-0.797226	0.000015	H	-4.420294	0.600489	-0.000050
C	1.253438	0.632500	0.000016	N	0.035386	1.191240	0.000003

N	0.349853	-1.624607	0.000001	H	-1.476422	2.617508	-0.000012
O	-2.398820	2.299936	-0.000023				

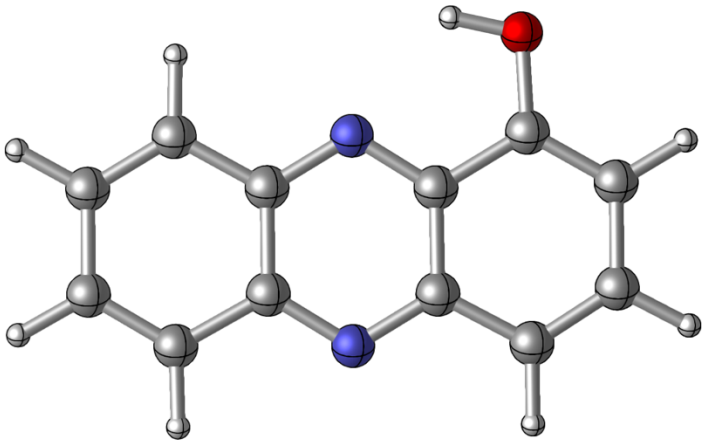

Zero-point correction= 0.176716 (Hartree/Particle)

Thermal correction to Energy= 0.186769

Thermal correction to Enthalpy= 0.187713

Thermal correction to Gibbs Free Energy= 0.141034

Sum of electronic and zero-point Energies= -646.485742

Sum of electronic and thermal Energies= -646.475689

Sum of electronic and thermal Enthalpies= -646.474745

Sum of electronic and thermal Free Energies= -646.521424

OH-phenazine_oxidized_open

E(scf) = -646.656242773 a.u.

C	3.838920	-0.493013	0.000043	C	-3.237008	-1.320985	-0.000040
C	2.755228	-1.324309	0.000029	C	-3.413361	0.093900	-0.000039
C	2.425899	1.483666	0.000031	C	-2.330632	0.935055	-0.000025
C	3.673294	0.927766	0.000044	C	-0.996213	0.379488	-0.000011
H	4.847109	-0.910280	0.000054	H	-1.849078	-2.970321	-0.000027
H	2.859538	-2.410205	0.000028	H	-4.126830	-1.952649	-0.000052
H	2.273461	2.563874	0.000032	H	-4.422946	0.509996	-0.000050
H	4.557737	1.566571	0.000056	N	0.049726	1.207291	0.000003
C	1.431485	-0.779973	0.000015	N	0.379206	-1.608702	0.000001
C	1.265920	0.645898	0.000016	O	-2.409479	2.279624	-0.000023
C	-0.838662	-1.051134	-0.000012	H	-3.340569	2.539090	-0.000033
C	-1.995723	-1.890223	-0.000027				

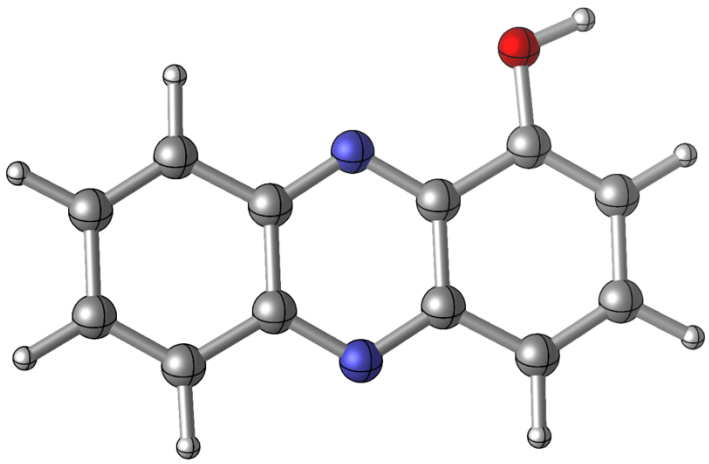

Zero-point correction= 0.176434 (Hartree/Particle)

Thermal correction to Energy= 0.186622

Thermal correction to Enthalpy= 0.187566

Thermal correction to Gibbs Free Energy= 0.140611

Sum of electronic and zero-point Energies= -646.479809

Sum of electronic and thermal Energies= -646.469621

Sum of electronic and thermal Enthalpies= -646.468677

Sum of electronic and thermal Free Energies= -646.515631

OH-phenazine_oxidized_open_octanol

E(scf) = -646.655107629 a.u.

C	3.838518	-0.493037	0.000043	H	4.557368	1.566578	0.000056
C	2.754896	-1.324305	0.000029	C	1.431202	-0.779924	0.000015
C	2.425620	1.483655	0.000031	C	1.265674	0.645895	0.000016
C	3.672920	0.927718	0.000044	C	-0.838402	-1.050944	-0.000012
H	4.846716	-0.910384	0.000054	C	-1.995481	-1.890166	-0.000027
H	2.858502	-2.410239	0.000028	C	-3.236670	-1.321178	-0.000040
H	2.272477	2.563727	0.000032	C	-3.412912	0.093802	-0.000039

C	-2.330305	0.935047	-0.000025	N	0.049741	1.207560	0.000003
C	-0.995851	0.379590	-0.000011	N	0.379168	-1.608788	0.000001
H	-1.848074	-2.970112	-0.000027	O	-2.409384	2.279628	-0.000023
H	-4.126434	-1.952964	-0.000052	H	-3.340448	2.538221	-0.000033
H	-4.422642	0.509816	-0.000050				

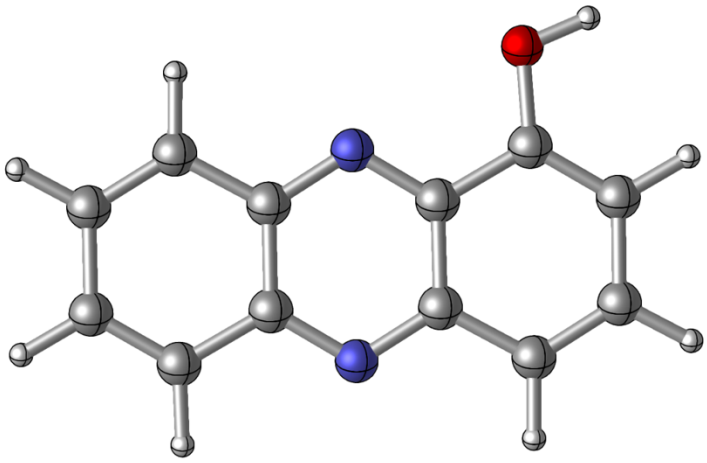

Zero-point correction= 0.176438 (Hartree/Particle)

Thermal correction to Energy= 0.186629

Thermal correction to Enthalpy= 0.187573

Thermal correction to Gibbs Free Energy= 0.140613

Sum of electronic and zero-point Energies= -646.478670

Sum of electronic and thermal Energies= -646.468479

Sum of electronic and thermal Enthalpies= -646.467535

Sum of electronic and thermal Free Energies= -646.514495

LogP prediction algorithms

We used four freely available, peer reviewed predictive algorithms relying on different methods of calculation to predict LogP values for neutral forms of the phenazines used in this study. We restricted our search to neutral forms of the molecules because several of these tools do not include charged molecules in their domains and thus give the same prediction for the protonated and deprotonated forms of, for example, PCA. iLOGP and XLogP3 were accessed through the SwissADME online tool[14]. The KOWWIN algorithm was accessed through the EPI (Estimation Program Interface) Suite[15].The molecular inspirations miLogP algorithm was accessed as a free tool on the molinspiration website, which has unfortunately been discontinued as of January 2026[16].

cLogP Algorithm descriptions

miLogP

miLogP is a free LogP prediction algorithm produced by Molinspiration[16]. It bases predictions on the contributions of known molecular fragments that it identifies within a molecule's structure. The empirical fragment contributions to lipophilicity are based on a training set of over 12,000 compounds, most of them drug-like, with measured LogP values. They include the influence of hydrogen bonding and charge interactions.

XLogP3

XLogP3 is based on the work of Wang et al., who developed an additive method based not on molecular fragments but on the individual atoms that constitute a molecule[17]. It includes contributions from element type, the identity of adjacent atoms, conjugation to a ring or extended pi system, and hybridization state. Summed atomic contributions are adjusted using correction factors to account for more complicated interactions attributable to halogens, intramolecular hydrogen bonds, etc. XLogP3 is the latest release of the software that, whenever possible, improves the accuracy of the original algorithm's calculations by using a structurally similar reference compound as a starting point for the additive, atom-based calculation[18].

KOWWIN:

Based on the work of Meylan and Howard[19-21], KOWWIN sums contributions from atoms and/or fragments identified within the molecule of interest. The 150 atom/fragment contributions recognized by the model were initially determined based on a training set of 2473 experimental LogP structure/value pairs for compounds with relatively simple structures. The model was then validated on an additional set of over 10,500 molecules of greater structural complexity. Correction factors account for interactions like steric hindrance and hydrogen bonding that might otherwise be missed by the atom/fragment approach.

iLOGP

iLOGP, short for “implicit log P”, is a physics-based prediction method correlating experimental LogP measurements with computed solvation energies of analytes in octanol and in water[22]. It approximates contributions to solvation free energies in both solvents using two terms: 1) the electrostatic contribution, assessed using a generalized Born (GB) model to approximate solutions to the Poisson-Boltzman equation; and 2) the nonpolar contribution, approximated by the computed surface accessible free surface area (SASA). The resulting GB/SA model was then regressed against experimental values for thousands of molecules in a test set. The resulting model requires no corrective terms because it considers the geometry and polarity of the whole molecule, a fact which differentiates it wholly from atomistic or fragmental approaches like those listed above.

For each algorithm, predictions were based on the following SMILES sequences:

PCA: O=C(O)C1=CC=CC2=C1N=C3C(C=CC=C3)=N2 (oxidized) and O=C(O)C1=CC=CC2=C1NC3=C(N2)C=CC=C3 (reduced);

PCN: O=C(N)C1=CC=CC2=C1N=C3C(C=CC=C3)=N2 (oxidized) and O=C(N)C1=CC=CC2=C1NC3=C(N2)C=CC=C3 (reduced);

PYO: O=C1C=CC=C(C1=N2)N(C)C3=C2C=CC=C3 (oxidized) and OC1=C2C(N(C)C3=CC=CC=C3N2)=CC=C1 (reduced);

1-OH-phenazine: OC1=CC=CC2=C1N=C3C(C=CC=C3)=N2 (oxidized) and OC1=CC=CC2=C1NC3=C(N2)C=CC=C3 (reduced);

phenazine: C12=NC(C=CC=C3)=C3N=C1C=CC=C2 (oxidized) and C1(NC(C=CC=C2)=C2N3)=C3C=CC=C1 (reduced).

Experimental Methods

No unexpected or unusually high safety hazards were encountered.

Chemicals

Unless otherwise noted, all chemicals were purchased from Sigma. All solvents were HPLC grade. Formic acid and Acetonitrile were purchased from Fisher. All water used was nanopore grade (resistivity > 18 MΩ). PCN was purchased from ChemScene. PCA was purchased from Princeton Biomolecules. These molecules were used without further purification.

PYO was synthesized according to an established method with slight modifications[23]. Briefly, an aqueous solution of sodium bicarbonate and phenazine methosulfate was exposed to broad spectrum light in a light box for 16 hours at room temperature, causing decomposition to PYO. PYO was then purified in three extraction steps: first

with DCM, then with 0.1 M HCl, and finally with DCM after neutralizing the acid with 10 M NaOH. DCM was removed by rotovap, and PYO was dissolved in a small volume of 80:20 DCM:MeOH solution. PYO was then precipitated by the addition of 200mL hexanes, and solids were vacuum filtered and washed with additional hexanes until flowthrough was clear. The identity and purity of PYO was confirmed against a lab standard by HPLC, and the powder was stored in the dark at -20 ^{o}C for future experiments.

To ensure no significant decomposition, phenazine purity was assessed by HPLC at the start of each experiment.

Phenazine solutions

Phenazine stocks were all prepared in 20 mM MOPS at pH 7.2. For those that did not dissolve readily in water, we first dissolved a known amount of the solid in a known mass of methanol, then diluted by a factor of at least 25 using 20 mM MOPS. Small amounts of carrier solvent are not expected to influence partitioning behavior[24].

Because of observed side reactions between octanol and phenazines, especially when exposed to light, oxygen, a continuous reducing potential, or long-term storage, we did not saturate any phenazine stock solutions with octanol prior to partition experiments. However, we pre-saturated all octanol with 20 mM MOPS at pH 7.2. The amount of octanol that dissolves in water ($7.5x10^{-5}$ mole fraction) is very small relative to the appreciable amount of water that dissolves in octanol (0.275 mole

fraction)[25-27]. Thus, we assumed that volume changes due to small amounts of octanol dissolving in the aqueous phase during partition experiments would be negligible. Furthermore, our HPLC method is insensitive to volume changes in the equilibration experiment because it relies on the detection of analyte in both the octanol and the water phases.

Electrochemical Phenazine Reduction

All reduced phenazine stocks were prepared in well-stirred glass reaction vessels using solutions containing 0.1 mM to 1 mM phenazine in 20 mM MOPS at pH 7.2. Reducing potentials were chosen to be at least 250mV lower than the midpoint potential of the phenazine to be reduced. We then used a potentiostat to apply the chosen potential via a graphite rod working electrode and a Ag/AgCl (3M KCl) reference electrode. In all cases, we used a platinum counter electrode submerged in oxidized phenazine solution and connected to the working electrode vessel either by a glass frit (for PCA, PCN, and PYO), or by a salt bridge made by solidifying a mixture of 4% agar saturated with 3 M KCl in a serological pipette tip (for phenazine and 1-OH phenazine). Reduction was considered complete when the current measured at the reference electrode dropped below 1% of its initial value.

Equilibration Conditions

Exploring our desired condition space of octanol-water partitioning required the development of a high throughput equilibration and measurement method that could make use of small amounts of expensive or difficult-to-acquire analytes. We settled

on a modified shake-flask method using sealable 2mL polypropylene eppendorf-style centrifuge tubes as reaction vessels and HPLC as an analytical method[28].

To minimize the influence of oxygen, we set up, equilibrated, and sampled all experiments in a Coy anaerobic chamber with an atmosphere of 95% N_2 and 5% H_2 . To perform an experiment, we used a syringe to dispense a small volume (typically 300μL, but volumes down to 150 μL in some cases) of octanol (pre-saturated with 20 mM MOPS at pH 7.2) into an eppendorf-style tube. Then, we used a pipette to dispense an aqueous phenazine solution (300μL) into the same tube. We then closed the tube and vortexed the mixture for 30s before placing it in a temperature-controlled shaker at 250 RPM for at least 16 hours, which was determined to be sufficient to reach equilibrium (**Figure A14**).

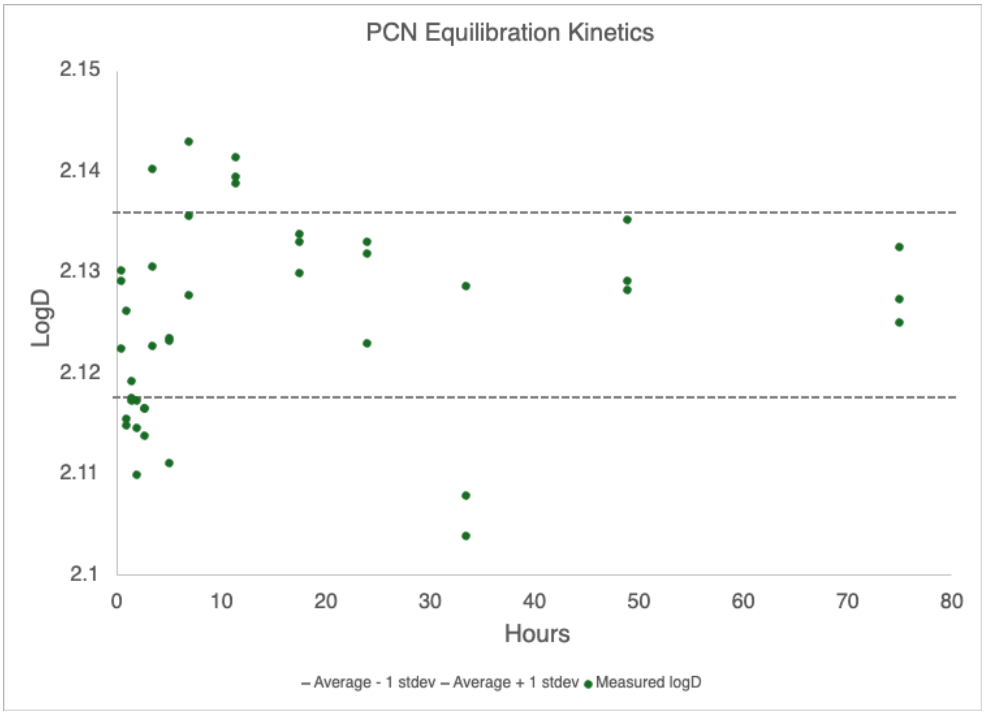

Figure A14. Control experiments to establish sufficient equilibration times with our experimental setup were carried out with oxidized PCN. Plotted points indicate individual replicates taken at each time point. Dashed lines indicate the average value from the last five time points plus or minus the standard deviation of those measurements. Based on these experiments, we determined that sampling after 16 hours was sufficient for PCA, PCN, and PYO. Out of an abundance of caution, we lengthened equilibration time to 24 hours for phenazine and 1-OH phenazine, which we worked with less frequently.

Sampling Procedure

To sample partition experiments after equilibration, we removed tubes from the heating block and centrifuged them for 90 s at 14,100xg using a microcentrifuge. We then collected about 100 µL of each of the fully separated octanol and water phases using separate 1 mL insulin syringes. Because the water phase sits below the octanol phase and small amounts of carryover can skew the measured partition coefficient significantly, we took great care to ensure no octanol contaminated the water samples. Before sampling the water phase, we pulled a small amount of air into the syringe. We then inserted the needle through the octanol phase, and, once the needle tip entered the water phase, ejected the air before drawing any of the water phase into the syringe. After withdrawing the needle and before dispensing the collected water phase into the HPLC vial for measurement, a small volume of the water phase was discarded to ensure no octanol remained at the tip of the syringe. All samples were measured in triplicate.

Because the reduced and oxidized forms of phenazines are known to absorb light differently, HPLC samples were removed from the Coy chamber and left uncapped under aluminum foil (to exclude light) on the benchtop for up to 2 hours prior to measurement to allow re-oxidation of reduced phenazine samples[29]. Samples were then capped and stored at 10°C until measurement. Samples were measured within 3 days of equilibration to avoid complications from reaction with octanol that were occasionally observed, especially in the case of PCA.

Liquid Chromatography Measurements

All HPLC separations were performed on a Waters Alliance HPLC connected to a Waters 2998 PDA detector set to detect wavelengths from 200-800nm at 20Hz with 1.2nm resolution. To minimize errors in equilibration experiments, especially those associated with dispensing small volumes of octanol, we chose to measure analyte in both octanol and water phases. To avoid on-column interference from octanol in the samples, we used a phenyl column rather than a C18 column as well as a large proportion of methanol in the mobile phase, which helped to solubilize both phenazines and octanol. Even so, the retention times for the same analyte often differed between octanol and water fractions.

For equilibration experiments, we used Methods A, B, and C. A and B were both isocratic 1.0 mL/min flows of 70:30 MeOH: H_2O with a phenyl column (XBridge BEH 5 µM particle size 4.6 x 250 mm), both solvents containing either 0.1% *v/v* formic acid (final pH ≤ 3, Method A) or 0.1% *v/v* NH_4OH (final pH ≥ 9, Method C). Method C was an acidic gradient method using the same phenyl column used in Methods A and B, using solvents X (H_2O + 0.1% *v/v* formic acid) and Y (70:30 MeOH: H_2O + 0.1% *v/v* formic acid) flowing at 1mL/min according to the following gradient: 0-5 minutes: linear gradient from 95% X, 5% Y to 40% X, 60% Y; 5-8 minutes: linear gradient to 5% X, 95% Y; 8-10 minutes: linear gradient to 95% X, 5% Y.

For measurements of PYO in cell culture supernatant for the cell pellet retention assay, we used a C18 column (XBridge BEH 2.5µm particle size, 3 x 100mm) and the following basic gradient method (final pH ≥ 9, Method D), using solvent A (H_2O + 2% *v/v* MeOH + 0.1% *v/v* NH_4OH) and Solvent B (acetonitrile + 2% *v/v* MeOH + 0.1% *v/v* NH_4OH) at 0.5 mL/min: 0-6 minutes: linear gradient from 98%A, 2%B to 80%A, 20%B; 6-8 minutes: linear gradient to 5%A, 95%B; 8-9 minutes hold at 5%A, 95%B; 9-9.1 minutes: linear gradient to 98%A, 2%B; 9.1-16 minutes: hold at 98%A, 2%B. A standard curve was prepared using the same method and was used to assess PYO concentrations down to 150nM. Prior to introducing them to the column, pellet supernatant samples were filtered using Costar SpinX centrifuge tube filters with 0.22 µm cellulose acetate filters.

Phenazine	Sample Type	Method A (acidic, isocratic, phenyl column)	Method B (basic, isocratic, phenyl column)	Method C (acidic, gradient, phenyl column)	Method D (basic, gradient, C18 column)	Detection Wavelengths (nm)	Retention Time (min)
PCA	abiotic partitioning	X				364	8.4

PCN	abiotic partitioning	X				287, 364	4.3 in oct. 4.5, 5.5[a] in water
PYO	abiotic partitioning		X[b]			313	3.6
PYO	abiotic partitioning			X		387	6.6
PYO	cell pellet and membrane retention				X	313	6.3
Colchicine	abiotic partitioning control	X				352	5.0

Table A5. Samples and corresponding HPLC methods. a: multiple peaks attributed to PCN and its protonated rotamer in aqueous fraction (see the following methods section and **Figures A2 and A3** for more information) b: Subsequent PYO samples were measured in basic conditions after recognizing an improvement in peak shapes compared to the acidic method.

Waters Empower 3 software was used to run the HPLC methods and to process the data. The built-in Apex Track Algorithm was used to extract chromatograms at wavelengths characteristic of each phenazine (**Table A5**). When strong partitioning

resulted in extremely dilute water fractions, equilibration volumes and HPLC injection volumes were adjusted to ensure signals remained within the linear range of the detector. Peak areas in octanol and water, corrected for injection volume, were used to calculate distribution coefficients directly according to Equation 2. For each sample, the same wavelength was monitored in both octanol and water fractions.

Treatment of PCN rotamer peak observed via HPLC

In most of our samples, only one peak attributable to the analyte was visible. However, aqueous fractions of PCN samples often exhibited two peaks with different retention times but identical absorbance spectra characteristic of PCN. To determine whether both peaks were attributable to PCN, we used the same chromatography settings and PDA detector then routed the outflow through a Waters Acquity QDa single quadrupole mass spectrometer. Mass scans were collected simultaneously from 100 to 900 Da in the positive mode and 100 to 600 Da in the negative mode. In addition, a selected ion recording channel was collected in the positive mode for 211.09, 224.08, and 225.07 Da, the masses expected for pyocyanin, phenazine-1-carboxamide, and phenazine-1-carboxylic acid, respectively. The probe temperature was 600°C and the capillary voltage was 0.8 kV. In all cases, one of the two peaks had a mass corresponding to PCN (~224.08 Da) while the other possessed a mass about one atomic mass unit greater than PCN (~224.94 Da). We speculate that the additional peaks are likely the result of a protonated rotamer preferentially stabilized in the water phase but not in the octanol phase (**Figures A2 and A3**). In these

samples, we assumed that the 224.9 Da peak possessed the same absorption coefficient as the ~224.08 Da peak observed in the water and in the octanol phases. We thus calculated the distribution coefficient using the sum of the peak areas in the water fraction as the aqueous peak area (**Figure A17**).

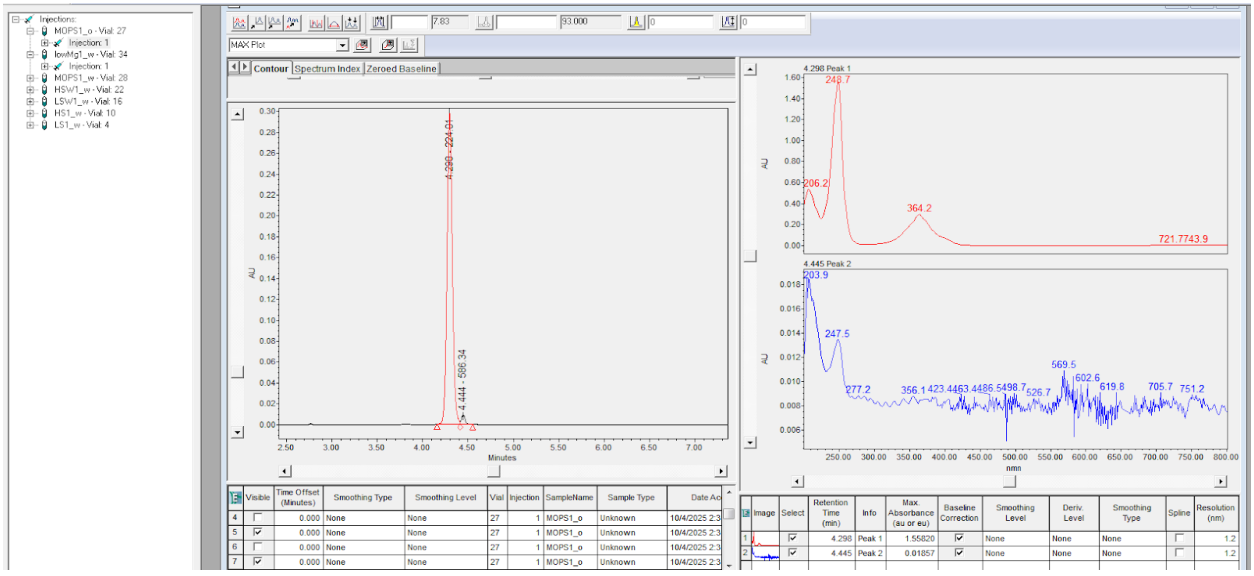

Figure A15. An example of a HPLC chromatogram extracted at 248nm to measure PCN in the octanol fraction of an equilibration experiment. The peak at 4.298 minutes has the absorbance spectrum (top right panel) and $[M+1]^+$ ion mass characteristic of protonated PCN (224.01Da). The small peak at 4.444 minutes has neither the correct mass nor the correct absorption spectrum for PCN. It was deemed an impurity, possibly related to the commercial synthesis of the PCN, and was not included in LogD calculations.

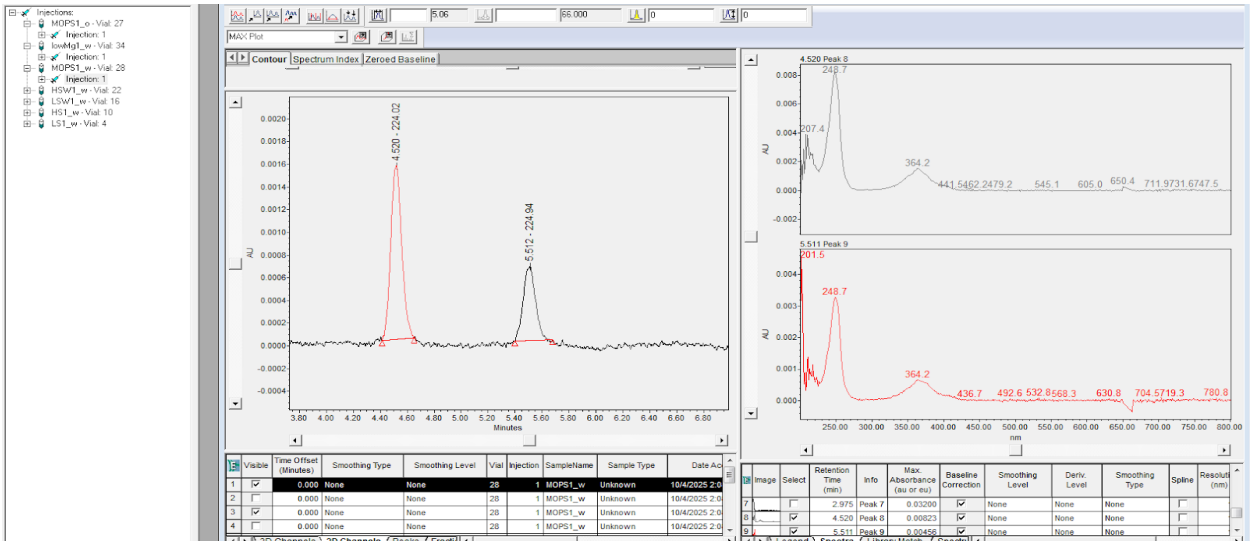

Figure A16. The HPLC chromatogram extracted at 248nm to measure PCN in the aqueous fraction of the same equilibration experiment sample as the panel above (Figure S2). The peak at 4.520 minutes has the characteristic absorbance spectrum and mass of the protonated PCN $[M+1]^+$ ion (224.02 Da) (top right panel), while the peak at 5.512 minutes has an essentially identical absorbance spectrum but a mass of 224.94 Da (bottom right panel). In this study, we attributed this peak to a rotamer of PCN stabilized in water but not in octanol, which would help justify its similar absorbance spectrum while accounting for its different retention time and mass. We assumed the absorption coefficient was not significantly different from PCN, and thus added the two measured peak areas in the water fraction together when calculating the distribution coefficient LogD according to **Figure A17**.

$$LogD = Log_{10} \sum_{i}^{n} \frac{[peak\ area\ octanol]_i}{[peak\ area\ water]_i} * \frac{injection\ volume\ water}{injection\ volume\ octanol}$$

Figure A17. Equation used to calculate octanol-water distribution coefficients for an analyte with n chromatographic peaks. For all samples, the same wavelength was monitored in octanol and water fractions. In rare cases when multiple peaks were present, mass and absorption spectra were used together to select and sum only peaks attributable to the intended analyte in its different ionization/rotamer forms and to exclude any peaks from impurities.

Ionic Strength Samples

To assess the effects of ionic identity and strength on phenazine partitioning, we used single-salt solutions at 0.1 M and 1 M ionic strengths. To check for constructive or destructive influences of multiple salts in an environmentally relevant mixture, we used a solution of artificial seawater (minus carbonate and trace metals, to avoid interference) consisting of the following salts and concentrations: $MgCl_2$, 46.6 mM; $CaCl_2$, 1.36 mM; NaCl, 456.88 mM; KCl, 7.00 mM; Na_2SO_4, 10.00 mM; K_2HPO_4, 1.00 mM; NH_4Cl, 2.00 mM. The ionic strength of the artificial seawater solution was 0.7 M, and we also used a 10x dilution of the same salt mixture (0.07 M ionic strength) to check for concentration effects.

Prior to equilibration with octanol, phenazine stock solutions were amended with volumes (up to 1/3rd of the final aqueous sample volume) of concentrated salt solutions prepared in water. pH changes were monitored with pH paper. Only the phosphate samples demonstrated a significant deviation from the buffered pH of 7.2 to a final pH of 8.5, a change which, based on the distance from the relevant pKa values, should not significantly affect the percentage of protonated and deprotonated species for any of the phenazines studied.

Samples were then equilibrated at 25 °C with shaking, sampled by syringe, and measured by HPLC as described above.

pH Samples

Phenazine stock solutions were prepared as above, buffered with 20 mM MOPS. To adjust the pH, small volumes (up to $1/30^{th}$ of the final aqueous sample volume) of 1 M HCl or NaOH were added to overwhelm the buffer, and pH was measured to the nearest 0.5 pH units in the anaerobic chamber using pH paper. When the pH was lowered to 3, PCA samples precipitated in the aqueous phase, but crystals dissolved fully when the octanol phase was introduced.

PYO Retention Samples

Experiment 1: cell pellets washed under normoxic or anoxic conditions

To assess the biological implications of the measured redox sensitivity of PYO's LogD, we conducted an experiment with late stationary phase *P. aeruginosa* cultures. *P. aeruginosa* PA14 cells were grown to late stationary phase (20 hours) in 5 mL of LB at 37 °C with vigorous shaking to ensure aeration. For each of three biological replicates, two 1 mL aliquots were taken from the same culture tube and washed either aerobically or anaerobically. While the aerobic aliquot was washed three times with PBS on the benchtop, the anaerobic aliquot was allowed to rest in an anaerobic chamber for 45 minutes, allowing the cells to reduce the PYO in the supernatant (a process that is visually apparent as the blue, oxidized PYO transforms to its colorless reduced form). Then the anaerobic aliquot was washed three times in the anaerobic chamber with N_2-sparged PBS. One wash consisted of spinning the cells down at 10,000xg for 1 minute, removing the supernatant, and resuspending the cell pellet in fresh PBS. After three washes, both the aerobic and the anaerobic cells were washed once more with aerobic PBS on the benchtop. In all conditions, supernatant was collected from the original culture, from the third wash, and from the fourth, aerobic wash. Supernatant samples were then analyzed by HPLC using method C listed in HPLC Conditions. Concentrations were calculated using a calibration curve constructed using pure PYO (**Figure A4**).

Experiment 2: membrane PYO retention measurement

A Pseudomonas aeruginosa culture (1 L) was grown under aerobic conditions in LB medium at 37 °C with shaking at 250 RPM to stationary phase (OD_{500} = 4.7). Cells were allowed to stand on the benchtop for 5 minutes before centrifugation, during

which time the color of the culture changed from blue (attributable to oxidized pyocyanin) to colorless (suggesting pyocyanin was reduced). Cells were harvested by centrifugation at 8000 RPM for 10 minutes. Culture supernatant was collected, mixed 1:1 with methanol, and stored at −20 °C until measurement. Cell pellets were resuspended in PBS (pH 7.0) supplemented with DNase I and lysed using an Avestin Emulsiflex C3 homogenizer (three passes at 15,000 PSI). The resulting lysate was subjected to ultracentrifugation at 38,000 RPM for 50 minutes at 4 °C to separate soluble and membrane fractions. Phenazines were extracted from the membrane fraction by adding 20 mL of methanol followed by vigorous vortexing and ultracentrifugation at 38,000 RPM for 10 minutes. During the first extraction, the color of the pellet changed from colorless (tinged with red, likely because of cytochrome hemes) to blue (attributable to oxidized pyocyanin). This extraction procedure was repeated three times, at which point both the membrane pellet and the methanol were colorless. The three resulting methanol fractions were pooled and evaporated on a rotovap to a volume of 4.7mL prior to LC–MS analysis. During the drying process, solids appeared in the solvent. These presumed protein aggregates were separated via centrifugation at 5300 RPM for 10 minutes, and the resulting supernatant was diluted 1:10 with fresh methanol prior to measurement. Medium and membrane fraction extract were both measured by HPLC method D described above, and concentrations were calculated based on the same standard curve as in PYO retention experiment 1 (**Figure A4**).

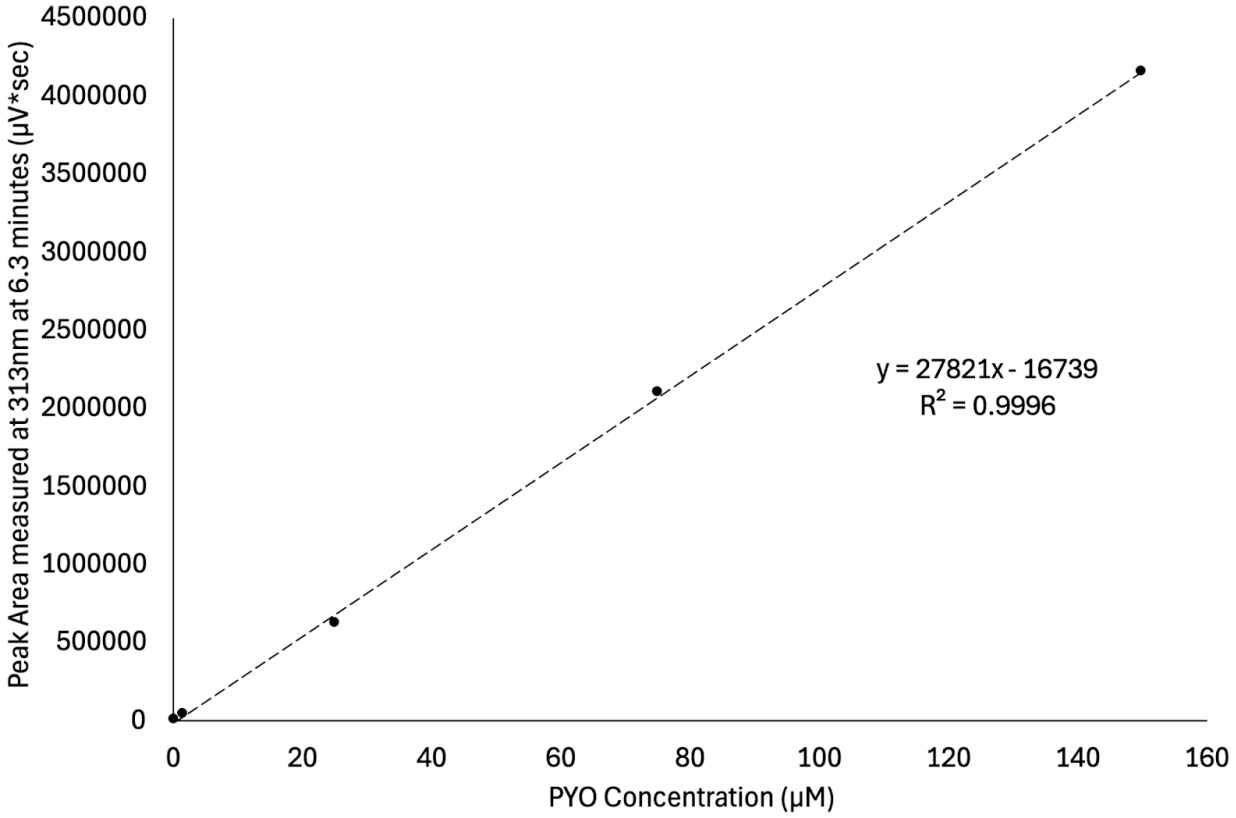

Figure A18. Standard curve used to calculate pyocyanin concentrations in supernatant samples from cellular retention assay and membrane retention assay. Standard solutions were prepared at concentrations of 150, 75, 25, 1.5, and 0.15 µM.

Ionic context exerts only minor control on phenazine lipophilicity

For most organic solutes, increasing ionic strength in the aqueous phase induces a "salting out" effect, increasing the observed lipophilicity. For the purposes of this discussion, we consider a "normal" salting out effect to be an increase in lipophilicity with an increase in ionic strength, while a "reverse" salting out effect is a decrease in lipophilicity with increasing ionic strength. Variations with a 10-fold change in ionic

strength were generally small for PCA, PCN, and PYO. For all the salts tested, PCN exhibited a normal salting out effect (**Figure A19 A**). While the differences in the lipophilicities are small enough that we hesitate to overinterpret them, PYO and PCA showed slightly different behavior when treated with different salts, only sometimes adhering to normal salting out expectations (**Figure A19 B**, **C**). Additionally, when treated with NaCl or KCl, the change in lipophilicity with increasing ionic strength was normal for the reduced species but reversed for the oxidized species. Particularly in the case of potassium phosphate, higher ionic strength actually made both oxidized and reduced PCA appreciably less lipophilic. This in spite of the fact that the phosphate salt overwhelmed the pH 7.2 MOPS buffer, resulting in an experimental pH of 8.5, which should have increased the proportion of deprotonated, charged PCA. Although not strong chelators, PCA and PYO are both known to bind to certain metals. Chelation of trace impurities in the salts may have contributed to the deviations we noted, but the effects were mostly small. Due to uncontrolled redox interactions and subsequent precipitation, we were unable to precisely characterize the effects of Cu^{2+}, Fe^{2+}, or Fe^{3+} in this study.

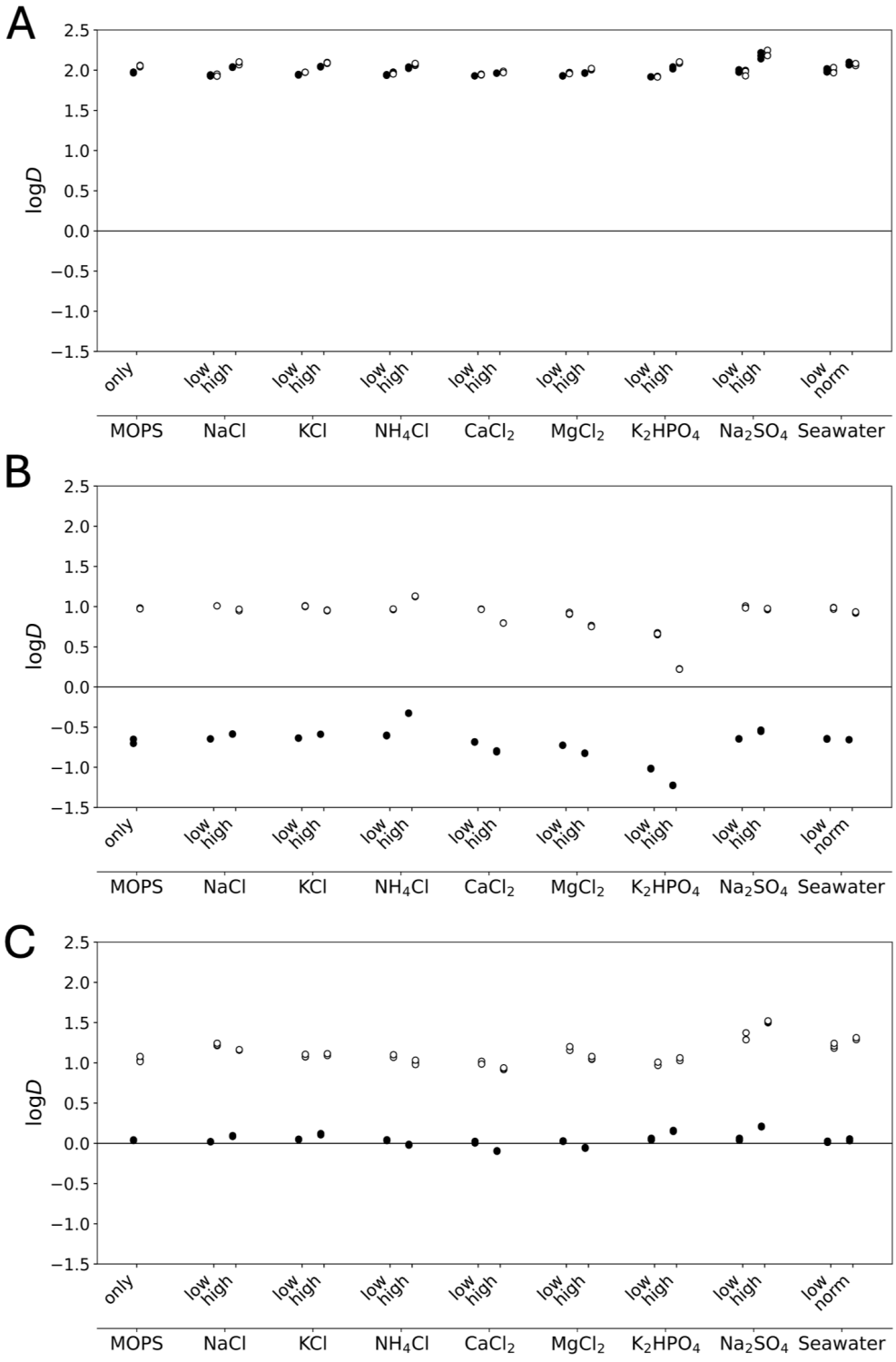
A
B
C
logD
2.5
2.0
1.5
1.0
0.5
0.0
−0.5
−1.0
−1.5
only
low
high
low norm
MOPS
NaCl
KCl
NH4Cl
CaCl2
MgCl2
K2HPO4
Na2SO4
Seawater

Figure A19. LogD measurements in various ionic strength conditions for PCN (A), PCA (B), and PYO (C). Ionic strength equilibrations were carried out at room temperature. In all cases, the aqueous fraction contained 20 mM MOPS at pH 7.2 amended to achieve final concentrations of either 0.1 M or 1 M concentrations of the salts listed. The phosphate salt overwhelmed the MOPS buffer and reached pH 8.5. All other salts were circumneutral at experiment's end. Each condition was conducted in triplicate (all data is shown). A table of exact experimental values is available below.

Tables of Experimental Values

In each table below, a line represents an average of experimental triplicates. All experiments were carried out in 20mM MOPS.

Colchicine method validation (pH 7.2)

Compound	Redox State	pH	$logD_{7.2\ (average\ of\ triplicates)}$	Standard Error (SE)	1.96*SE
Colchicine	N/A	7.2	1.06	0.002	0.004
Colchicine	N/A	7.2	1.06	0.004	0.008

Table A6. Method validation using Colchicine. Values conformed well to the literature[28].

Phenazine and 1-OH phenazine (pH 7.2)

Compound	Redox State	pH	$logD_{7.2\ (average\ of\ triplicates)}$	Standard Error (SE)	1.96*SE
phenazine	oxidized	7.2	2.66	0.015	0.030
phenazine	**reduced**	**7.2**	**2.63**	**0.037**	**0.073**
1-OH phenazine	oxidized	7.2	2.65	0.019	0.037
1-OH phenazine	**reduced**	7.2	**2.45**	**0.003**	**0.005**

Table A7. Experimental values for phenazine and 1-OH phenazine.

Ionic Strength Experiments (pH 7.2)

Phenazine	Redox State	Salt	Salt Conc. (M)	$logD_{7.2}$ (average of triplicates)	Standard Error (SE)	1.96*SE
PCA	oxidized	NaCl	0.1	-0.65	0.001	0.002
PCA	oxidized	NaCl	1	-0.59	0.001	0.002
PCA	oxidized	KCl	0.1	-0.64	0.002	0.003
PCA	oxidized	KCl	1	-0.59	0.001	0.002
PCA	oxidized	CaCl2	0.1	-0.68	0.002	0.004
PCA	oxidized	CaCl2	1	-0.80	0.004	0.008
PCA	**reduced**	**NaCl**	**0.1**	**1.01**	**0.001**	**0.001**
PCA	**reduced**	**NaCl**	**1**	**0.96**	**0.006**	**0.011**
PCA	**reduced**	**KCl**	**0.1**	**1.01**	**0.003**	**0.007**
PCA	**reduced**	**KCl**	**1**	**0.95**	**0.003**	**0.006**
PCA	**reduced**	**CaCl2**	**0.1**	**0.97**	**0.002**	**0.004**
PCA	**reduced**	**CaCl2**	**1**	**0.80**	**0.001**	**0.001**
PCA	oxidized	MgCl2	0.1	-0.72	0.001	0.003
PCA	oxidized	MgCl2	1	-0.82	0.002	0.004
PCA	oxidized	NH4Cl	0.1	-0.60	0.003	0.005
PCA	oxidized	NH4Cl	1	-0.33	0.001	0.003
PCA	oxidized	K2HPO4	0.1	-1.02	0.002	0.005
PCA	oxidized	K2HPO4	1	-1.22	0.002	0.004

PCA	**reduced**	**MgCl2**	**0.1**	**0.92**	**0.007**	**0.015**
PCA	**reduced**	**MgCl2**	**1**	**0.76**	**0.005**	**0.010**
PCA	**reduced**	**NH4Cl**	**0.1**	**0.97**	**0.002**	**0.005**
PCA	**reduced**	**NH4Cl**	**1**	**1.13**	**0.002**	**0.005**
PCA	**reduced**	**K2HPO4**	**0.1**	**0.66**	**0.007**	**0.014**
PCA	**reduced**	**K2HPO4**	**1**	**0.22**	**0.002**	**0.004**
PCA	oxidized	Na2SO4	0.1	-0.65	0.002	0.003
PCA	oxidized	Na2SO4	1	-0.54	0.005	0.010
PCA	oxidized	artificial seawater	1/3 strength	-0.64	0.003	0.005
PCA	oxidized	artificial seawater	normal	-0.66	0.001	0.001
PCA	oxidized	MOPS only	N/A	-0.67	0.018	0.035
PCA	**reduced**	**Na2SO4**	**0.1**	**0.99**	**0.008**	**0.016**
PCA	**reduced**	**Na2SO4**	**1**	**0.97**	**0.004**	**0.008**
PCA	**reduced**	**artificial seawater**	**1/3 strength**	**0.98**	**0.007**	**0.013**
PCA	**reduced**	**artificial seawater**	**normal**	**0.93**	**0.005**	**0.009**
PCA	**reduced**	**MOPS only**	**N/A**	**0.98**	**0.004**	**0.008**
PYO	oxidized	NaCl	0.1	0.02	0.001	0.003
PYO	oxidized	NaCl	1	0.09	0.004	0.007
PYO	oxidized	KCl	0.1	0.05	0.002	0.004

PYO	oxidized	KCl	1	0.12	0.005	0.009
PYO	oxidized	CaCl2	0.1	0.02	0.007	0.014
PYO	oxidized	CaCl2	1	-0.09	0.003	0.006
PYO	**reduced**	**NaCl**	**0.1**	**1.23**	**0.009**	**0.018**
PYO	**reduced**	**NaCl**	**1**	**1.16**	**0.002**	**0.005**
PYO	**reduced**	**KCl**	**0.1**	**1.09**	**0.011**	**0.021**
PYO	**reduced**	**KCl**	**1**	**1.11**	**0.008**	**0.015**
PYO	**reduced**	**CaCl2**	**0.1**	**1.00**	**0.011**	**0.021**
PYO	**reduced**	**CaCl2**	**1**	**0.93**	**0.006**	**0.013**
PYO	oxidized	MgCl2	0.1	0.03	0.003	0.005
PYO	oxidized	MgCl2	1	-0.06	0.003	0.006
PYO	oxidized	NH4Cl	0.1	0.04	0.004	0.008
PYO	oxidized	NH4Cl	1	-0.02	0.004	0.007
PYO	oxidized	K2HPO4	0.1	0.05	0.007	0.013
PYO	oxidized	K2HPO4	1	0.16	0.004	0.008
PYO	**reduced**	**MgCl2**	**0.1**	**1.17**	**0.015**	**0.030**
PYO	**reduced**	**MgCl2**	**1**	**1.06**	**0.011**	**0.022**
PYO	**reduced**	**NH4Cl**	**0.1**	**1.08**	**0.010**	**0.020**
PYO	**reduced**	**NH4Cl**	**1**	**1.01**	**0.016**	**0.031**
PYO	**reduced**	**K2HPO4**	**0.1**	**0.98**	**0.013**	**0.026**
PYO	**reduced**	**K2HPO4**	**1**	**1.04**	**0.012**	**0.023**
PYO	oxidized	Na2SO4	0.1	0.05	0.008	0.015
PYO	oxidized	Na2SO4	1	0.21	0.003	0.006
PYO	oxidized	artificial seawater	1/3 strength	0.02	0.006	0.011
	oxidized	artificial seawater	normal	0.04	0.008	0.016

PYO

PYO	oxidized	MOPS only	N/A	0.04	0.003	0.006
PYO	**reduced**	**Na2SO4**	**0.1**	**1.32**	**0.028**	**0.056**
PYO	**reduced**	**Na2SO4**	**1**	**1.51**	**0.007**	**0.013**
PYO	**reduced**	**artificial seawater**	**1/3 strength**	**1.21**	**0.018**	**0.034**
PYO	**reduced**	**artificial seawater**	**normal**	**1.30**	**0.007**	**0.014**
PYO	**reduced**	**MOPS only**	**N/A**	**1.04**	**0.019**	**0.038**
PCN	oxidized	NaCl	0.1	1.94	0.005	0.009
PCN	oxidized	NaCl	1	2.04	0.003	0.005
PCN	oxidized	KCl	0.1	1.94	0.003	0.005
PCN	oxidized	KCl	1	2.05	0.002	0.004
PCN	oxidized	CaCl2	0.1	1.93	0.001	0.001
PCN	oxidized	CaCl2	1	1.96	0.001	0.002
PCN	**reduced**	**NaCl**	**0.1**	**2.44**	**0.008**	**0.015**
PCN	**reduced**	**NaCl**	**1**	**2.57**	**0.011**	**0.022**
PCN	**reduced**	**KCl**	**0.1**	**2.45**	**0.000**	**0.001**
PCN	**reduced**	**KCl**	**1**	**2.57**	**0.004**	**0.007**
PCN	**reduced**	**CaCl2**	**0.1**	**2.42**	**0.004**	**0.007**
PCN	**reduced**	**CaCl2**	**1**	**2.46**	**0.005**	**0.010**
PCN	oxidized	MgCl2	0.1	1.93	0.002	0.003
PCN	oxidized	MgCl2	1	1.96	0.002	0.003

PCN	oxidized	NH4Cl	0.1	1.94	0.003	0.007
PCN	oxidized	NH4Cl	1	2.03	0.006	0.011
PCN	oxidized	K2HPO4	0.1	1.92	0.001	0.002
PCN	oxidized	K2HPO4	1	2.03	0.009	0.017
PCN	**reduced**	**MgCl2**	**0.1**	**2.44**	**0.005**	**0.010**
PCN	**reduced**	**MgCl2**	**1**	**2.49**	**0.006**	**0.011**
PCN	**reduced**	**NH4Cl**	**0.1**	**2.44**	**0.007**	**0.014**
PCN	**reduced**	**NH4Cl**	**1**	**2.53**	**0.003**	**0.006**
PCN	**reduced**	**K2HPO4**	**0.1**	**2.40**	**0.003**	**0.006**
PCN	**reduced**	**K2HPO4**	**1**	**2.42**	**0.006**	**0.011**
PCN	oxidized	Na2SO4	0.1	1.99	0.010	0.019
PCN	oxidized	Na2SO4	1	2.18	0.023	0.044
PCN	oxidized	artificial seawater	1/3 strength	2.00	0.012	0.024
PCN	oxidized	artificial seawater	normal	2.08	0.011	0.022
PCN	oxidized	MOPS only	N/A	1.97	0.004	0.007
PCN	**reduced**	**Na2SO4**	**0.1**	**2.45**	**0.021**	**0.041**
PCN	**reduced**	**Na2SO4**	**1**	**2.68**	**0.022**	**0.043**
PCN	**reduced**	**artificial seawater**	**1/3 strength**	**2.48**	**0.019**	**0.038**
PCN	**reduced**	**artificial seawater**	**normal**	**2.55**	**0.008**	**0.015**
PCN	**reduced**	**MOPS only**	**N/A**	**2.53**	**0.005**	**0.011**

Table A8. Ionic strength experiments were conducted by adding small amounts of concentrated salt solutions to 20mM MOPS buffered phenazine stock solutions. Phosphate solutions overwhelmed the buffer and became more basic (pH 8.5), but this was not expected to interfere with the ionization state of the phenazines used in this portion of the study.

pH Experiments

Phenazine	Redox State	pH	$logD_{pH}$ (average of triplicates)	Standard Error (SE)	1.96*SE
PYO	oxidized	3.0	-2.21	0.013	0.026
PYO	oxidized	6.0	-0.12	0.003	0.005
PYO	oxidized	9.0	0.03	0.004	0.009
PYO	**reduced**	**3.0**	**0.42**	**0.020**	**0.039**
PYO	**reduced**	**6.0**	**1.13**	**0.100**	**0.196**
PYO	**reduced**	**9.0**	**1.02**	**0.053**	**0.104**
PCA	oxidized	3	2.12	0.006	0.011
PCA	oxidized	3	2.12	0.004	0.009
PCA	oxidized	9	-2.01	0.014	0.028
PCA	oxidized	4	2.11	0.039	0.076
PCA	oxidized	6	-0.09	0.001	0.002
PCA	**reduced**	**3**	**3.42**	**0.046**	**0.091**

PCA	**reduced**	**5.5**	**1.54**	**0.017**	**0.033**
PCA	**reduced**	**9.5**	**-1.08**	**0.007**	**0.014**
PCA	**reduced**	**4.5**	**3.35**	**0.049**	**0.097**
PCN	oxidized	3	2.13	0.010	0.020
PCN	oxidized	9.5	1.94	0.008	0.016
PCN	**reduced**	**2.5**	**2.26**	**0.016**	**0.031**
PCN	**reduced**	**9**	**2.10**	**0.001**	**0.002**

Table A9. For pH experiments, 20mM MOPS starting solutions were overwhelmed with small amounts of concentrated HCl or NaOH. Values from the Ionic Strength MOPS only condition (**Table A8**) were used to assess LogD at pH 7.2.

Intracellular pyocyanin concentration estimation

Goal:

This calculation is designed to estimate a lower bound for intracellular $PYO_{reduced}$ concentrations in a reduced subsample by comparing measured concentrations of extracellular PYO in oxidized and reduced subsamples of the same starter culture.

Calculation:

1. The intracellular concentration of PYO in the reduced subsample is defined as the intracellular amount of PYO in moles divided by the intracellular volume:

$$[PYO]_{reduced,\,intracellular} = \frac{nPYO_{reduced,\,intracellular}}{V_{reduced,\,intracellular}}$$

2. The intracellular volume is the product of the cellular volume (L/cell), the culture density (cells/L) and the subsample volume (L):

$$V_{reduced,\,intracellular} = V_{cell} * \rho_{culture} * V_{subsample}$$

3. To calculate the intracellular moles of PYO in the reduced subsample, we begin with an assumption. Because both subsamples are taken from the same starter culture and are not allowed sufficient time to produce significant additional PYO (45 min for sample preparation), we assume that oxidized and reduced subsamples contain the same total moles of PYO:

   $nPYO_{reduced} = nPYO_{oxidized}$

4. Our HPLC measurements show that, for a given starter culture, oxidized subsamples contain significantly more extracellular PYO than reduced subsamples. For simplicity, we will assume that oxidized subsamples contain only extracellular PYO:

   $nPYO_{oxidized} = nPYO_{oxidized,\,extracellular}$.

5. And we will assume that reduced subsamples contain both extracellular and intracellular PYO:

$$nPYO_{reduced} = nPYO_{reduced,\,extracellular} + nPYO_{reduced,\,intracellular}\ .$$

This simplifying assumption will ultimately result in an underestimation of intracellular PYO if, as is likely, oxidized subsamples also contain some intracellular PYO.

Because no PYO degradation mechanism is currently known in *P. aeruginosa PA14*, we then assume that the PYO deficit consistently observed in the reduced condition compared to the oxidized condition is due solely to uptake (whether due to passive partitioning and/or active processes). In other words, the difference between measured extracellular amounts in the two subsamples is exactly the amount of intracellular PYO in the reduced condition:

6. $$nPYO_{oxidized,\,extracellular} - nPYO_{reduced,\,extracellular} = nPYO_{reduced,\,intracellular}$$

Molar amounts of extracellular PYO in an oxidized or reduced subsample can be calculated directly from the concentrations measured by HPLC and the volumes of the subsamples:

7. $[PYO]_{subsample,\,extracellular} * V_{subsample} = nPYO_{subsample,\,extracellular}$

Substituting Equation 7 into Equation 6 gives the total moles of intracellular PYO:

8.

$$nPYO_{reduced,\,intracellular} = [PYO]_{oxidized,\,extracellular} * V_{oxidized} - [PYO]_{reduced,\,extracellular} * V_{reduced}$$

The intracellular PYO concentration in the reduced subsample is then given by substituting Equation 8 and Equation 2 into Equation 1 as numerator and denominator, respectively:

9.

$$[PYO]_{reduced,\,intracellular} = \frac{[PYO]_{oxidized,\,extracellular} * V_{oxidized} - [PYO]_{reduced,\,extracellular} * V_{reduced}}{V_{cell} * \rho_{culture} * V_{reduced}}$$

Quantities used for calculation:

- A dense culture of WT PA14 cells (measured OD_{500} = 7.5) typically contains about $7x10^9$ cells per mL, or $7x10^{12}$ cells per L [30].
- The volume of each cell is approximately one cubic micron, or one 1fL (10^{-15}L) [31].

- The average extracellular concentration in oxidized subsamples was 60μM.
- The average extracellular concentration in reduced subsamples was 35μM.
- The volumes of oxidized and reduced subsamples were 1mL

Substituting, we find the moles of intracellular PYO in the reduced sample (Equation 8) is

$$nPYO_{intracellular,reduced} = (60 \times 10^{-6}M) * (1 \times 10^{-3}L) - (35 \times 10^{-6}M) * (1 \times 10^{-3}L)$$

$$nPYO_{intracellular,\,reduced} = 25 \times 10^{-9} moles.$$

The intracellular volume in the reduced fraction (Equation 2) is

$$V_{intracellular,\,reduced} = V_{cell} * \rho_{culture} * V_{reduced} = \left(1 \times 10^{-15}\ \frac{L}{cell}\right) * \left(7 \times 10^{12}\ \frac{cells}{L}\right) * (1 \times 10^{-3}\ L)$$

$$V_{intracellular,\,reduced} = 7 \times 10^{-6}\ L.$$

The intracellular concentration is then

$$[PYO]_{intracellular,\,reduced} = \frac{nPYO_{intracellular,\,reduced}}{V_{intracellular,\,reduced}} = \frac{25 \times 10^{-9} moles}{7 \times 10^{-6} L} = 3.6mM.$$

Membrane fraction PYO retention experiment calculation

Goal: These calculations are designed to determine the concentration of PYO on a per gram basis in the media and in the recovered membrane fraction of a dense *P. aeruginosa* culture.

Calculations:

The concentration of extracellular PYO found in the media is given by the measured concentration of the diluted media multiplied by the dilution factor (2):

$$16.8\ \mu M * 2 = 33.6\ \mu M$$

If we assume the media has a density of 1g/mL, the concentration on a per gram basis is

$$33.6 \frac{\mu mol}{L} * \frac{1\ L}{1000\ mL} * \frac{1\ mL}{1\ g} = 0.0336 \frac{\mu mol}{g\ media}$$

For the membrane fraction extract, which, after pooling and evaporation, consisted of 4.7mL MeOH, the measured concentration (diluted 1:10) was 125.9µM, making the true concentration in the extract

$$125.9\ \mu M * 10 = 1259.0\ \mu M$$

To find the number of moles per gram wet membrane, we can find the total moles in the 4.7mL extract and divide by the mass of the wet membrane fraction (separated by ultracentrifugation as described above):

$$1259 \frac{\mu mol}{L} * \frac{1\ L}{1000\ mL} * 4.7\ mL * \frac{1}{2.75\ g\ wet\ membrane}$$

$$= 2.15\ \frac{\mu mol}{g\ wet\ membrane}$$

When calculated for the whole cell pellet (mass 7.92g), we find

$$1259\,\frac{\mu mol}{L} * \frac{1\,L}{1000\,mL} * 4.7\,mL * \frac{1}{27.92\,g\ wet\ pellet} = 0.75\,\frac{\mu mol}{g\ wet\ pellet}$$

References:

1. (a) J.-D. Chai and M. Head-Gordon, "Systematic optimization of long-range corrected hybrid density functionals," *J. Chem. Phys.*, **128** (2008) 084106. (b) J.-D. Chai and M. Head-Gordon, "Long-range corrected hybrid density functionals with damped atom-atom dispersion corrections," *Phys. Chem. Chem. Phys.*, **10** (2008) 6615-20
2. T. H. Dunning Jr., "Gaussian basis sets for use in correlated molecular calculations. I. The atoms boron through neon and hydrogen," *J. Chem. Phys.*, **90** (1989) 1007-23
3. (a) Klamt, A.; Schüürmann, G. COSMO: a new approach to dielectric screening in solvents with explicit expressions for the screening energy and its gradient. *J. Chem. Soc. Perkin Trans. 2* **1993**, *0*, 799-805. (b) Tomasi, J.; Persico, M. Molecular Interactions in Solution: An Overview of Methods Based on Continuous Distributions of the Solvent. *Chem. Rev.* **1994**, *94*, 2027-2094. (c) Andzelm, J.; Kölmel, C.; Klamt, A. Incorporation of solvent effects into density functional calculations of molecular energies and geometries. *J. Chem. Phys.* **1995**, *103*, 9312-9320. (d) Barone, V.; Cossi, M. Quantum Calculation of Molecular Energies and Energy Gradients in

Solution by a Conductor Solvent Model. *J. Phys. Chem. A* **1998**, *102*, 1995-2001. (e) Cossi, M.; Rega, N.; Scalmani, G.; Barone, V. Energies, structures, and electronic properties of molecules in solution with the C-PCM solvation model. *J. Comput. Chem.* **2003**, *24*, 669-681.

4. Gaussian 16, Revision C.01, Frisch, M. J.; Trucks, G. W.; Schlegel, H. B.; Scuseria, G. E.; Robb, M. A.; Cheeseman, J. R.; Scalmani, G.; Barone, V.; Petersson, G. A.; Nakatsuji, H.; Li, X.; Caricato, M.; Marenich, A. V.; Bloino, J.; Janesko, B. G.; Gomperts, R.; Mennucci, B.; Hratchian, H. P.; Ortiz, J. V.; Izmaylov, A. F.; Sonnenberg, J. L.; Williams-Young, D.; Ding, F.; Lipparini, F.; Egidi, F.; Goings, J.; Peng, B.; Petrone, A.; Henderson, T.; Ranasinghe, D.; Zakrzewski, V. G.; Gao, J.; Rega, N.; Zheng, G.; Liang, W.; Hada, M.; Ehara, M.; Toyota, K.; Fukuda, R.; Hasegawa, J.; Ishida, M.; Nakajima, T.; Honda, Y.; Kitao, O.; Nakai, H.; Vreven, T.; Throssell, K.; Montgomery, J. A., Jr.; Peralta, J. E.; Ogliaro, F.; Bearpark, M. J.; Heyd, J. J.; Brothers, E. N.; Kudin, K. N.; Staroverov, V. N.; Keith, T. A.; Kobayashi, R.; Normand, J.; Raghavachari, K.; Rendell, A. P.; Burant, J. C.; Iyengar, S. S.; Tomasi, J.; Cossi, M.; Millam, J. M.; Klene, M.; Adamo, C.; Cammi, R.; Ochterski, J. W.; Martin, R. L.; Morokuma, K.; Farkas, O.; Foresman, J. B.; Fox, D. J. Gaussian, Inc., Wallingford CT, 2016.
5. Legault, C. Y. (2009) CYLview, 1.0b, Université de Sherbrooke: Sherbrooke, Canada, http://www.cylview.org.

6. Winget, P.; Dolney, D.; Giesen, D.; Cramer, C.; Truhlar, D. *Minnesota Solvent Descriptor Database*. https://comp.chem.umn.edu/solvation/mnsddb.pdf.
7. Michalík, M.; Vladimír Lukeš. The validation of quantum chemical lipophilicity prediction of alcohols. *Acta Chimica Slovaca* **2016**, *9* (2), 89–94.
8. Ho, J.; Ertem, M. Z. Calculating free energy changes in continuum solvation models. *Journal of Physical Chemistry B* **2016**, *120* (7), 1319–1329.
9. Marenich, A. V.; Cramer, C. J.; Truhlar, D. G. Universal solvation model based on solute electron density and on a continuum model of the solvent defined by the bulk dielectric constant and atomic surface tensions. *The Journal of Physical Chemistry B* **2009**, *113* (18), 6378–6396.
10. José Manuel Guevara-Vela; Gallegos, M.; Valentín-Rodríguez, M. A.; Costales, A.; Tomás Rocha-Rinza; Ángel Martín Pendás. On the relationship between hydrogen bond strength and the formation energy in resonance-assisted hydrogen Bonds. *Molecules* **2021**, *26* (14), 4196–4196.
11. Anslyn, E. V.; Dougherty, D. A. *Modern Physical Organic Chemistry*; Univ. Science Books: Sausalito, Calif., 2008.
12. Glendening, E. D.; Landis, C. R.; Weinhold, F. NBO 6.0: Natural bond orbital analysis program. *Journal of Computational Chemistry* **2013**, *34* (16), 1429–1437.

13. Reed, A. E.; Curtiss, L. A.; Weinhold, F. Intermolecular interactions from a natural bond orbital, donor-acceptor viewpoint. *Chemical Reviews* **1988**, *88* (6), 899–926.
14. Daina, A., Michielin, O. & Zoete, V. SwissADME: a free web tool to evaluate pharmacokinetics, drug-likeness and medicinal chemistry friendliness of small molecules. *Sci Rep* 7, 42717 (2017). https://doi.org/10.1038/srep42717
15. US EPA. [2026]. Estimation Programs Interface Suite™ v 4.11]. United States Environmental Protection Agency, Washington, DC, USA.
16. Molinspiration Cheminformatics free web services. https://www.molinspiration.com, Slovensky Grob, Slovakia.
17. Wang, R., Fu, Y., & Lai, L. (1997). A new atom-additive method for calculating partition coefficients. *Journal of Chemical Information and Computer Sciences*, 37(3), 615–621. https://doi.org/10.1021/ci960169p
18. Cheng, T., Zhao, Y., Li, X., Lin, F., Xu, Y., Zhang, X., Li, Y., Wang, R., & Lai, L. (2007). Computation of octanol−water partition coefficients by guiding an additive model with knowledge. *Journal of Chemical Information and Modeling*, 47(6), 2140–2148. https://doi.org/10.1021/ci700257y
19. Meylan, W. M., & Howard, P. H. (1995). Atom/fragment contribution method for estimating octanol–water partition coefficients. *Journal of Pharmaceutical Sciences*, 84(1), 83–92. https://doi.org/10.1002/jps.2600840120

20. Meylan, W. M., Howard, P. H., & Boethling, R. S. (1996). Improved method for estimating water solubility from octanol/water partition coefficient. *Environmental Toxicology and Chemistry*, 15(2), 100–106. https://doi.org/10.1002/etc.5620150205

21. Meylan, W. M., & Howard, P. H. (2000). Estimating log P with atom/fragments and water solubility with log P. *Perspectives in Drug Discovery and Design,* 19(1), 67–84. https://doi.org/10.1023/a:1008715521862

22. Daina, A., Michielin, O., & Zoete, V. (2014). iLOGP: A simple, robust, and efficient description of n-octanol/water partition coefficient for drug design using the GB/SA approach. *Journal of Chemical Information and Modeling*, 54(12), 3284–3301. https://doi.org/10.1021/ci500467k

23. Cheluvappa, R. (2014). Standardized chemical synthesis of *Pseudomonas aeruginosa* pyocyanin. *MethodsX,* 1, 67–73. https://doi.org/10.1016/j.mex.2014.07.001

24. J. Sangster. (1997). Octanol-water partition coefficients: fundamentals and physical chemistry. Ch. 3 p. 55. J. Wiley, Cop.

25. Apelblat, A. (1983). Correlation between activity and solubility of water in some aliphatic alcohols. *Berichte Der Bunsengesellschaft Für Physikalische Chemie*, 87(1), 2–5. https://doi.org/10.1002/bbpc.19830870104

26. Marcus, Y. (1990). Structural aspects of water in 1-octanol. *Journal of Solution Chemistry*, 19(5), 507–517. https://doi.org/10.1007/bf00650383

27. J. Sangster. (1997). Octanol-water partition coefficients: fundamentals and physical chemistry. Intro. p. 5. J. Wiley, Cop.

28. Schönsee, C. D., & Bucheli, T. D. (2020). Experimental determination of octanol–water partition coefficients of selected natural toxins. *Journal of Chemical Engineering Data*, 65(4), 1946–1953. https://doi.org/10.1021/acs.jced.9b01129

29. Wang, Y., & Newman, D. K. (2008). Redox reactions of phenazine antibiotics with ferric (hydr)oxides and molecular oxygen. *Environmental Science Technology*, 42(7), 2380–2386. https://doi.org/10.1021/es702290a

30. Dong-ju Kim,. (2012). Relation of microbial biomass to counting units for *Pseudomonas aeruginosa*. *African Journal of Microbiology Research*, 6(21). https://doi.org/10.5897/ajmr10.902

31. Milo, R., & Phillips, R. (2015). *Cell Biology by the Numbers*. CRC Press. https://book.bionumbers.org/how-big-is-an-e-coli-cell-and-what-is-its-mass/